IMPROVING SCALE-UP PROCEDURES FOR SOLIDS FRICTION AND MINIMUM TRANSPORT BOUNDARY FOR FLUIDIZED DENSE-PHASE PNEUMATIC CONVEYING SYSTEMS

A thesis submitted in fulfillment

of the requirement for the award of the degree of

DOCTOR OF PHILOSOPHY

Submitted by

GAUTAM SETIA

Registration No.: 901208004

DEPARTMENT OF MECHANICAL ENGINEERING

THAPAR UNIVERSITY, PATIALA-147004,

PUNJAB, INDIA

June 2016

This thesis is dedicated to my parents

Shashi and Darshan Lal

THESIS CERTIFICATION

I, Gautam Setia, declare that the work presented in this thesis report entitled, **"Improving Scale-up Procedures for Solids Friction and Minimum Transport Boundary for Fluidized Dense-Phase Pneumatic Conveying Systems"** submitted in fulfillment of requirement for the award of degree of Doctor of Philosophy in Department of Mechanical Engineering, Thapar University Patiala, is an authentic record of my own work carried out under the supervision of Dr. S.S. Mallick (Associate Professor, Department of Mechanical Engineering, Thapar University, Patiala) from July 2012 to June 2016. The matter presented in this thesis has not been submitted either in part or full to any other University or Institute for the award of any other degree.

Gautam Setia Date: June16, 2016

Registration No.: 901208004

It is certified that the above statement made by the student is correct to the best of my knowledge and belief.

Dr. S.S. Mallick, PhD Supervisor Date: June16, 2016

Associate Professor,

Department of Mechanical Engineering, Thapar University, Patiala

ACKNOWLEDGEMENTS

Abilities require opportunities for achievements which should be created if are not there. However, I was not even aware of my abilities. I would always be thankful to Dr. S.S. Mallick who not only believed in my abilities but also provided me the opportunities to achieve this degree. I feel there is always a special bonding between a PhD student and his supervisor in which later plays the role of a mentor whereas, in my case Dr. S. S. Mallick was more like a co PhD Student and a close friend to me. Here, I feel blessed to share this kind of relation with my PhD supervisor.

I was also fortunate to have guidance and sincere advice given time to time from Professor Peter Wypych, Director, Centre for Bulk Solids and Particulate Technologies, University of Wollongong, Australia. I thank him for his generous support and continuous encouragement.

I shall remain grateful to Dr. Rehnu Pan, Vice General Manager, Fujian Longking Co., Ltd., China; for providing me the opportunity and support to carry out the experimental studies at Fujian Longking's experimental test facility in Longyan, China. This has equipped me with very valuable data, which I have used extensively in this thesis. I acknowledge the support of the technical staff of the Bulk Materials Handling Laboratory, Fujian Longking Co., Ltd., China for the experimental work.

I express my sincere gratitude to Mr. Atul Sharma, Lecturer, Mechanical Engineering Department, Thapar University, and Patiala; for his presence and moral support during my good and difficult times.

I acknowledge my heartiest gratitude to my grandfather Sh. Ram Gopal and my maternal grandmother Mrs. Hukmai whom I lost during the course of my PhD. They always prayed for me and had given me their continuous blessings to achieve successes. I really regret not being able to spend sufficient time with them.

I am highly indebted to Department of Science and Technology (DST), Science and Engineering Research Board, Ministry of Science and Technology, Government of India (Young Scientist Scheme No: SR/FTP/ETA-15/2011; PI: Dr. S.S. Mallick), and Council for Scientific and Industrial Research (CSIR) Government of India, (Scheme no: 22(0614)/12/EMR-II; PI: Dr. S.S. Mallick), for the financial support to pursue the research work.

I owe special thanks to all the staff of Central Workshop, Thapar University for their help and support, for their help in manufacturing various components and commissioning of dense phase pneumatic conveying facility in Thapar University.

Finally, I thank, Thapar University, Patiala, for providing me such a great atmosphere to learn and perform my research. The support from the library and research staff has been remarkable.

ABSTRACT

This thesis presents results of an ongoing investigation into developing a validated modeling procedure of important design criteria, such as solids friction factor (for the accurate prediction of pressure drop) and minimum transport condition for the fluidized dense-phase pneumatic conveying of powders. In spite of having the potential of being energy economic mode of pneumatic transport, reliable design of fluidized dense-phase pneumatic conveying systems is still a difficult task due to the highly turbulent and complex nature of the flow of fine powders under high concentrations, where it is difficult to model the particle-wall-air interactions.

Major efforts in this thesis have gone to develop pneumatic conveying test facility at the Laboratory for Particle and Bulk Solids Technologies, Thapar University, India for the fluidized dense-phase flow of fine powders having different pipeline configurations, such as 43 mm I.D. × 24 m long, 54 mm I.D. × 24 m long and 69 mm I.D. × 24 m long and 54 mm I.D. × 70 m long pipes. Indian fly ash was conveyed in fluidized dense-phase. Additional tests (under scale-up condition) were performed by conveying of cement and a different sample of fly ash through the 65 mm I.D × 254 m long and 80/100 mm I.D × 407 m long test rigs of Fujian Longking Co., China. Existing data of other researcher (from the laboratory of University of Wollongong, Australia), where ESP dust and fly ash were conveyed through 69 mm I.D. × 168 m long, 105 mm I.D. ×168 m long and 69 mm I.D. × 554 m long pipelines, were also used for comprehensive scale-up validation of the developed models.

A new technique of modeling solids friction factor has been developed using new dimensionless numbers, volumetric loading ratio and dimensionless velocity (the ratio of particle free settling velocity to superficial conveying air velocity) by replacing the solids loading ratio and Froude numbers, respectively, present in the existing models. The volumetric loading ratio term incorporates the effect of product volume occupancy inside the pipeline, which was considered in this study to be a better representation of the flow conditions compared to the mass flow rate ratio of solids to air (solids loading ratio). The dimensionless velocity term is aimed at addressing the flow condition (transition from non-suspension to suspension flow). Models have been developed using the straight-pipe conveying data of three types of fly ash, cement and ESP dust (median particle diameter: 7 to 30 μm; particle density: 1950 to 3637 kg/m^3; loose-poured bulk density: 610 to 1080 kg/m^3). The models were evaluated for their accuracy and stability under significant scale-up conditions by comparing the predicted versus experimental pneumatic conveying characteristics obtained from longer and larger sized pipelines. Results have shown that the new model has considerably improved pressure drop predictions (up to 66.2%) compared to the prediction capability of the existing model, especially in the dense-phase region.

In another approach, a two-layer based model has been developed by separately considering the solids friction contributions of the non-suspension (dense) bed of powders flowing along the bottom of pipe and the suspension (dilute-phase flow) of particles occurring on top of the non-suspension layer. Volumetric loading ratio and dimensionless velocity have been used to represent the non-suspension dune flow layer. A solids impact and friction term has been employed to represent the dilute-phase flow due their established reliability. The developed models for solids friction were validated for their scale-up accuracy by using them to predict

the pressure drops in above mentioned larger and longer pipelines and by comparing the experimental versus predicted pneumatic conveying characteristics. The two-layer model provided further considerable improvement in prediction indicating that the model is able to adequately address the dense- to dilute-phase transition criteria.

For the reliable design of fluidized dense-phase pneumatic conveying systems, it is of paramount importance to accurately estimate blockage conditions or the minimum transport boundary. Based on the test results of 22 different powders conveyed through 38 pipelines, a unified model for the minimum transport boundary has been developed that represents gas Froude number as a function of solids loading ratio and particle Froude number. The model has been validated by predicting the minimum transport boundary for 3 different products, conveyed through 6 different pipelines. Various other existing models have been validated for the same products and pipelines. Comparisons between experimental blockage boundary and predicted results have shown that the newly developed model provides more accurate and stable predictions compared to the other existing models. The model incorporates both pipe diameter effect and some important physical properties of the particles. The model is believed to be useful in predicting minimum conveying velocities for various fine powders that are fluidizable to ensure optimum operating point for industrial pneumatic conveying systems.

TABLE OF CONTENTS

LIST OF FIGURES

CHAPTER 4

APPENDIX A

LIST OF TABLES

CHAPTER 6

LIST OF SYMBOLS AND ABBREVIATIONS

A	Cross sectional area of the pipe [m^2]
A1	Portion of cross sectional area of pipe occupied by the non-suspension layer in dense-phase regime [m^2]
A2	Portion of cross sectional area of pipe occupied by the suspension layer in dense-phase regime [m^2]
Ar	Archimedes number ($Ar = [g \rho (\rho p-\rho)d^3]/(\mu)^2$)
B	Bend loss factor
Be	Equivalent length for bends [m]
C	Particle velocity [m/s]
CD	Drag coefficient
D	Internal diameter of pipe [m]
d, ds, dp	Particle diameter [m]
d_{50}	Median particle diameter [μm]
d_b	Bubble diameter, m
Fr	Sliding friction factor between of solids and pipe wall
Fr	Froude number ($Fr = V/(gD)^{0.5}$)
Fr	Sliding friction factor between of solids and pipe wall
Fr_{bo}	Froude number of flow at bend outlet
Fr_d	Froude number based on superficial air velocity and particle diameter ($Fr_d = V/(gd)^{0.5}$)
Fr_i	Froude number at pipe inlet

Fri	Friction number
Fr_m	Mean Froude number related to the section of pipe ($Fr_m = V_m/(gD)^{0.5}$)
Fr_{min}	Minimum Froude number at the inlet to the pipe ($Fr_{min} = V_{min}/(gD)^{0.5}$)
Fr_p ,Fr_s	Particle Froude number based on single particle terminal velocity and particle diameter ($Fr_p = w_{fo}/(gd)^{0.5}$)
Fr_{sD}	Particle Froude number based on single particle terminal velocity and pipe diameter ($Fr_{sD} = w_{fo}/(Dg)^{0.5}$)
G	Acceleration due to gravity [m/s^2]
G_s	Product mass flow rate per unit area ($G_s = m_s/A$), [$kg/s.m^2$]
K, K_1, K_2	Constant of power function
K_b	Bend loss coefficient
L	Length of pipe or test section [m]
L_h	Length of a horizontal portion of pipe [m]
L_v	Height of a vertical section of pipe [m]
m*	Solids loading ratio ($m^* = m_s/m_f$)
M_f	Mass of air in a control volume [kg]
m_f	Mass flow rate of air [kg/s]
$m_{non\text{-}sus}$	Mass flow rate of solids being conveyed in non-suspension layer in dense-phase regime[kg/s]
M_s	Mass of solids in a control volume [kg]
m_s	Mass flow rate of solids [kg/s]
m_{sus}	Mass flow rate of solids being conveyed in suspension layer in dense-phase regime [kg/s]

n	Flow index
N	Number of bends
P	Pressure [N/m^2]
R	Radius of pipe [m]
R_B	Centerline radius of bend [m]
Re	Reynolds number of gas ($Re = \rho VD/\mu_f$)
Re^*_p	Reynolds number modified by pipe diameter ($Re_p^* = Re_p/(1.4 – 0.8\ e^{-((d/d_{50})/1.5)})$)
Re_b	Bubble Reynolds number
Re_m	Modified Reynolds number
Re_p	Reynolds number of particle ($Re_p = \rho_s Vd/\mu_f$)
R_h	Hydraulic radius [m]
S_1	Wetted perimeter on the pipe wall due to non-suspension layer in dense-phase regime [m]
S_2	Wetted perimeter on the pipe wall due to suspension layer in dense-phase regime [m]
t/h	Tones per hour
U_{mf}	Minimum fluidization velocity [m/s]
V	Superficial air/gas velocity [m/s]
V_{min}	Minimum conveying air velocity requirement at pipe inlet [m/s]
V_f	Volume of air in a control volume [m^3]
V_i,V_{entry}	Superficial air/gas velocity at the inlet or entry of a pipe section [m/s]
VLR	Volumetric loading Ratio ($VLR= (m_s/\rho_s)/(m_f/\rho_s)$)

$V_{non\text{-}sus}$	Conveying velocity for the non-suspension layer in dense-phase regime [m]
V_s	Volume of solids in a control volume [m^3]
w_f	Particle settling velocity in a cloud [m/s]
w_{fo}	Single particle settling (or terminal) velocity in undisturbed fluid [m/s]
$\dot{\gamma}$	Strain rate [1/sec]
$\emptyset$	Volume fraction of the material
ΔP	Pressure drop through a straight horizontal pipe or pipe section [Pa]
ΔP_{accel}	Pressure drop due to initial acceleration [Pa]
ΔP_b	Pressure drop through a bend [Pa]
ΔP_f	Pressure drop due to air only in a pipe [Pa]
ΔP_T	Total pipeline pressure drop [Pa]
ΔPv	Pressure drop due to verticals [Pa]
u_{bu}	Bubble rise velocity [m/s]
v_θ	Angular velocity of the inner rotating cylinder [radians/s]
β	Velocity ratio related to particle fall velocity in a cloud ($\beta = w_f/V$)
β_o	Velocity ratio related to particle fall velocity in a cloud ($\beta = w_{fo}/V$)
γ	Strain [rad]
E	Bed voidage
E	Void fraction of the strand
ε_f	Fluid volumetric fraction ($\varepsilon_f = 1- \varepsilon_p$)
ε_{mf}	Bed voidage at minimum fluidization
ε_p	Particle volumetric fraction
ε_p	Volumetric concentration of particles

θ_M	Angular rotation of motor shaft [rad]
λ_{bs}	Solids friction factor through bends
λ_f	Air/gas only friction factor
λ_{fb}	Air only friction factor in bend
$\lambda_{non\text{-}sus}$	Friction factor for the non-suspension layer in dense-phase regime
λ_s	Solids friction factor through straight pipe
λ_s*	Impact and friction factor
λ_{sus}	Friction factor for the suspension layer in dense-phase regime
λ_T, λ_e	Combined solids-air friction factor
μ_{app}	Apparent viscosity of powders [Pa.s]
μ_f	Dynamic viscosity for single fluid (e.g. air) [Pas]
$\mu_{non\text{-}sus}$	Apparent viscosity for the non-suspension layer in dense-phase regime [Pas]
μ_r	Relative viscosity to the Newtonian fluid [Pa.s]
ρ, ρ_f	Density of air [kg/m^3]
ρ_{app}	Apparent density [kg/m^3]
ρ_{bf}	Bulk density of fluidized bed [kg/ m^3]
ρ_{bl}	Loose-poured bulk density [kg/m^3]
ρ_{bo}	Density of air bend outlet [kg/m^3]
ρ_m	Mean air density for a pipeline section [kg/m^3]
$\rho_{non\ sus}$	Apparent density of the non-suspension layer in dense-phase regime [kg/m^3]
ρ_s, ρ_p	Particle density [kg/m^3]
ρ_{sus}	Suspension density ($\rho_{sus} = (M_s+M_f)/(V_s+V_f)$) [kg/m^3]
ρ_t	Tapped bulk density [kg/m^3]

σ_z	Normal stress in the z direction [Pa]
T	Shear stress [Pa]
τ_o	Yield stress [Pa]
τ_w	Wall shear stress [Pa]
τ_1	Shear stress on the pipe wall due to non-suspension layer in dense-phase regime [Pa]
τ_2	Shear stress on the pipe wall due to suspension layer in dense-phase regime [Pa]

Superscripts

a,b,c,d	Exponents of the power function

Subscripts

Bl	Bulk
E	Equivalent
F	Fluid (air)
H	Horizontal
I	Inlet condition
M	Mean value for the section/interval of pipe, based on average air density
min	Minimum
P	Particle
S	Solids
V	Vertical
T	Total

Abbreviations

BD	Bottom discharge
I.D.	Internal diameter of pipe
MTB	Minimum transport boundary
PCC	Pneumatic conveying characteristics
PMC	Pressure minimum curve
TD	Top discharge

CHAPTER 1

Introduction and Objectives

1.1 Introduction

The pneumatic transportation of bulk solids through pipelines is being selected for several industrial applications and is playing a more vital and integral role in numerous bulk handling operations and processes. Some benefits of pneumatic conveying include: totally enclosed conveying, environment friendly and hygienic mode of transport, enhanced workplace safety, relatively low capital and maintenance costs (for well-designed systems), flexibility in layout, ease of automation and installation and increased security. The traditional flow mode of conveying is known as dilute-phase (or suspension flow), where the velocity of the carrier gas is sufficiently high to entrain and suspend all the particles along the pipeline. Due to the dispersed and suspended nature of flow mechanism, researchers have enjoyed decent success in modeling the relevant particle interactions and flow phenomenon (e.g. friction, impact, drag, slip velocity etc) and in developing several solids friction factor and pressure drop models (Klinzing et al., 2010; Mallick, 2009). However, the high gas velocity requirement (to ensure suspension of particles) calls for larger size of compressors and higher operating power. The high particle velocities cause increased rate of wear of pipelines and bends. The impact of particles with other particles and the pipeline during high velocity flow results in product attrition in case of fragile products (thus poor quality control and product wastage). Moreover, larger gas flow requires bigger size of filtration equipment (e.g. bag filter), hence additional capital and space requirements. To prevail over these limitations of conventional suspension or dilute-phase flow, low velocity dense-phase pneumatic conveying is acquiring popularity within industries in recent years. In this mode of conveying, due to the lower operating gas and particle velocities, material is transported in non suspension flow and the size of the air mover is considerably reduced (therefore, lower energy consumption). There

can be different types of dense-phase mode of flow depending on the air retention capability and permeability of the bulk solids, which are as follows (Wypych, 1989; Pan, 1992):

- Fluidized dense-phase (FDP) pneumatic conveying for air-retentive powders
- Low-velocity slug-flow (LVSF) of granular materials having natural slugging ability
- Low-velocity plug-flow of cohesive fine powders (e.g. cocoa powder)
- Single-slug conveying of relatively coarse/abrasive products (e.g. crushed coal)

Typically, the fine powders, such as fly ash, cement, pulverized coal etc that have good air retention capabilities, are good candidates for fluidized dense-phase (FDP)mode of transport, where the flow through the pipes is in the form of a moving fluidized bed or non-suspension dunes (Klinzing et al., 2010). Also, the FDP mode of conveying can sustain much higher solids-to-gas mass flow rate ratio (m*), referred to as "solids loading ratio". Hence, fluidized dense-phase is the most preferred mode of dense-phase conveying used by various industries conveying fine powders, such as fly ash in coal fired thermal power plants, pulverized coal, cement, calcium carbonate, fine chemical powders etc. Due to the high amounts of solids conveyed per unit mass of gas flow (e.g. solids loading ratio - m* can go to as high as 100, Mallick 2009), FDP offers the following advantages compared to the conventional dilute-phase mode:

(a) Relatively low conveying velocity, e.g. conveying velocities at feed points are normally in the range of 3 to 6 m/s (Mallick and Wypych, 2009) compared to about 15 m/s for dilute phase (Mills, 2004).

(b) Reduced gas flow rates and hence smaller compressor with lesser power consumption, e.g. a well designed FDP system could result in 50% energy saving (i.e. reduced kW consumption of the transport air compressors) compared to the conventional dilute-phase system. Hence,

considering the wide industrial application (especially applications such as the huge amount of fly ash that is usually conveyed in pneumatic conveying mode in coal fired thermal power plants in India), FDP would provide substantial amount of savings in power consumption.

(c) Due to the higher value of product flow rates per unit mass of conveying air (e.g. $m^* > 50$ in dense-phase, compared to $m^* < 15$ in dilute-phase), higher conveying capacities can be achieved through smaller sizes of pipes, e.g. typically 4 inch Nominal Bore (NB) pipe size in dense-phase compared to 6 in NB pipe in dilute-phase for the same solids flow rate. This also results in the requirement of smaller sized pipe-fittings and support sizes/structures.

(d) Reduced amounts of particle attrition or product degradation.

(e) Reduction of wear rate of pipeline and bends.

(f) Due to the higher concentrations of product along the pipeline, FDP can offer a natural explosion barrier preventing dust explosions propagating and accelerating along the pipeline, as well as avoiding the risk of explosion detonation (Eckhoff, 1997). Such potentially dangerous incidents are possible in dilute-phase pneumatic conveying.

(g) Reduction in the size of solid-gas separation equipment due to reduced gas flow rate.

Despite these potential benefits, widespread industrial use of fluidized dense-phase type of conveying is still limited due to the following design difficulties, attributed by:

- The nature of flow is quite complex - highly turbulent moving fluidized bed of powders.
- Very difficult to model the relevant particle and wall interactions (Li et al., 2014).
- Due to the above, it is extremely difficult to link the particle/bulk properties and the interactions/mechanisms to actual conveying parameters and operating conditions (Rao and Nott, 2008)

Because of the above flow complexities, only limited progress has been achieved so far in fundamentally understanding the flow mechanism (i.e. the powder/wall/air interactions) and accurately modeling important system design parameters for fluidized dense-phase pneumatic conveying of powders, such as the accurate prediction of:

- Horizontal straight-pipe pressure loss (towards estimating total pipeline pressure drop)
- Minimum transport boundary (i.e. the minimum conveying velocity requirement to ensure flow blockage would not take place for a given pipeline length and diameter and product, especially under industrial scale-up conditions)

Due to the turbulent and complex nature of fluidized dense-phase flow, empirical power function based models using different dimensionless groupings have been employed over the years by various researchers (Pan, 1992; Pan and Wypych, 1998; Jones and Williams, 2003; Williams and Jones, 2004; Mills, 2004; Ratnayake, 2005) to represent important key design parameters, such as total pipeline pressure drop and minimum transport conditions. These models provided good results when employed to the researchers' own data, but had not been investigated under proper scale-up conditions of pipeline lengths and/or diameters. Recent examination (Mallick, 2009) to test the scale-up accuracy of the existing and/or popular models by comparing the predicted PCC against experimental plots have shown that the existing models for pressure drop generally provide significant inaccuracy under industrial scale-up conditions. Also, the existing method to determine the minimum transport condition and flow-mode transition criteria have been found to be inadequate (Mallick, 2009), as they do not consider important factors, such as the particle and bulk properties, pipeline diameter and gas density effects. Therefore, use of these models in industrial design would likely to cause either a grossly over designed system (large compressor, pipe sizes etc) and ultimately

running the system at a low efficiency points, or an under-rated system not able to provide the required product throughput (e.g. resulting in slow rate of evacuation of fly ash from ESP hoppers in a power plant, ultimately causing the disruption in plant operations). Lack of confidence to design good dense-phase system is likely to cause selection (wrongly) of an operating point having large gas flows. This would result in higher gas-velocity that would increase the rate of pipe and bend erosion and also the product degradation. The present criteria of predicting minimum transport boundary (such as, Mallick and Wypych, 2009) have not been adequately tested for scale-up accuracy against a wide range of pipe and product data. Incorrect estimation of minimum transport boundary would cause pipeline blockage. In addition, determination of the conveying mode (dilute and fluidized dense-phase) of flow is also important. For fluidized dense-phase type conveying with fine powders, the transition from the dilute-phase (suspension) to dense-phase (non-suspension) mode is quite gradual i.e. without any sudden changes in flow characteristics resulting in instability (Wypych and Yi, 2003; Klinzing et al., 2010). Very little work has been done so far to investigate into the flow mode transition criteria (dense-to-dilute phase). Because of the above limitations of the existing design methods due to the lack of fundamental understanding of the flow phenomenon and much rely on empirical methods (using parameter groupings whose physical significances are often difficult to rationale), there is a need for further research with greater emphasis on proper understanding of the complex flow (particle/air/wall) interactions of the highly turbulent moving dune to provide the industry an improved validated modeling and scale-up technique.

1.2 Objectives

Particular research objectives include:

(1) Development of dense-phase pneumatic conveying test rig with different pipeline configurations and having pressure transducers and sight-glass located at strategic locations for conducting testing to generate a unique and extensive database comprising relevant conveying parameters (such as wide range of air and solids flow rates, straight-pipe and total pipeline pressure drop data) by conveying different fine powders (such as fly ash and cement).

(2) Development of Pneumatic Conveying Characteristics (PCC) for total and straight-pipeline pressure drop and identification of dense- to dilute-phase transition location from the straight-pipe conveying characteristics.

(3) Development of improved straight-pipe model for solids friction factor and scale-up validation of the same by comparing predicted versus experimental conveying characteristics.

(4) Development of models for solids friction contribution for the non-suspension dense-phase flow of fine powders using the measured apparent viscosity data and scale-up validation of the same by comparing predicted versus experimental conveying characteristics.

(5) Modeling of minimum transport boundary (i.e. minimum conveying velocity requirement to ensure pipeline blockage does not occur) for different pipe diameters, lengths and powders and validation of the same.

The resulting outcome of this thesis would help others researchers by providing a better detailed understanding of the turbulent fluidized nature of dense-phase solids-gas flow.

Having a validated reliable modeling and scale-up procedure would benefit the industry in the following ways:

(a) Minimization of air flows: reduced sized compressor and power consumption

(b) Optimal pipe sizing for a given product, capacity and pipe layout – large capacity, long distance conveying

(c) Accurate predictions of pressure drop – reduction in safety margins in design

(d) Improved ability to troubleshoot existing systems

(e) Minimization of filtration equipment and workplace/ environmental emissions

(f) Increased acceptance of FDP within the industry

CHAPTER 2

Literature Review

2.1 Introduction

Various studies that have been are carried out over the years in the area of dense-phase pneumatic conveying of fine powders are presented here to illustrate the various approaches used by different researchers. The studies reported here are divided into two areas: pressure drop and solids friction factor and minimum conveying velocity. Suitable references to other literatures (such as the rheology of bulk solids) have been provided in the subsequent chapters, where found appropriate.

2.2 Pressure drop of solids-gas flows

Total pipeline pressure drop mainly consists of pressure drops in horizontal straight-pipe sections, verticals and around the bends. For pipelines having relatively longer horizontal straight-pipe length (e.g. fly ash conveying pipelines in coal fired power plants that run from the buffer hopper to remote silo), accurate prediction of pressure drop for the horizontal straight-pipe is of paramount importance. Details about previous studies carried out over the years (by different researchers) on the estimation of pressure drop for dense-phase pneumatic conveying system of powders are listed underneath. Initial studies conducted were related to the system approach concepts and afterwards the studies regarding micro approach of pressure drop (expression for solid friction factor) are presented.

2.2.1 Scale-up models in system approach

System approach includes initially generating test rig pneumatic conveying characteristics (PCC) for a bulk solid and then applying scale-up equations to predict the pressure drop characteristics for the proposed plant (Mills et al., 1982; Wypych and Arnold, 1987). The method does not address fundamental flow phenomenon, such as the particle-particle/wall/air interactions. This method has been in existence for more than two decades (Mills et al., 1982 to Wypych and Arnold, 1987 to Mills, 2004). Mills et al. (1982) conveyed fine "pulverized fuel ash" for a wide range of product flow rates through a 50 mm I.D. × 100 m long pipe including 13 numbers of 90^{o} bends. The derived PCC were then scaled-up to generate predicted PCC for 50 mm I.D. × 150 m, 75 mm I.D. × 150 m and 100 mm I.D. × 150 m long pipes using the following scale-up laws for constant air mass flow rate per unit area and pressure drop due to product.

Length scale-up: $m_{s2} = m_{s1} (L_1/L_2)$ (2.1)

Diameter scale-up: $m_{s2} = m_{s1} (D_2/D_1)^2$ (2.2)

Where, m_s is mass flow rate of solids, L is length of pipe and D is internal diameter of pipe. Subscript 1 refers to the test rig and 2 to the actual (scale-up) conveying set-up. These scale-up laws do not make any allowance for the losses due to the bends and verticals. Also, authors did not provide any basis for this approach. However, a complete review of this can be found in Mallick (2009). As commented by Mallick (2009) the technique wasn't suitable for dense–phase flow. Hence, not much emphases has been given to this approach in the present study.

Wypych and Arnold (1987) later presented the original scale-up relationships as "generalized scale-up equations", given by:

$$m_{f2} = m_{f1} (D_2/D_1)^2 \quad (2.3)$$

$$m_{s2} = m_{s1} (L_1/L_2) (D_2/D_1)^2 \quad (2.4)$$

Generalized scale-up equations for total pipeline pressure drop (ΔP_T) were given as:

$$\Delta P_{T2} = \Delta P_{T1} + \Delta P_{f1} \{(L_2/L_1) (D_1/D_2) -1\} \quad (2.5)$$

Where, ΔP_f is pressure drop due to air only in a pipe and subscript 1 refers to the test rig and 2 to the actual (scale-up) conveying set-up. Wypych and Arnold (1987) also examined the validity of scale-up laws provided by Mills et al. (1982) by conveying fly ash and cement mixture, PVC powder and screened coke through test rigs of different diameters and lengths. It was found that for diameter scale-up, the criteria proposed by Mills et al. (1982) resulted in significant over-predictions. They suggested that for an improvement in prediction capability, the following equation should be used:

$$m_{s2} = m_{s1} (L_1'/ L_2') (D_2/D_1)^{2.8} \quad (2.6)$$

Where, L_1' and L_2' represents the adjusted values of L_1 and L_2 to allow for any differences between the number and type of bends used in the test rig and the actual plant. Originally the exponent of diameter ratio was 2. However, Wypych and Arnold (1986) when evaluated Mills model in their experimental data, found that the exponent value of 2 provides over prediction of pressure drop in case of diameter scale-up while a number 2.8 was found to provide more

accurate predictions for diameter scale-up. Here, for the verticals, a length of $2L_v$ was proposed to be added with L_h. It appears that the suggested adjustment value represents bend losses corresponding to an additional 4 m length of straight-pipeline length, which is to be added for each bend in the line. Mills (2004) provided system approach by incorporating certain modifications to his original work (Mills et al., 1982). This principally assumes that the losses due to the bends are all equal (for example four meters of additional straight length) and are irrespective of particle, pipe/bend properties, for example location of the bend in the pipeline, radius of curvature of the bend etc. For the length scale-up criteria, Mills (2004) suggested:

$$m_{s2} = m_{s1} (L_{e1}/L_{e2}) \quad (2.7)$$

$$\text{Where, } L_e = L_h + 2L_v + Nb_e \quad (2.8)$$

It appears that the term "L_e" is actually same as L' (Wypych and Arnold, 1987). The suggested adjustment factor by Mills (2004) for the verticals actually matches with that proposed by Wypych and Arnold (1987). For diameter scale-up, Mills (2004) reused his original relationship given by equation (2.4). Recent evaluation work by Mallick (2009) proved that the system approach can provide significantly inaccurate predictions for total pipeline pressure drop under certain scale-up conditions, especially in the dense-phase region. However, it was found that the length scale-up criteria (Mills, 2004) worked well for the dilute-phase regime. It was stated that the accuracy of the system approach is dependent on the system layout and prediction may get highly inaccurate where the layout of laboratory scale test rig and industrial pipelines are considerably different (in terms of relative distribution of the bends in the pipeline), which limits the applicability of this technique.

2.2.2 Micro or component approach

In this approach, the models of solids friction are normally represented in terms of different dimensionless parameter groupings. Barth (1958) was one of the earlier researchers to suggest an expression for pressure drop for solids-gas flows in straight horizontal pipes (equation 2.9) where, total losses due to the solids-gas mixture can be represented as the sum of individual losses due to the solids and gas only.

$$\Delta P = (\lambda_f + m^* \lambda_s) L/D \rho V^2/2 \quad (2.9)$$

In the above equation ΔP is pressure drop for solids-gas flows in straight horizontal pipes, λ_f is air/gas only friction factor and λ_s is solids friction factor through straight pipe. Where, ρ represents air density and V denotes air velocity. This is the most popular form for representing pressure drop for a solids-gas mixture flowing through a straight horizontal section of pipe. There is an assumption in above equation (2.9) that pressure drop due solids and air are independent of each other. The main task in equation (2.9) is to model the solids friction factor (λ_s) accurately, for which generally empirical based solids friction factor models were suggested by various researchers. It is believed that this equation is valid for dilute-phase flow of coarse particles. However, this equation has been used subsequently by various researchers (Stegmaier, 1978; Rizk, 1982; Wypych, 1989; Pan, 1992; Pan and Wypych, 1998; Jones and Williams, 2003; Williams and Jones, 2004, to list a few) to predict the pressure loss for the dense-phase pneumatic transport of fine powders, such as fly ash, for horizontal straight-pipes.

Undoubtedly, Barth's representation has remained as the most popular equation for accounting solids friction in pneumatic conveying systems (for dilute- and fluidized dense-phase).

Stegmaier (1978) developed a power function based model (equation 2.10) for the data obtained on a number of fine and coarse particles, including fly ash, alumina, quartz powder, sand, catalyst for horizontal transport (particle size and particle density varying from 15 to 112 μm and 1500 to 4100 kg/m^3, respectively) for different pipe sizes. It is believed that the data used by Stegmaier (1978) was obtained from straight-pipe sections.

$$\lambda_s = 2.1\ m^{*-0.3} Fr_m^{-2}\ Fr_s^{0.5}\ (D/d_s)^{0.1} \qquad (2.10)$$

Where, m_s is mass flow rate of solids, L is length of pipe, D is internal diameter of pipe and d_s is particle diameter. Subscript 1 refers to the test rig and 2 to the actual (scale-up) conveying set-up. Here, Stegmaier (1978) seemed to have assumed the particle size is spherical and/or particle size distribution effect can be adequately represented by using a single particle diameter term. This assumption seems o have been repeated in subsequent models.

Weber (1981) presented a modified form of Stegmaier (1978) model, as given in equation 2.11, by modifying the particle Froude number term denoted by Fr_{sD} (from being based on particle diameter to pipe diameter).

$$\lambda_s = 2.1\ m^{*-0.3} Fr_m^{-2}\ Fr_{sD}^{0.5}\ (D/d_s)^{0.1} \qquad (2.11)$$

Rizk (1982) suggested that solids friction factor can be divided into two components– losses due impact and friction between particle-particle/air/pipe wall interactions and that due to keeping the particles in suspension. The model developed is given in equation 2.12.

$$\lambda_s = \lambda_s^* C/V + 2\beta/\{(C/V)\, Fr^2\} \quad (2.12)$$

Where, λ_s^* is the impact and friction of the solid particles, C refers to particle velocity and β is the particle fall velocity in a cloud. Here, the term $[2\beta/\{(C/V)\, Fr^2\}]$ considers the energy required to keep the particles in suspension.

Wirth and Molerus (1983) developed the following model for pressure drop for strand conveying using a new dimensionless terms, friction number term Fri (given in the equation 2.13)

$$Fri = V / [(\rho_s/\rho)\,(1 - \rho_s/\rho)\,(1 - \varepsilon)\, D\, g\, f_r]^{0.5} \quad (2.13)$$

Where, f_r is the wall friction angle, ρ_s is particle density and ρ_{bl} is the bulk density of powder and $\varepsilon = 1 - (\rho_{bl}/\rho_s)$; ρ_{bl} is the bulk density of powder. Here, it is a point of concern that whether ρ_s can adequately represent the solid density under actual flow conditions. In the experience of the author the bulk density of the particles under fluidized state can be as low as half of the loose pour bulk density (however, this depends upon the fineness of the particles). Also, the term voidage is difficult to be determine experimentally for fine powders flowing in dense-phase.

Chambers and Marcus (1986) presented an empirical model to calculate the pipeline pressure drop including the bend loss, vertical lift loss and pressure loss due to the initial acceleration. The model consisted of the following:

Acceleration loss : $\Delta P_{accel} = \rho V^2 (1+2 m^* C/V)/2$ (2.14)

Vertical loss : $\Delta P_v = m^* \rho g L_v V/C$ (2.15)

Straight-pipe loss : $\Delta P = (\lambda_f + m^* \lambda_s) L/D \rho V^2/2$ (2.16)

Bend loss : $\Delta P_b = N B (1+ m^*) \rho V^2/2$ (2.17)

$\lambda_s = 2.1 m^{*-0.3} Fr_m^{-1} Fr_s^{0.25} (D/d_s)^{0.1}$ for d_s <0.5 mm (2.18)

Where, L_v represents the height of a vertical section of pipe and g denotes acceleration due to gravity and N is the no. of bend.

Weber (1991) suggested that the flow of air-solid mixture is inseparable in nature as given by equation (2.20) (i.e. the pressure drop due to air only and that due to the solids are difficult to be separated) and came out with a new format of pressure drop, which was expressed as given below:

$\Delta P= \lambda_T \rho V^2 L/2D$ (2.19)

Where, λ_T is the total friction factor of the mixture. The underline assumption of this representation is that the particles and the air form a combined mixture which doesn't seemed to be realistic for non suspension type of flows as a dune appears to flow at bottom of the pipe

and on top of which air flows with dilute suspension. Weber (1991) did not validate his method against scale-up data. For λ_T he suggested the following relation:

$$\lambda_T = K(m^*)^a \ (Fr_m)^b \qquad (2.20)$$

'K' is the constant and 'a' and 'b' are the exponents of power function, which can be found by using minimizing the sum of square error method.

Pan (1992) wrote a thesis, which was aimed at improving the scale-up procedures for the design of pneumatic conveying systems. Based on dimensional analysis, semi-empirical correlations were derived predicting the solids friction factor through straight-pipe (λ_s) and bends (λ_{bs}) and provided the same by equations (2.21) and (2.22), respectively. An air density term was introduced in the power function format. Fly ash was used as the test material for majority of the experiments with d_{50}, ρ_s and ρ_{bl} as 15.5 μm, 2197 and 634 kg/m^3, respectively.

$$\lambda_s = K_1 \ (m^*)^a \ (Fr_m)^b \ (\rho_m)^c \qquad (2.21)$$

$$\lambda_{bs} = K_2 \ (m^*)^{a1} \ (Fr_{bo})^{b1} \ (\rho_{bo})^{c1} \qquad (2.22)$$

Where, 'K_2' is the constant and 'a1', 'b1' and 'c1' are the exponents of power function. λ_{bs} represents the solids friction factor through bends. ρ_{bo} represents the density of air at bend outlet. Fr_{bo} represents Froude number of flow at bend outlet. From experimental data, the values of the constants and exponents of power functions were determined by using the technique of "minimizing the sum of square errors". Similar approach can also be found in Pan and Wypych (1992) and Arnold et al. (1994).

Keys and Chambers (1995) employed power function approach for solids friction with different fly ash samples and using different test rigs. By expressing the pressure drop of the entire pipe as $\Delta P_T = (\lambda_f + m^*\lambda_s)\ L\rho V^2/2D$, solid friction factor (λ_s) model was derived (equation 2.23). Incorporating the effect of d_s/D, equation (2.23) was modified to equation (2.24).

$$\lambda_s = 0.75\ (m^*)^{-0.3}\ (Fr_m)^{-0.58} \quad (2.23)$$

$$\lambda_s = 0.553\ (m^*)^{-0.3} (Fr_m)^{-0.73} (d_s/D)^{0.1} \quad (2.24)$$

Pan and Wypych (1998) transported four different fly ash samples (ρ_p: 2197 to 2540 kg/m^3; ρ_{bl}: 634 to 955 kg/m^3; d_{50}: 4 to 58 μm) through various test rigs (I.D: 52.5 to 105 mm; L: 70 to 564 m). Combining the data of all four fly ash samples, the following models for solids friction for horizontal straight-pipes and bends were proposed:

$$\lambda_s = 3.2343\ (m^*)^{-0.47}\ (Fr_m)^{-1.56}\ (\rho_m)^{-0.43} \quad (2.25)$$

$$\lambda_{bs} = 0.0097\ (m^*)^{0.57}\ (Fr_{bo})^{0.97}\ (\rho_{bo})^{-0.62} \quad (2.26)$$

Jones and Williams (2003) obtained a model for solids friction (equation 2.27) by applying "back calculation" method using the conveying data of pulverised fuel ash, iron powder, copper ore and flour (ρ_p: 1470 to 5710 kg/m^3; "mean diameter": 42 to 90 μm) through a test pipe (L: 50 m, D: 53 mm, 9 bends).

$$\lambda_s = 83/\{(m^*)^{0.9}\ Fr^2\} \quad (2.27)$$

Williams and Jones (2004) proposed a combined friction factor (λ_e) model (equation 2.28) representing the losses due to both air and solids. They conveyed cement material, having diameter of solid particles as 22 μm, and fluidized bulk density as 930 kg/m^3 through a 50 mm nominal bore pipeline, having length of 176 m with 14 short radius bends. λ_e was suggested to be calculated by using a back calculation method.

$$\Delta P = (m^* \lambda_e) \rho_m V_m^2 L/2D \quad (2.28)$$

$$\lambda_e = K(m^*)^a (Fr_m)^b \quad (2.29)$$

A new approach of has been employed by Datta and Ratnayaka (2003) and Ratnayake (2005) using various products. Five different test rigs were used. Rather considering air and solids friction drop separately (as given by Weber, 1981), they considered the solids-air mixture as a combined entity. The total pressure drop due to solids-air mixture was provided by a combined "pressure drop coefficient" ('K') and the concept of "suspension density", as given by equations (2.30) and (2.31), was introduced. Barite (ρ_s: 4200 kg/m^3; "mean particle size": 12 μm) and cement (ρ_s: 3100 kg/m^3; "mean particle size": 15.5μm) were conveyed. Plots of 'K' versus V_{entry}^2 for both the products and different pipelines were obtained, from where 'K' was supposed to be found out for a given value of V_{entry}.

$$\Delta P = K L \rho_{sus} V_{entry}^2/2D \quad (2.30)$$

Where, V_{entry} is the superficial air/gas velocity at the inlet and ρ_{sus} is the Suspension density given as:

$$\rho_{sus} = (M_s + M_f)/(V_s + V_f) \quad (2.31)$$

Where, M_s is the mass of solids in a control volume and M_f is the mass of air in a control volume. V_s is the volume of solids in a control volume and V_f is the volume of air in a control volume. The equation (2.30) has an assumption that the entry condition of the flow at pipe section represents the flow situation in the entire section.

Williams et al. (2008) attempted to investigate into the flow mechanism of cement meal (fluidized dense-phase conveying) by capturing the flow structure using high speed digital camera. The flow was found to have faster dilute-phase layer flowing in the upper portion of the pipe and a slower dense-phase flow travelling as the lower layer (along the pipe bottom). Jones et al. (2008) conducted Electrical Capacitance Tomography (ECT) study for fly ash (ρ_p: 2450 kg/m^3; ρ_b: 700 kg/m^3; d_{50}: 12 µm). They transported the powders through a 20 m long, 53 mm I.D. pipe in fluidized dense-phase mode. The results of contour plots indicated that the velocity of solids particles increased and the bulk density decreased across the bed height measured from the bottom of pipe. In a recent study, Mallick (2009) examined the accuracy of various existing friction factor models and scale-up procedures by developing models using the "straight-pipe" data of fly ash and ESP dust and by comparing the predicted versus experimental total pipeline pneumatic conveying characteristics for larger and longer pipes. The results (Mallick, 2009) showed that the various existing models and formats for solids friction factors generally provide significant inaccuracy under proper scale-up conditions. Mallick (2009) also provided a "Modified Weber A4" method, by modifying a particle settling velocity in free air term to that in cloud. This approach showed some improvements under limited scale-up validation, but would still require further extensive validation.

Maa et al. (2010) performed numerical study to predict the pressure drop in a pneumatic conveying system and compared it's the results with experimental data. The experiments were conducted on fly ash with 26 m long pipeline and 53 mm internal diameter with the values of solid loading ratio ranging from 20 to 70. A three dimensional gas solid system was modeled in commercial CFD (Computational Fluid Dynamics) software. The simulations used Euler-Euler approach accounting for 4 way coupling. The results of computational model reported to have provided good agreement with the experimental data. The authors found that the pressure gradient increased rapidly with particle size up to 150 mm and showed a decrease in slope of rise with further increase in particle diameter. Pressure gradient was found to increase with an increase in pipe roughness. Total pressure drop across the bends increased with bend radius. The bend pressure gradient increased significantly when the bend radius was increased from 1 to 3 as compared to when the bend radius was further increased from 3 to 6.

Behera et al. (2013a) performed CFD modeling of dense-phase pneumatic conveying of fine powders using commercial CFD software. Particle size distribution was incorporated in the model by using different solid phases of different mean particle diameter. Simulations were performed by using Euler-Euler approach, which accounts for the 4 way coupling for 2 m horizontal pipeline. The pressure drop predicted by the CFD model was within ± 25% in comparison to the experimental data. Solid volume fraction was analyzed for different sections of the pipe showing major portions of solids flow along the bottom of the pipe. Behera et al. (2013b) used one dimensional model including particle size distribution to simulate pneumatic conveying of fine powders through a straight-pipeline. Experimental data was used for the inlet pipe conditions for air and solid mass flow rate to predict pressure drop for different pipeline diameter and lengths.

Guoa et al. (2013) proposed a correlation for solid friction factor based on the extensive experimental data of pulverized coal conveyed in fluidized dense-phase pneumatic conveying mode through horizontal pipes. They also evaluated pressure drop model proposed by Mallick and Wypych (2011) and found its prediction as satisfactory. The solid friction factor model was derived from investigations on bench scale systems at pressure less than 0.4 MPa. They advocated that their model should be applied for the stable flow ranges specified by them. Chen et al. (2014) identified and analyzed the pulsating movement of gas and fly ash mixture by using electrical capacitance tomography method. Pulse produced within the mixture was classified as pulse growth phase and pulse decay phase. Pulse growth phase represented the superficial fluidization and pulse decay represented de-aeration during conveying. It was found that solids mass flow rate had minor influence on pulse structure.

2.3 Minimum transport boundary

Minimum conveying air velocity is one of the key parameters in the pneumatic transport of particulate bulk materials. An unnecessarily high conveying velocity would result in higher energy costs due to an increased pressure drop in the system, solids degradation and pipe erosion that can result in an economically unattractive operation. On the other hand, systems designed with extremely low conveying velocities or extremely high solid flow rates are subject to erratic operation due to solids disposition or they may be completely inoperable because of blocking (Ratnayake, 2005). According to Ratnayake (2005), “A reduction in gas flow rate beyond the good steady state dense-phase region would cause the formation of unsteady dunes, characterized by enhanced pressure fluctuations. A further decrease of gas

flow would cause a build-up of product along the line in the form of deposits. This would result in an inability of the system to attain a consistent steady-state conveying condition (i.e. the pressure signal would continue to gradually increase with time). Keeping gas velocity above the minimum conveying velocity requirement in all horizontal sections of a pipeline ensures no deposition of solids in the system and a continuous, safe and steady transport."

Mills et al. (1982) was one of the first researchers who worked for minimum transport boundary for FDP conveying systems. He conveyed cement through a 81mm I.D. × 95 m test rig and seemed to propose a test rig based criteria. Later, from this conveying data, Mill (2004) presented a plot of initial conveying velocity (V_i) versus solids loading ratio (m^*) to represent the minimum conveying conditions. However, the finding of Mills (2004) on the minimum transport boundary is only based on certain product (cement) data and pipeline geometry and does not include pipeline diameter and length scale-up effects. Mills (2004) defined the dense-phase minimum transport boundary limit as 3 m/s. Similar inferences can be found in Mills (2004a).

Weber (1981) provided correlation for minimum conveying velocity for dilute phase conveying. Model for PMC is provided in equation 2.32 and 2.33. Weber (1981), however, did not clearly indicate whether the models are applicable for both fine and coarse particles.

For $w_{fo} \leq 3$m/s $\quad Fr_i = [(8/3)\, w_{fo} + 7]\, m^{*0.25}\, (d_p/D)^{0.1}$ (2.32)

For $w_{fo} \geq 3$m/s $\quad Fr_i = 15\, m^{*0.25}\, (d_p/D)^{0.1}$ (2.33)

Where, w_{fo} represents the single particle settling (or terminal) velocity in undisturbed fluid and d_p denotes the particle diameter.

Hilgraf (1988) in his investigation identified that the minimum conveying velocity depends on the absolute conveying pressure, the product properties and the pipeline diameter, which was represented as:

$$V_{min} = K\ (D^a/\rho^b) \qquad (2.34)$$

Where, V_{min} represents the minimum conveying air velocity requirement at pipe inlet and K, a and b are defined as material dependent numerical constants that can be found by using minimizing sum of square error method.

Wypych and Reed (1990) used an empirical method to find out the minimum transport velocity in the process of designing stepping pipeline and proposed the following equation for the minimum conveying velocity for a given product by using dimensional analysis method.

$$V_{min} = K\ m^{*a}\ \rho_f^b\ D^c \qquad (2.35)$$

Where, K, a, b and c are the coefficients to be determined by minimizing sum of square error method.

Martinussen (1996**)** used experimental set-up having horizontal pipeline of 53 mm inner diameter and 15 m length. By applying the fluid flow analogy, he developed the following model to determine the minimum conveying velocity, which was given by:

$$(V_{min})^2 = K\ D\ g\ (\rho_{bl}/\rho_f)\ [1 - \mu\ (\rho_f/\rho_{bl})]^3 \qquad (2.36)$$

Where K; geometrical factor = Π/4 at the filling level of D/2.

Ratnayake (2005) conveyed nine different fine materials (barite, cement, alumina etc; all capable of fluidized dense-phase conveying) through five different pipelines up to 130 m in length and 75 mm in diameter. He proposed the following model for minimum conveying velocity determination, as given by:

$$V_{min} = K\, w_{fo}\, (D/d_p)^{0.5}\, (m^*)^a \qquad (2.37)$$

Where, 'K' and 'a' are the material dependent constant that have to be determined using the pilot plant test data.

Mallick and Wypych (2009) examined the accuracy of Mills (2004) work on minimum conveying boundary criteria using the experimental data of twelve different powders conveyed over a wide range of pipe lengths and diameters and found that the representation of minimum V_i as a function of m^* may not be adequate under diameter scale-up conditions and also that the pipe diameter term needs to be incorporated in the minimum conveying boundary criteria. They developed a Froude number based criteria (Fr_i = 6) to represent the minimum transport criteria using different fly ash, ESP dust and cement data conveyed through pipelines of various diameters and length. However, Mallick (2009) and Mallick et al. (2011) indicated that a constant Froude number value to predict the blockage boundary may provide only limited accuracy under a wide range of scale-up conditions.

In addition to the above, few other dimensionless numbers have found (equation 2.38 to 2.42) popularity in recent years in modeling important flow characteristics, such as the flow mode transition criteria. Dense to dilute-phase transition criteria is generally represented by the location of pressure minimum curve (PMC) in the straight-pipe pneumatic conveying characteristics (Klinzing et al., 2010; Yi et al., 1998, Mallick, 2009), which is the lower boundary of dilute-phase or suspension flow. Because of the relatively distinct location of pressure minima for coarser particles compared to fine powders (the change in flow mechanism from dense to dilute-phase is gradual for fine powders, i.e. there is no distinct location of PMC for fine powders), majority of the previous efforts to model PMC were limited to only coarser particles.

Kalman et al. (2005) provided a pickup velocity model (equations 2.38 to 2.40) using a modified Reynolds number (Re_p*) and Archimedes number term by conveying glass, zirconium, alumina, iron, salt sand, talk and ammonium oxide.

For Ar> 16.5	$Re_p^* = 5\ Ar^{(3/7)}$	(2.38)
For 0.45 <Ar< 16.5	$Re_p^* = 16.7$	(2.39)
For Ar< 4.5	$Re_p^* = 21.8\ Ar^{(1/3)}$	(2.40)

Where, Ar represents the Archimedes number and Re_p^* represents the Reynolds number modified by pipe diameter ($Re_p^* = Re_p/(1.4 - 0.8\ e^{-((d/d_{50})/1.5)})$). Re_p^* was provided to incorporate pipe diameter effect, as practically it is expected that the model should be used in cases of diameter scale-up. It is understood that using only Re_p (Reynolds number) would result in larger scatter obtained from different experimental data sets having different pipe

diameters. The use of pipe diameter term in the definition of Re_p* is aimed to reduce the variation coming due to different pipe diameters.

Bansal (2012) provided a new model to represent pressure minimum curve for fine powders. The model was developed for fine fly ash (particle density: 2300 kg/m^3, bulk density: 700 kg/m^3 and d_{50} :30 μm) and white powder (particle density: 1600 kg/m^3, bulk density: 620 kg/m^3 and d_{50}: 55 μm) and is given as:

For Fly ash, $Re_p = 8.027\ Ar^{1.001}$ (2.41)

For White powder, $Re_p = 1.694\ Ar^{1.004}$ (2.42)

It is evident from the above literature review that the majority of the previous attempts have included empirical models. This is possibly due to the complex and highly turbulent nature of the dunes under dense-phase flow conditions where it is extremely difficult to address solids friction using fundamental flow models. However, it must be noted that Knowlton et al. (1986) and Mountziarjs and Jackson (1991) carried out comprehensive work to fundamentally represent the gas-solids flow. Starting with governing equations (mass and momentum equations provided in the following) for the gas and solid phases and suitable incorporating Ergun's equation into the same they provided the following equation for energy loss.

Gas continuity: $\frac{d(\rho'\epsilon)}{dt'} + \nabla.(\rho'\epsilon u') = 0$ (2.43)

Solids continuity: $\frac{d(1-\epsilon)}{dt'} + \nabla.[(1-\epsilon)v')] = 0$ (2.44)

Gas momentum: $$\rho'\epsilon\left[\frac{du'}{dt'} + u'.\nabla u'\right] = \epsilon\nabla.T'_f - \epsilon F' + \epsilon\rho' g' \quad (2.45)$$

Solids momentum:

$$\rho'_s(1-\epsilon)\left[\frac{dv'}{dt'} + v'.\nabla v'\right] = (1-\epsilon)\nabla.T'_f - \epsilon F' + (1-\epsilon)\rho'_s g' - \nabla.T'_s \quad (2.46)$$

Here, ϵ denotes the void fraction and u' and v' are the local average velocities of the gas and the particles, respectively. while ρ' and ρ'_s are the intrinsic densities of the gas and the solid materials. The force F' is the local average force (per unit volume of gas) exerted by the gas on the particles, while T'_f and T'_s are effective stress tensors associated with the gas phase and with contact interactions between the particles, respectively, and g' is the specific gravitational force vector.The term $\nabla.T'_f$ appearing in the solids momentum balance corresponds to the buoyancy force exerted by the fluid on the particles. However, these efforts where for coarse particles flowing through vertical pipe whereas flow understudy in this thesis is of fine powders flowing through horizontal pipes. Therefore, it is prudent to think that there will be certain mechanistic changes compare to that described in Mountziarjs and Jackson (1991) and Knowlton et al. (1986). For example, Ergun's equation is presumably valid for packed bed flow and therefore this may not work well under fluidized state. Preliminary attempts of Bansal (2012) by using Ergun's equation to represent fluidized dense-phase flow of flyash (fine powder) through horizontal straight pipe has provided gross over predictions in the values of pressure drop. In spite of this the author is of the view that fundamental representation of Fluidized dense-phase flow is necessary to provide long term solutions. Therefore, the efforts of Mountziarjs and Jackson (1991) and Knowlton et al. (1986) are worth commending.

CHAPTER 3

Development of Test Facilities and

Experimental Procedures

3.1 Introduction

To carry out meaningful modeling and scale-up validation work on fluidized dense-phase pneumatic conveying, it is important to have an extensive database of different products conveyed through different pipelines (different lengths and pipeline diameters). The conveying characteristics obtained from the testing of products in small test rigs, can be directly used to predict the pressure drop and minimum transport boundaries in larger and/or longer pipelines using suitable scale-up techniques. This facility was not available during the start of the PhD program, so it was decided to develop such a facility. As such large infrastructure development required a significant amount of time, hence initial investigations were carried out with the help of existing data of Wypych et al. (2005) (also shown by Mallick, 2009) where ESP dust and Australian power station fly ash were conveyed through three test rigs at the University of Wollongong, Australia (pipelines A1, A2 and A3, refer to Tables 3.1 and 3.2).

Table 3.1 presents the pipeline details for test rigs (A1, A2 and A3) at the University of Wollongong, Australia and Table 3.2 presents physical properties of powders conveyed through these rigs. Dentailed description of the test set-up can be found in Mallick (2009).

Table 3.1: Pipeline details for test rigs (A1, A2 and A3) at the University of Wollongong, Australia (Mallick, 2009)

Pipeline (Test Rig)	**Blow tank type**	**D (mm)**	**L (m)**	**L_h (m)**	**Lv (m)**	**Number and type of bends**
A1	BD	69	168	161	7	5 × 1m radius 90° bend
A2	BD	105	168	161	7	5× 1m radius 90° bend
A3	BD	69	554	547	7	17× 1m radius 90° bend

Table 3.2: Physical properties of powders conveyed in test rigs A1, A2 and A3

Powder Conveyed	**d_{10} (µm)**	**d_{50} (µm)**	**d_{90} (µm)**	**ρ_s (kg/m3)**	**ρ_{bl} (kg/m3)**	**Pipeline (Laboratory)**
ESP Dust	3	7	25	3637	610	A1, A2 and A3 (University of Wollongong, Australia)
Fly ash	2	30	110	2300	700	A1, A2 and A3 (University of Wollongong, Australia)

3.2 Development of pneumatic conveying test facility at Thapar University

Fluidized dense-phase pneumatic conveying test facility test facility has been developed at Thapar University, India in the first year of the PhD program to meet the following specific needs:

- Conveying powders in fluidized dense-phase mode for a wide range of air and solids flow rates
- Different combinations of pipe diameters
- Pressure measurement at strategic points
- Flow visualization arrangements located at strategic points so that flow mechanism could be studied in greater detail (e.g. change in the nature of the dune flow with change in air and solids flow rates)

The test facility mainly comprises of air compressor, air dryer, air receiver, control valves, blow tank and receiver bin (the blow tank and receiver bin are mounted on load cells to measure the change in weight w.r.t time during the experimentation), pipelines of different configurations, static pressure transducers, air flow meter and data acquisition system. Detailed descriptions of the above mentioned equipment and instrument are given below.

An electric powered rotary screw compressor (suitable for wide range of tests conditions) has been installed as a prime air mover. The technical specification of the air compressor is given below:

- Model: KES 18-7.5
- Operating Pressure: 7 bar

- Maximum / unloading pressure: 7.5 bar
- Free air delivery: 3.37 m^3/min
- Power supply conditions: 415 V/50 Hz, 3 phase
- Main motor rating: 18.5 kW
- Rated speed of main motor: 2940 rpm

A refrigerant type air dryer has been provided in order to get moisture free compressed air for conveying and instrumentation purposes. It works with dew point of +4°C. After the treatment of air in the refrigerant dryer, compressed air is supplied and stored in air receiver.

One blow tank of 0.2 m^3 capacity (water fill volume) and capable of dense-phase conveying has been used. The blow tank can withstand a maximum pressure of 4 bar and was manufactured/supplied by Mcgale Pneumatics Ltd, Nagpur. The air was supplied to the blow tank with the help of an orifice plate installed at its air inlet. Blow tank was equipped with solenoid operated dome type material inlet, outlet and vent valves. Inside the blow tank, there are porous fluidizing membranes at the sloped portion of the side walls to fluidize the conveying material. Six different independent compressed air streams are provided to ensure even fluidization of powders inside the blow tank. Figure 3.2 shows a view of the blow tank together with the receiving tank on top of it. On the top of the blow tank, a receiver bin of 0.7 m^3 capacity was mounted. It was fitted with bag filters having reverse pulse jet type cleaning mechanism. For the measurements of solid mass flow rates, blow tank and receiver bin were supported on shear beam type load-cells.

Figure 3.1: A view of the blow tank together with the receiving tank

Figure 3.2 shows A schematic diagram for the operation distribute and control the compressed air supply from the dryer to conveying line, through the blow tank, which is controlled by

manually operated and pneumatically driven valves. A pressure regulator and flow control valve were installed in compressed air line before the blow tank to set the maximum pressure and to vary the air flow rates over a wide range of air flows (0 to 0.06 kg/s). The main compressed air line is initially divided into two lines. One is for instrumentation purpose and the other is for operating and controlling the blow tank operation. The pressure of instrumentation line is generally maintained at 5 bar, whereas the pressure in the conveying air line was varied using a pressure regulator between 2 to 4 bar according to the conveying requirements. This main conveying line is then passed through a 40 mm N.B., 12~24VDC flange connection vortex air flow meter (Make: N.I.C. Jaipur) and then further divided into 3 different air lines i.e. top air, fluidization air and conveying air line with the help of a 50 mm air header. The valve G3 is functioning as the main air supply switch and an emergency stop valve for the whole air supply to the pneumatic conveying rig. Compressed air is supplied to the pneumatically driven valves and mechanical filter at the receiving tank by branching out from the main air supply line. The pressure of supply air to the blow tank is controlled by a pressure regulating valve, PR 1, which controls air pressure at a set value. PR 2 is used to control the pressure of air to the pneumatically operated control panel. A bank of manually operated valves is used to control the air supply to the different regions of the blow tank to ensure an evenly distributed fluidization of bulk material. During conveying, this arrangement helps to attain different distribution of air in top, fluidization and conveying air. This eventually helps in attaining and maintaining the wide range of different flow conditions in the conveying pipeline. During the experimentations, different conveying air flow rates could be achieved with different combinations of settings of this bank of valves. Valve G3, G4 and G5 are used to supply or cut off the conveying or secondary air to the pipeline, fluidization air and top air to the blow tank. To release the pressure of blow tank after each conveying test,

valve V3, which can be operated from the control panel is used. Here, two pneumatically driven valves, V1 and V2 are placed in between the receiving tank and the blow tank so that the material collected in the receiving tank after each test run can be redirected to the blow tank for the successive test runs.

Legend and Abbreviation	
Symbol	**Name**
G1,G2, G3,G4,G5	Manually operated Air Flow On /Off Valves
GL1, GL2, GL3	Air Flow Control Valves (Globe)
PR1,PR2	Pressure Regulator Valves
BL1,BL2, BL3	Automated Blow off Valves
NR1,NR2, NR3,NR4,NR5	Non Return Valves

Legend and Abbreviation	
Symbol	**Name**
MIV	Manually operated Material Intake Valve
V1	Vent off Valve
V2	Material Intake Valve
V3	Blow Tank Discharge Valve

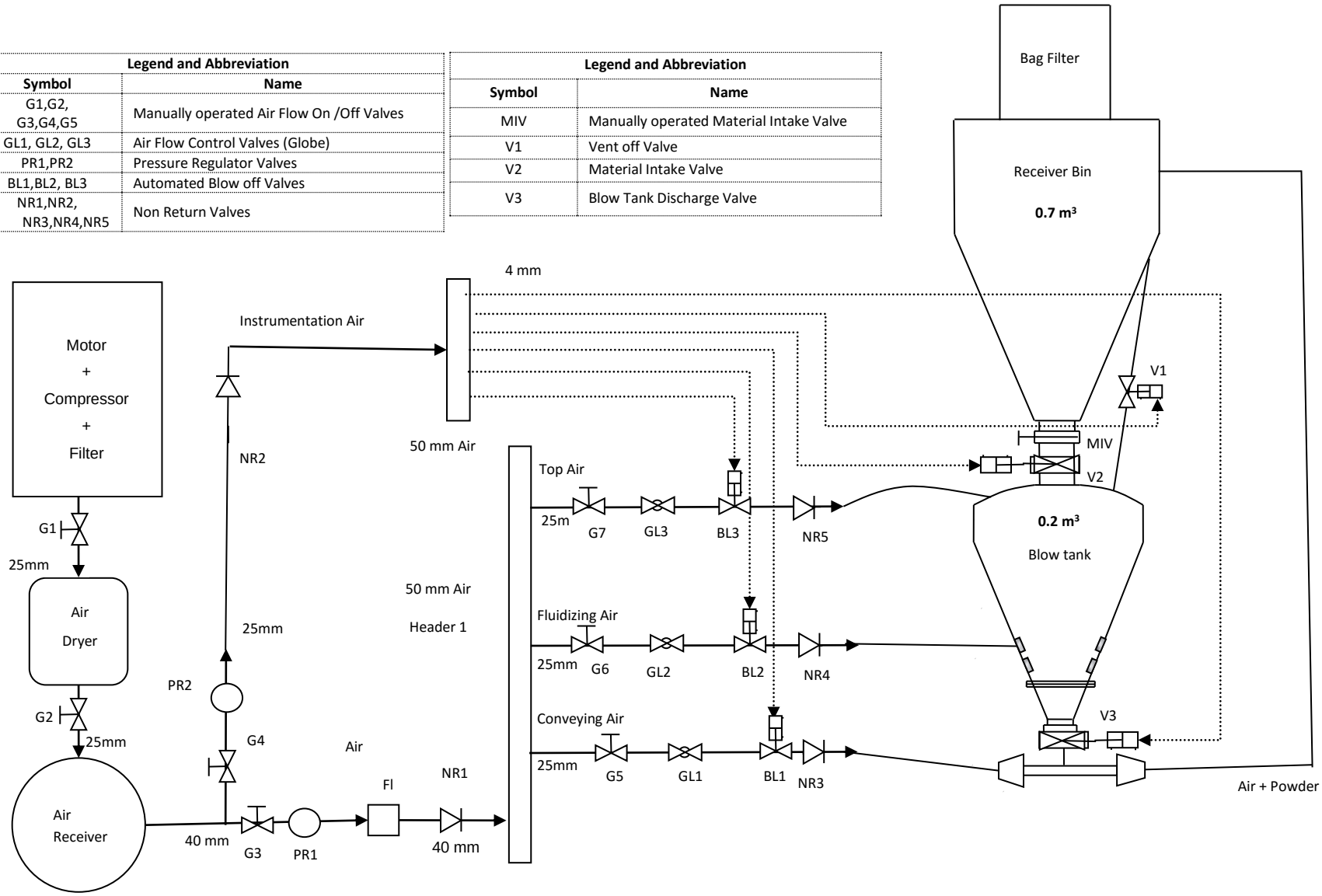

Figure 3.2: Schematic diagram for the operation distribute and control the compressed air supply from the dryer to conveying line, through the blow tank

For the measurement of air flow rates, a vortex air flow meter of 40 NB diameter and of capacity up to 320 m^3/h) was installed in compressed air line. This flow meter had a digital display which showed the reading of volumetric flow rate of air; at the same time it also generated an analog signal, which was fed to the data logger and after further processing of signal, data logger also displayed the volumetric flow rate. Pressure data at the inlet to the flow meter was recorded with the help of pressure transducer to calculate density of inlet air to flow meter, so that its mass flow rate can be obtained. During the pneumatic conveying experimentations, it is required to measure the solids transport rate. The blow tank and the receiving tank (where the solids are being collected after the transportation) both were mounted on four load cells. The technical data of a load cell are given below:

- Manufacturing Company : Rudrra Sensor
- Model : RSL 803
- Nominal load : 500 kg
- Sensitivity (output at nominal load) : 3 mV/V
- Accuracy : ±0.1%
- Nominal range of supply voltage : 0.5-12 V

Four different mild steel pipelines (IS: 1239, heavy grade) of 43 mm I.D. × 24 m length, 54 mm I.D. × 24 m length, 69 mm I.D. × 24 m length and 54 mm I.D. × 70 m length were installed and used as the test pipelines. From this point onwards in this thesis, these pipelines will be referred to as Pipeline B1, B2, B3 and B4. All the pipeline configurations included a vertical lift of 3 m and 4 × 90^0 bends of 1 m radius of curvature. All the pipelines were equipped with three sight-glasses made of toughened borosilicate materials at different

strategic locations for flow visualization (using high speed digital camera). Table 3.3 shows the pipeline details for the test rigs (B1, B2, B3 and B4) at Thapar University, India.

Table 3.3: Pipeline details for test rigs (B1, B2, B3 and B4) at Thapar University, India

Pipeline (Test Rig)	**Blow tank type**	**D (mm)**	**L (m)**	**L_h (m)**	**L_v (m)**	**Number and type of bends**
B1	BD	43	24	21	3	4 × 1m radius 90° bend
B2	BD	54	24	21	3	4 × 1m radius 90° bend
B3	BD	69	24	21	3	4 × 1m radius 90° bend
B4	BD	54	70	67	3	4 × 1m radius 90° bend

Figure 3.3 shows the schematic of a typical pipeline B4, i.e. 54 mm I.D. × 70 m long test rig.

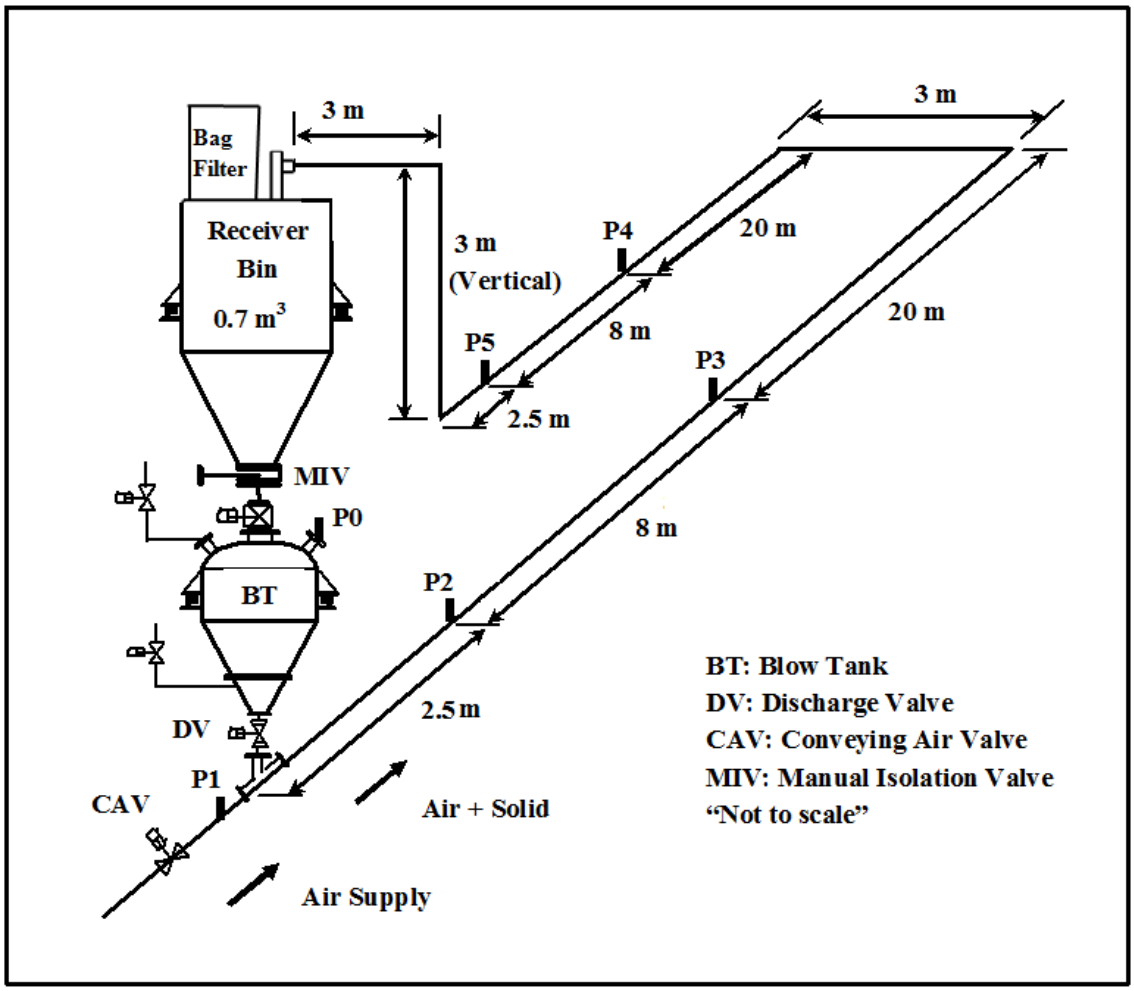

Figure 3.3: Schematic of pipeline B4: 54 mm I.D. × 70 m long test rig at Thapar University, India

Various static pressure measurement points were installed along the pipeline and bends, where P1 was used to measure the total pipeline pressure drop and all other transducers (i.e. P2 to P5) were installed to measure static pressures at the respective points, which were used to model solids friction factor for straight horizontal pipe. The static pressure transducers used were made by Endress & Hauser (Model: Cerabar PMC131), which can be used for pressure range of 0-2 and 0-4 bar. For the operations of the various valves mentioned in Figure 3.2, a

control panel was used. The variations of the pressures at different locations, volume flow rate, mass flow rate can be observed and controlled from the control panels and the computer. To record the electrical output signals from the load cells, pressure transducers and flow meter, a portable PC compatible data logger was used. The data logger had 16 different channels with 14 bit resolution. All recorded measurements from load cells, static pressure points, air flows etc are then converted to usable output (e.g. in MS Excel plots etc) as described in Figure 3.4.

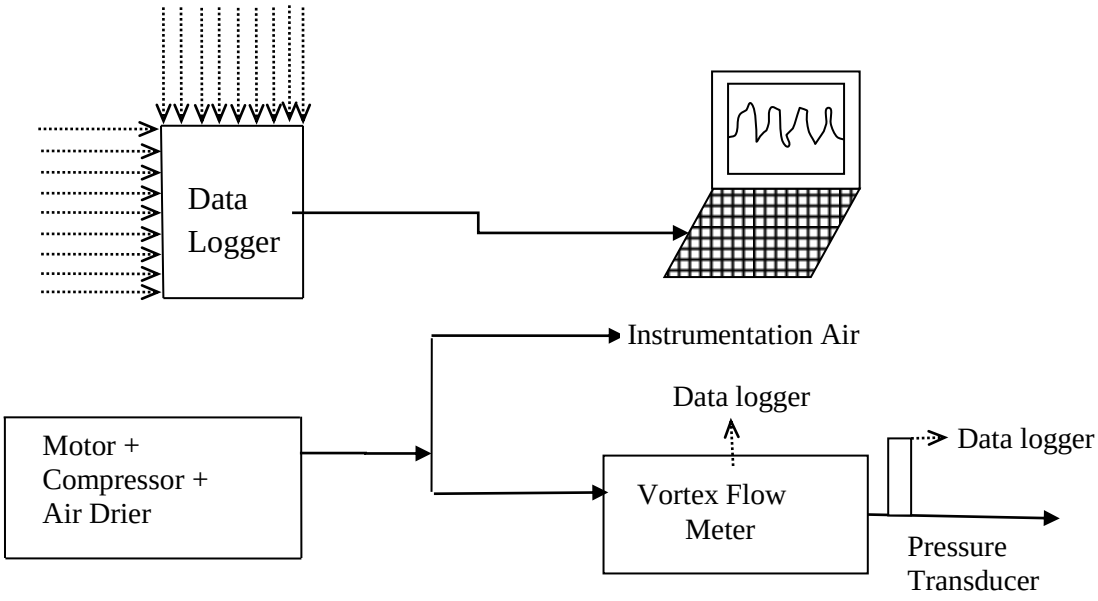

Figure 3.4: Schematic layout of data acquisition system

3.3 Test facility at Fujian Longking Co. , Ltd., China

Test facility of Fujian Longking Co., Ltd., China was also used to generate wide range of experimental data during second year of PhD program by the author for evaluation and validation scale-up design procedures for fluidized dense-phase conveying. Schematic diagrams of the test pipelines used for fly ash and cement conveying at Fujian Longking Co., Ltd., China are shown in Figure 3.5 and 3.6. Rotary screw compressor was used having the maximum delivery pressure of 750 kPa and 660 m^3/hr of capacity (Free Air Delivery). The compressor was fitted with a dryer and air receiver. A 0.75 m^3 capacity bottom-discharge type blow tank was used. A receiver bin of 2 m^3 capacity was installed on top of the blow tank and fitted with bag filters having reverse pulse jet type cleaning mechanism. Mild steel pipelines of different pipeline diameters and lengths (see Table 3.4) were used. The test rigs included a 13.4 m vertical height. All the pipelines had 90^o bends of 1 m radius of curvature. Static pressure measurement points were installed along the pipeline to measure the total pipeline pressure drop (P1) and static pressures along the straight-pipe lengths (P2-P3). The receiver bin and blow tank were supported on shear beam type load cells to provide data for mass flow rates of solids. Air flow rates were obtained using annubars with differential pressure measurements. Flow control valve was used to change the air mass flow rate to achieve dense-to dilute-phase (wide range of air flow). Variation of solids flow rates was achieved through different blow tank pre-pressurization and combinations of different amounts of blow tank aeration and transport air. Calibrations of the pressure transducer, load cells and flow meter were performed using a standardized calibration procedure (Pan, 1992). A portable PC compatible data logger was used to convert and record the electrical output signals from the load cells, pressure transducers and flow meter.

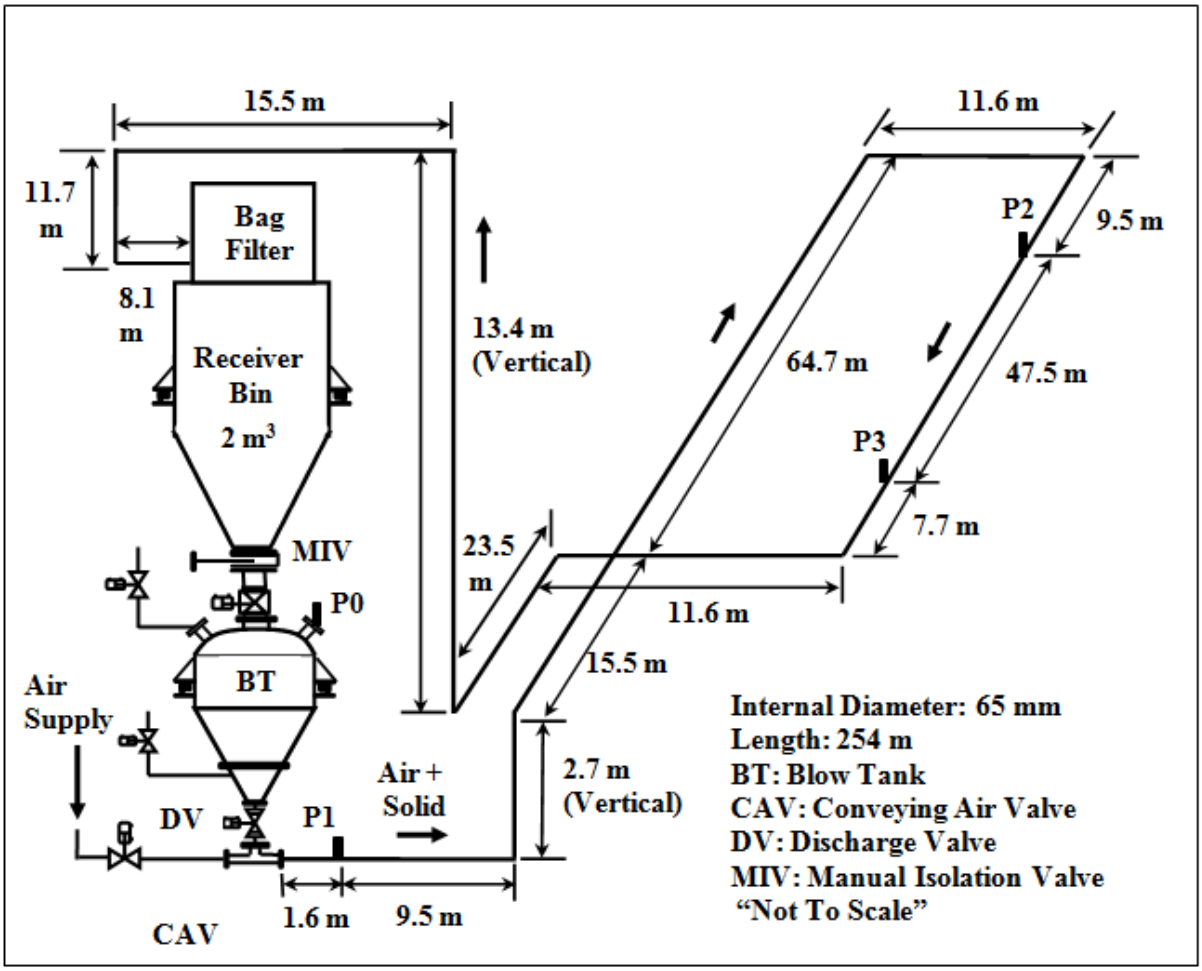

Figure 3.5: Schematic of pipeline C1: 65 mm I.D. × 254 m test rig at Fujian Longking Co., Ltd., China

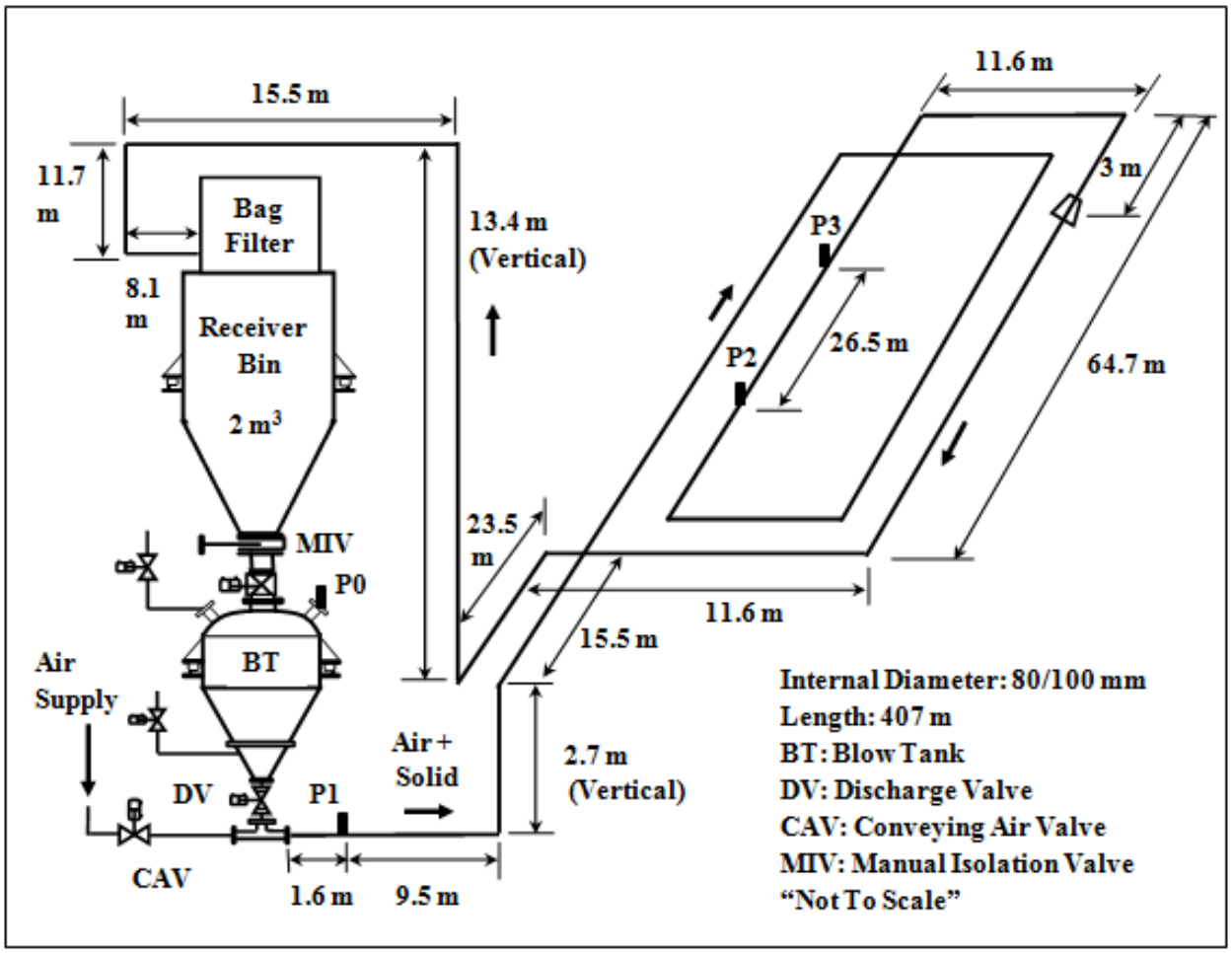

Figure 3.6: Schematic of pipeline C2: 80 and 100 mm I.D. × 407 m stepped pipeline test rig at Fujian Longking Co., Ltd., China

Table 3.4: Pipeline details for test rigs (C1 and C2) at Fujian Longking Co., Ltd., China

Pipeline (Test Rig)	Blow tank type	D (mm)	L (m)	L_h (m)	L_v (m)	Number and type of bends
C1	BD	65	254	238	16	10× 1m radius 90° bend
C2	BD	80/100	407	391	16	14 × 1m radius 90° bend

3.4 Products conveyed and properties

Fly ash from an Indian power plant was tested in Thapar University, India test set-up (Pipelines B1, B2, B3 and B4). Cement and a different sample of fly ash from China were conveyed from fluidized dense- to dilute-phase at the pneumatic conveying test facilities of Fujian Longking Co., Ltd., China (Pipelines C1, C2). These fine powders were conveyed for different solids and air mass flow rates. The physical properties of the products and pipeline lengths are diameters are provided in Table 3.5.

Table 3.5: Physical properties of powders conveyed in test rigs B1, B2, B3, B4, C1 and C2

No.	Powder	d_{10} (μm)	d_{50} (μm)	d_{90} (μm)	ρ_s (kg/m^3)	ρ_{bl} (kg/m^3)	Pipeline (Laboratory)
1	Fly ash	3	19	140	1950	950	B1, B2, B3 and B4 (Thapar University, India)
2	Fly ash	4	22	79	2370	660	C1 and C2 (Fujian Longking Co., Ltd., China)
3	Cement	3	19	75	2910	1080	C1 and C2 (Fujian Longking Co., Ltd., China)

Particle size distribution of all three above mentioned products was determined using a laser diffraction analyzer (Malvern Mastersiser 2000). The particle density was determined using water displacement method, as referred in Wypych (2006).

3.5 Development of test facility for fluidization and de-aeration tests

Besides pneumatic conveying test facility, another test facility for carrying out fluidization and deaeration tests was also developed (during the thesis tenure) at the Laboratory for Particle and Bulk Solid Technologies, Thapar University. A schematic diagram of test facility for fluidization and de-aeration is shown in Figure 3.7.

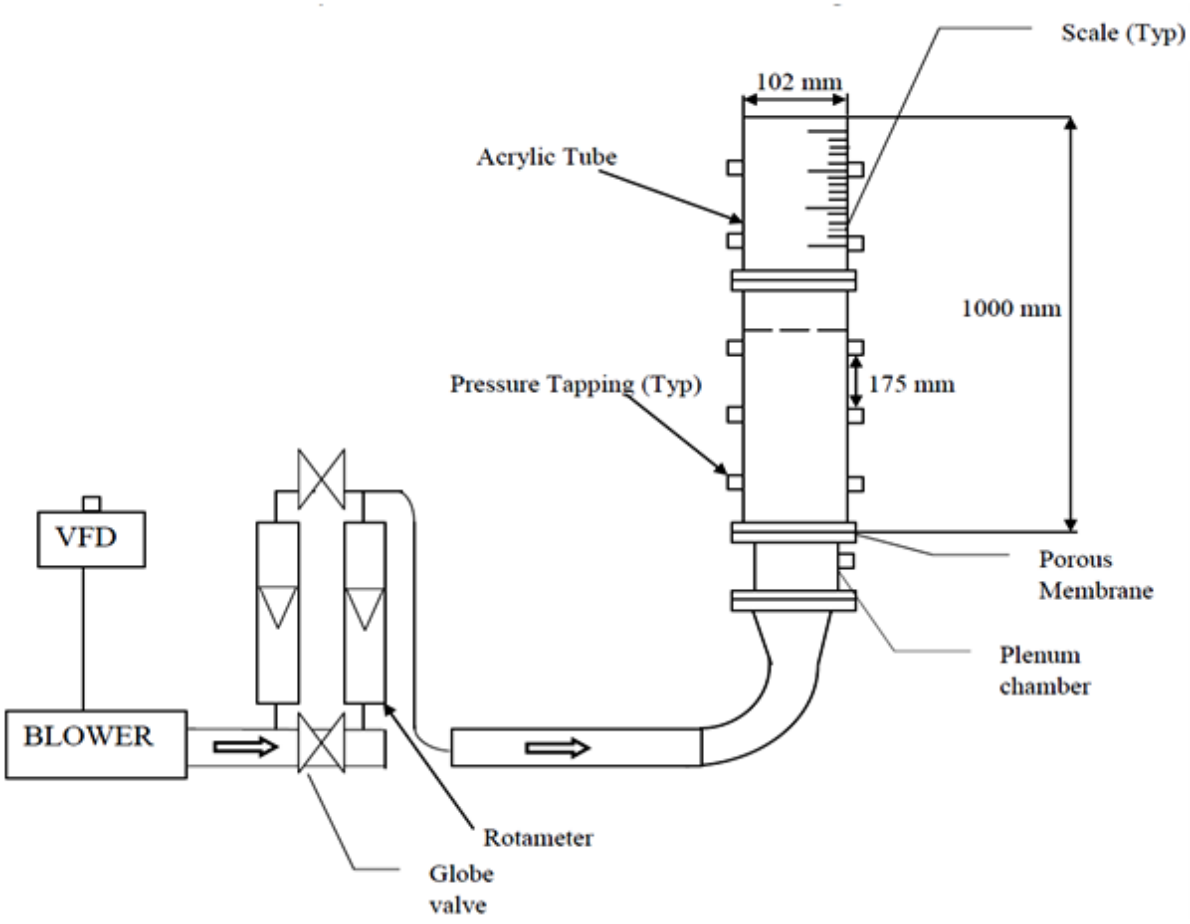

Figure 3.7: Fluidization and de-aeration chamber

Major components of the above set up are as follows:

- Blower with maximum pressure of 160 mbar
- Variable frequency drive (VFD)

- Two rotameters
- Air plenum chamber
- Fluidization column of internal diameter of 1 m
- U-Tube manometers

A side channel centrifugal type blower (1 hp and maximum air delivery capacity of 145 m^3/hr) was used to supply air. A variable frequency drive was attached to the blower to control the air flow rate by changing the frequency, i.e. by controlling the rpm of the blower. Two rotameters were installed (in parallel connection) in the air line to measure the air flow. The regulating valves were installed in the air pipeline to achieve different air flow rates. A mild steel plenum chamber of internal diameter of 102 mm and height of 150 mm was attached to the fluidization column for uniform distribution of air. A porous membrane was placed between the plenum chamber and fluidizing column for supporting the material (powder). Fluidizing column of internal diameter of 102 mm and height of 1 m was attached in vertical position above the plenum chamber as shown in Figure 3.7. The column was made of acrylic tube for clear visibility of the fluidization behavior of powders. Five pressure tappings were installed at equal distances from each other along the height of the column for the measurement of pressure drop across the bed material. The bed height was measured by attaching a centimeter scale on the column. The manometers were used to measure the pressure from each tapping. Figure 3.8 shows the fluidization curve (typical) developed for the fly ash conveyed at Thapar University.

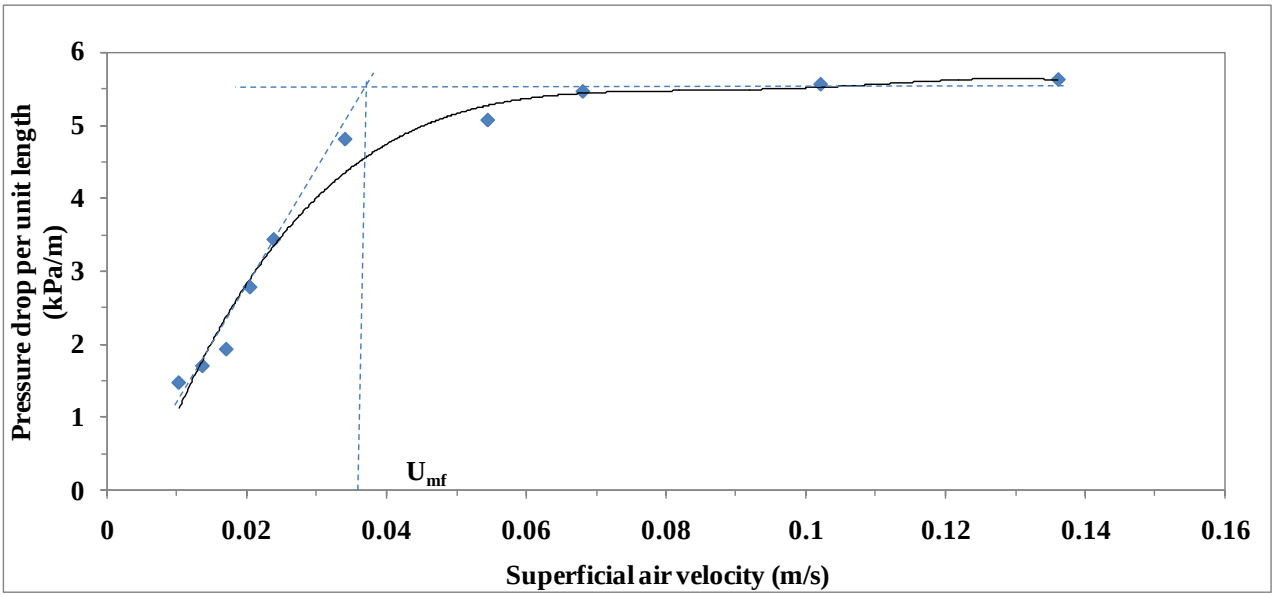

Figure 3.8: Fluidization curve for fly ash conveyed at Thapar University, India

3.6 Calibration of instruments and test procedure

The load cells, pressure transducers and flow meter were calibrated before performing experiments using a standard calibration procedure as described by Pan (1992). The procedure for calibration of static pressure transducer is described below:

(a) The pressure transducers were installed at the desired locations along the pipeline and connected to the data logger.

(b) Conveying pipeline upstream of the receiver bin was closed by using a blind flange.

(c) The pipeline was checked for air leakages and then the globe valve was opened to release the air.

(d) Pressure regulator was set to desired pressure value (e.g. 100 kPa) and then the conveying pipeline valve was opened.

(e) A pressure gauge was used to measure pressure in the pipeline and simultaneously pressure transducer reading was also recorded using the data logger.

(f) Step (e) was repeated by adjusting the pressure regulator to different pressure readings.

The calibration graph for pressure transducer P1 (typical plot) is shown in Figure 3.9.

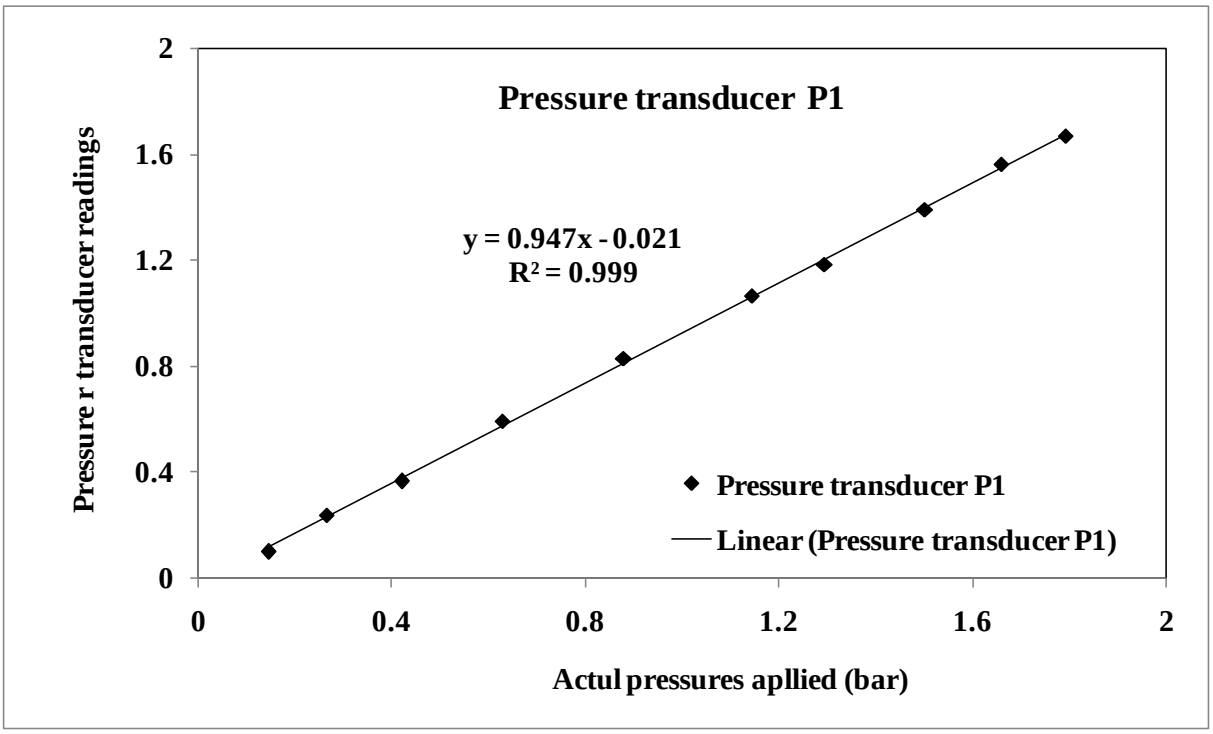

Figure 3.9: Calibration curve for pressure transducer "P1" in Thapar University, India, test set-up

According to the calibration curve, the percentage error is well within the accuracy margin given in pressure transducer specification. To calibrate load cells, known weights were put on the structure and its values were recorded in the data logger. Calibration curve for load cell 2 is given in Figure 3.10.

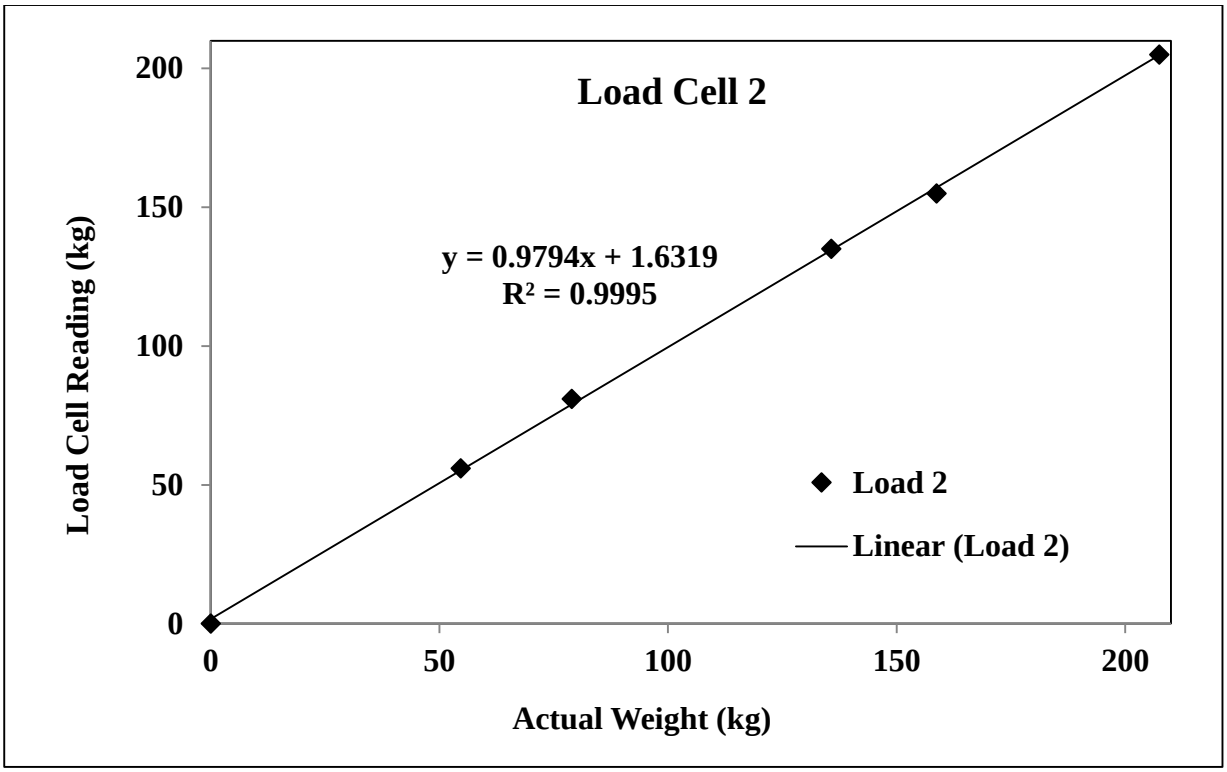

Figure 3.10: Calibration curve for load cell "L2" in Thapar University, India, test set-up

A standard test procedure was used to conduct the experiments over a wide range of air and solid flow rates (Wypych, 1989, Ratnayake, 2005 and Mallick, 2009). In each experiment, data logger recorded the readings of the load cell, flow meter and pressure transducer. All these data points were plotted with respect to time and steady state conditions were identified. One set of such type of signal curves obtained for fly ash conveyed at Thapar University, India is shown in Figure 3.11 Initial conveying trials were conducted with medium ranges of air flows and then the air flow rate was gradually reduced to achieve highly dense-phase flow. The air flow rate was then further reduced till large pressure fluctuations, indicating unstable flow condition and eventually pipeline blockage. Then the air flow was increased to high velocities (dilute-phase) to develop pneumatic conveying characteristics from fluidized dense-to-dilute-phase region.

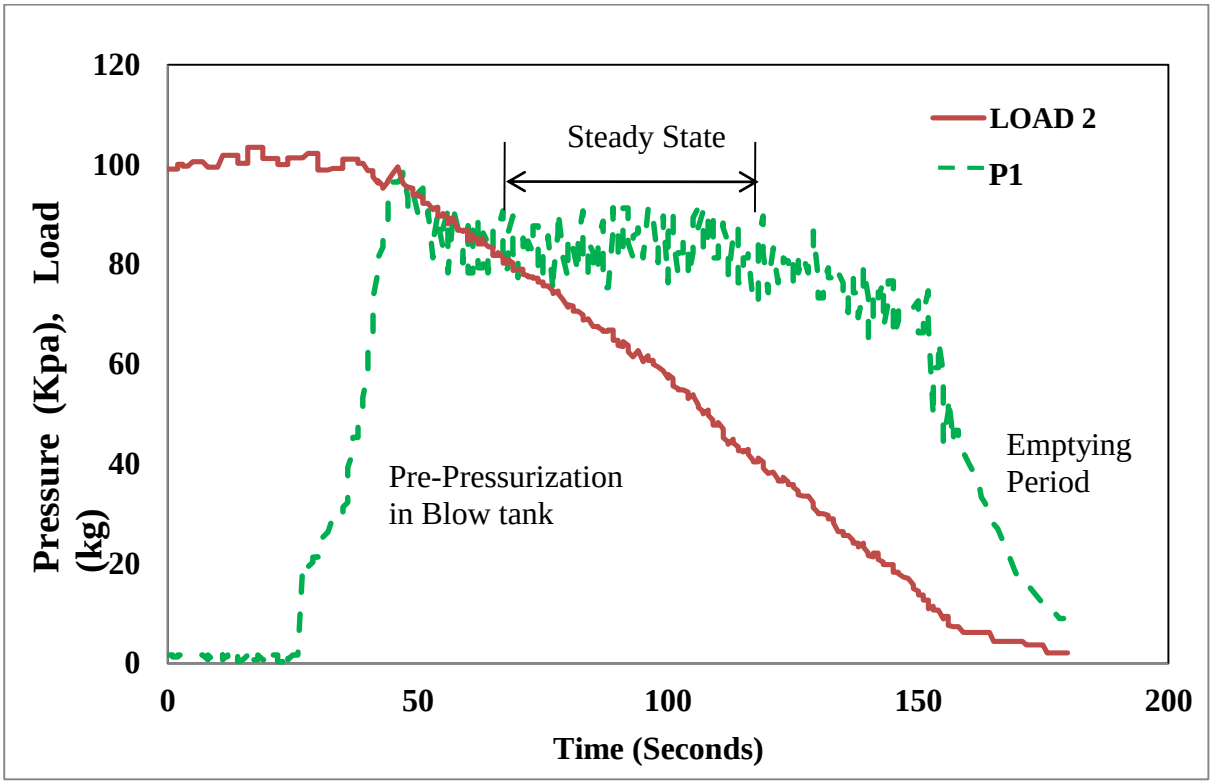

Figure 3.11: Signals for load cells "L2" at blow tank and pressure transducer "P1" obtained during a typical conveying cycle of fly ash conveyed at Thapar University, India.

CHAPTER 4

Development of Pneumatic Conveying Characteristics

4.1 Introduction

In each individual experiment, data logger recorded the load cell, flow meter and pressure transducer readings with time. All these data points were plotted with time and only the steady state portion of the data were taken for further analysis, such as to obtain Pneumatic Conveying Characteristics (PCC), study of reliable transport limits and solids friction. The products were conveyed in all the pipelines over a range of air and solid mass flow rates. An extensive data-base of total pipeline, straight-pipe pressure loss and minimum conveying condition was generated by conveying various powders (Indian power plant fly ash at Thapar University, fly ash and cement at Fujian Longking Co., Ltd.) for a wide range of flow conditions through different pipelines. Total pipeline pressure drop data were obtained from the static pressure tapping point located under the blow tank and straight-pipe pressure drop data were obtained using static pressure tapping points strategically installed along the pipe length. Sufficient numbers of tests were conducted in an attempt to clearly identify the blockage boundary. Some of these tests were repeated to monitor any changes to the product flow over time (product degradation due to repeated testing). To ensure accuracy in the data taken from the pressure transducers, these were checked for calibration during and after the test program. High speed digital movie camera (with sufficient background light) was used to observe the physical nature of the fluidized dense-phase flow, especially the dense- to dilute-phase transition phenomenon with the increase in conveying gas velocity. Continuous dune flow was observed in the conveying pipeline with gradual reduction of air flow, which in turn changed to discontinuous dune flow with the further reductions in air flow rates. Even further decrease in air flow rates resulted in unstable conveying characterized by high pressure fluctuations and lead to complete pipeline blockage. In the unstable conveying zone, the

amount of material discharged by the blow tank into conveying pipeline did not completely return to the receiver bin, which led to the gradual deposition of material in the conveying line. As this gradual deposition of material would result in complete blockage of pipeline in few conveying cycles, hence, it was considered as the initiation of blockage. Blow tank initial pressure was varied to obtain different solid flow rates.

4.2 Pneumatic Conveying Characteristics

Pneumatic Conveying Characteristics (PCC) is an effective way to describe the solid-gas transportation process. PCC provide a quantitative representation of a given product being conveyed through a particular pipe and may be considered as "performance curves" similar to pumps, fans and blowers (i.e. variation of pressure drop for a given air flow rate and operating speed) (Zhang et al., 2015; Klinzing et al., 2010; Mills 2004). If a pneumatic conveying system is to be designed to ensure satisfactory operation and to achieve maximum efficiency, it is necessary to know the conveying characteristics of the material to be handled. The conveying characteristics will provide a designer the minimum conveying velocity requirement and the optimum operating point for the material for a given pipeline diameter and length (Mills, 2004). To form the PCC, the discrete steady state conveying data were obtained from the experiments, plots of pressure drop (Y-axis) versus mass flow rate of conveying air (X-axis) were drawn. In these plots, different constant lines for mass flow rate of solid (m_s) were drawn by using the plotted data points with the help of interpolation technique. This technique has been described in much detail in Mallick (2009). The extensive amount of data obtained from the test program for this thesis were analyzed to develop

pneumatic conveying characteristics for the total and straight-pipe pressure drops, which benefited in:

(a) Determination of experimental dense- to dilute-phase transition condition from the straight-pipe characteristics (and relating the same with flow visualization observations) or identifying pressure minimum zone from the straight-pipe conveying characteristics.

(b) Determination of variation of experimental total pipeline pressure drop with varying condition of air and solid mass flow rates for different products and pipeline diameters.

(c) Determination of experimental minimum transport line, especially the minimum conveying velocity requirement with varying conditions of air and solid mass flow rates for different products and different pipeline diameters and lengths.

(d) Forming the basis of comparison for accuracy in scale-up prediction for solids friction factor (and hence straight-pipe pressure drop) and minimum transport boundary.

4.3.1 Straight-pipe Pneumatic Conveying Characteristics

Using the pressure drop data between tapping points installed on the straight-pipe lengths P2-P3 on the 54 mm I.D. × 70 m long pipeline, pneumatic conveying characteristics for straight-pipe have been developed for different solids and air flow rates for fly ash, which is shown in Figure 4.1. Location for Pressure Minimum Curve, PMC is also indicated using the bold line, also it should be noted that defining the exact location for the PMC is a difficult task to be achieved with precision because of the gradual change in the flow mechanism.

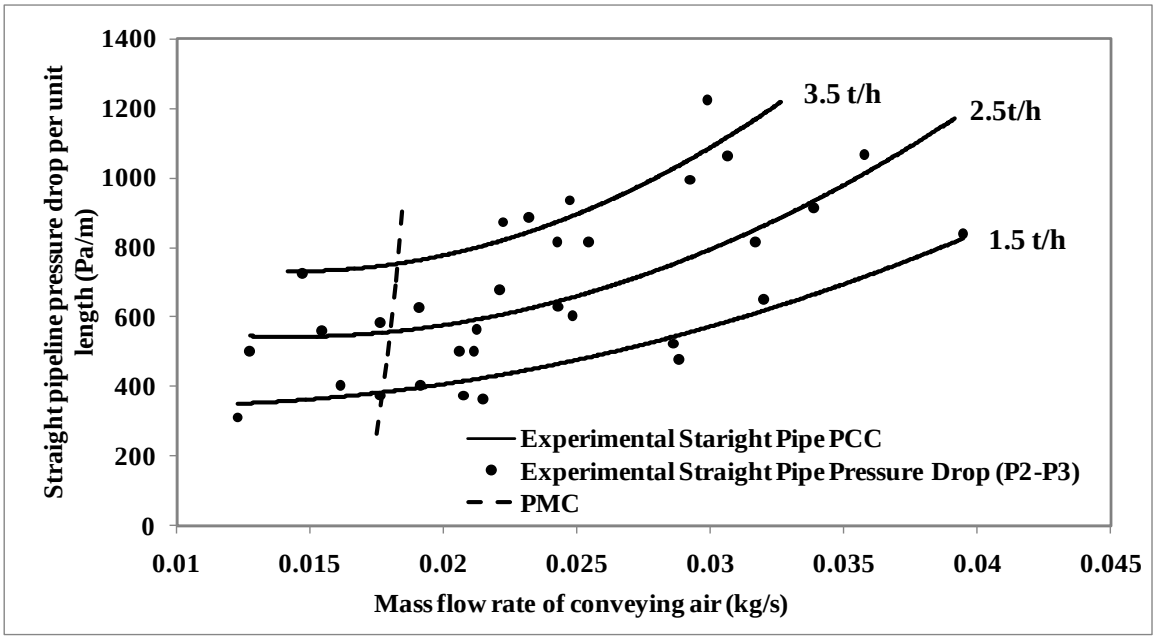

Figure 4.1: Straight-pipe PCC for fly ash, straight section length P2-P3: 8 m, through pipeline B4 (54 mm I.D. × 70 m long pipe)

It can be seen from Figure 4.1 that below the air flow rate of 0.02 kg/s, the pressure drop values almost do not change with an increase in air flow rates. However with further rise in air flow rates, the pressure drop values have increased with an increase in air flow rate, thus indicating a change from non-suspension to suspension mode of flow. Steady state straight-pipe static pressure drop data were obtained from the P2-P3 transducers of both the pipelines of Fujian Longking Co. (pipelines C1 and C2) over a wide range of solids and air flow rates (fluidized dense- to dilute-phase flows) for fly ash and cement. Straight-pipe pneumatic conveying characteristics have been developed using the above data, as given by Figures 4.2 and 4.3 for cement. Figures 4.4 and 4.5 show the same for fly ash. Once again, the bold lines indicate the tentative location of the PMC.

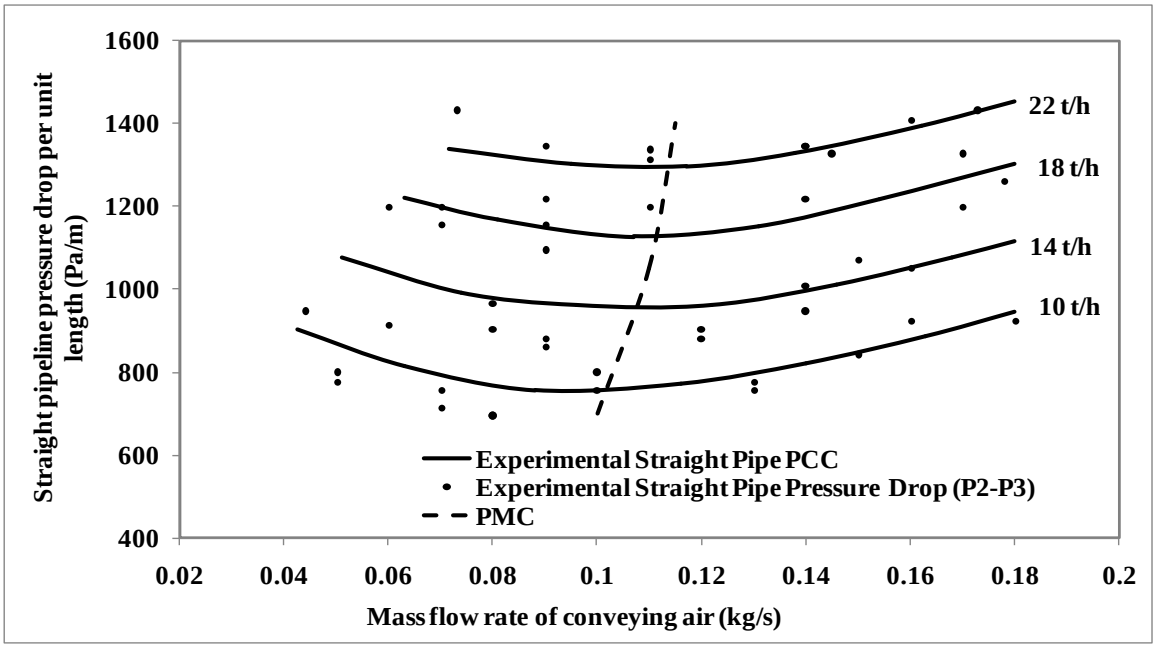

Figure 4.2: Straight-pipe PCC for cement at different solids mass flow rates for straight section length P2-P3: 47.5 m, through pipeline C1 (65 mm I.D. × 254 m long pipe)

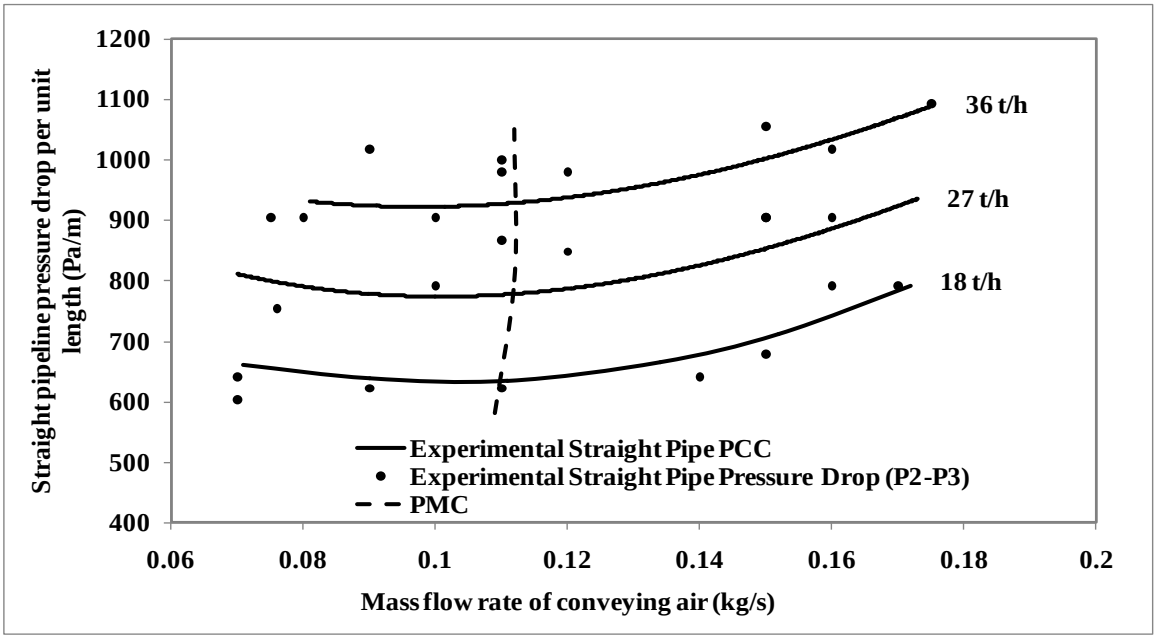

Figure 4.3: Straight-pipe PCC for cement at different solids mass flow rates for straight section length P2-P3: 26.5 m, through pipeline C2 (80/100 mm I.D. × 407 m long pipe)

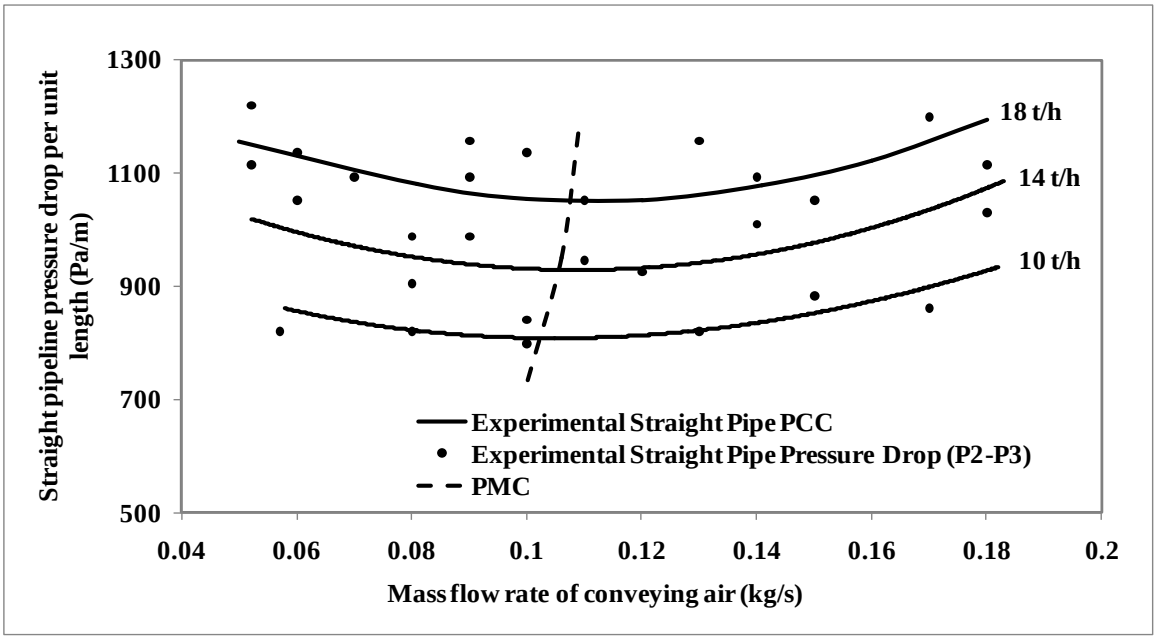

Figure 4.4: Straight-pipe PCC for fly ash at different solids mass flow rates for straight section length P2-P3: 47.5 m, trough pipeline C1 (65 mm I.D. × 254 m long pipe)

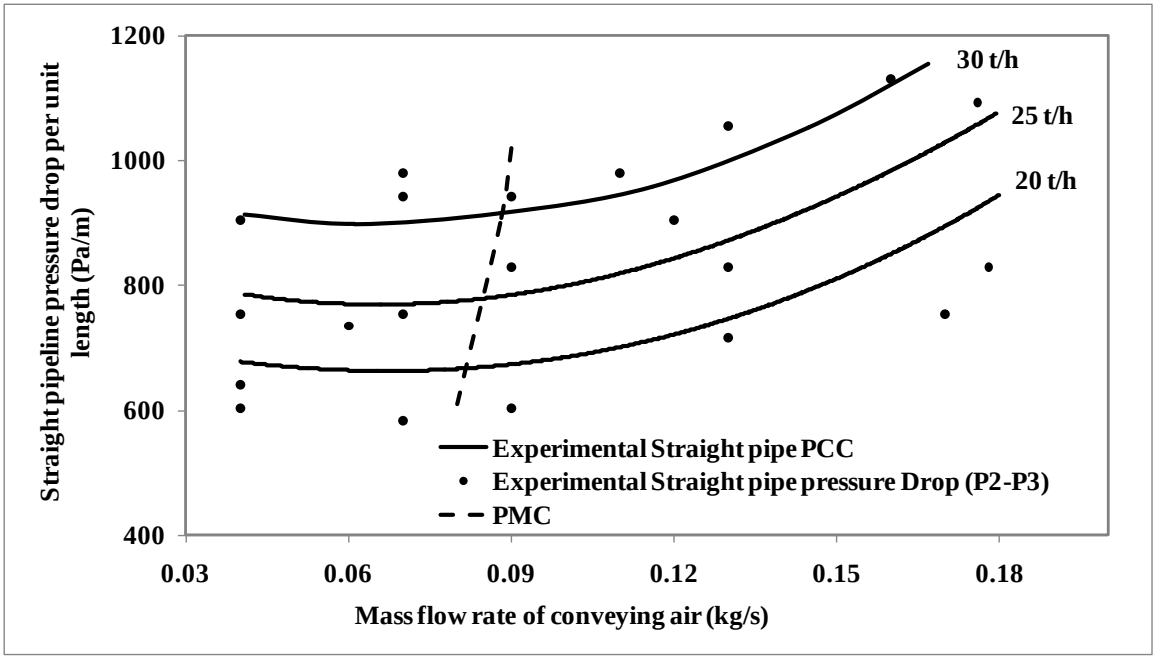

Figure 4.5: Straight-pipe PCC for fly ash at different solids mass flow rates for straight section length P2-P3: 26.5 m, through pipeline C2 (80/100 mm I.D. × 407 m long pipe)

It can be seen that the straight-pipe PCC (Figure 4.2 to 4.5) show some 'U' shaped characteristics (though not very prominent) with a PMC, although the location of the PMC is not very specific. The change in slope through the 'U' shape indicates a change in flow mechanism from fluidized dense to dilute-phase (Mallick, 2009). Absence of a distinct PMC (i.e. no sharp change in slopes of straight-pipe PCC) indicates that the flow mode transition from fluidized dense- to dilute-phase is gradual.

4.3.2 Total-pipe Pneumatic Conveying Characteristics

All the selected test data for total pipeline (P1 for Thapar university, India and Fujian Longking Co. Ltd., China test set-up) for different test materials in different pipeline configurations were plotted in terms of PCC and a line (dot-dash line) corresponding to constant velocity at pipeline inlet (for Minimum Transport Boundary, MTB) was superimposed on them. With each constant velocity line, corresponding inlet constant Froude number (Fr_i) values are also given. Here, the V_i values indicate that conveying is possible for all the mass flow rates of solids having velocities higher than this. These values ensure that conveying is possible for all the mass flow rates of solid within the experimental boundary. Total pipeline PCC for Thapar University test data are shown in Figures 4.6 to 4.9. As these PCC did not provide any PMC, hence lines corresponding to MTB are only shown. Only selected unstable and blockage points have been shown in these Figures.

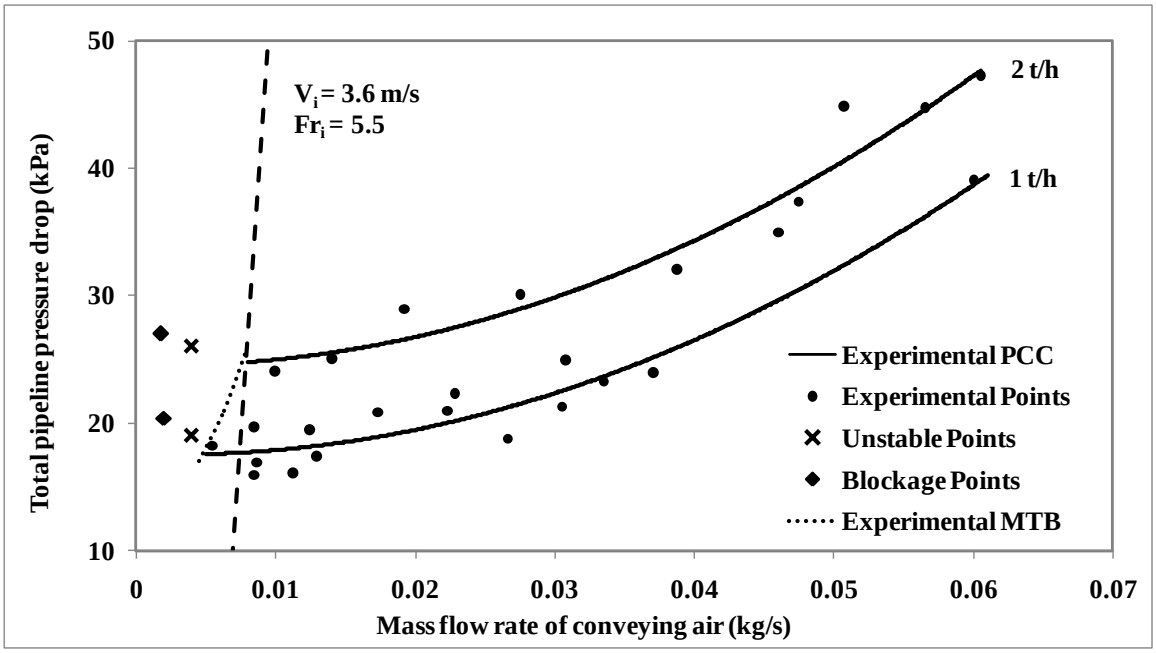

Figure 4.6: PCC for total pipeline pressure loss for fly ash at different solids mass flow rates through pipeline B1 (43 mm I.D. × 24 m long pipe)

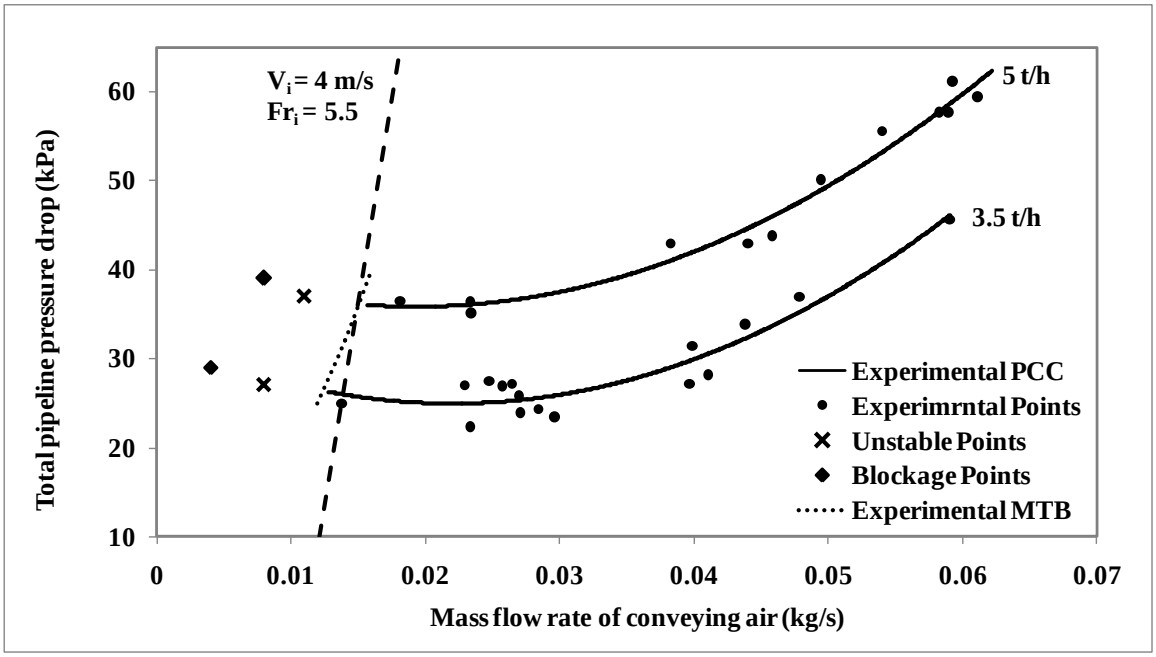

Figure 4.7: PCC for total pipeline pressure loss for fly ash at different solids mass flow rates through pipeline B2 (54 mm I.D. × 24 m long pipe)

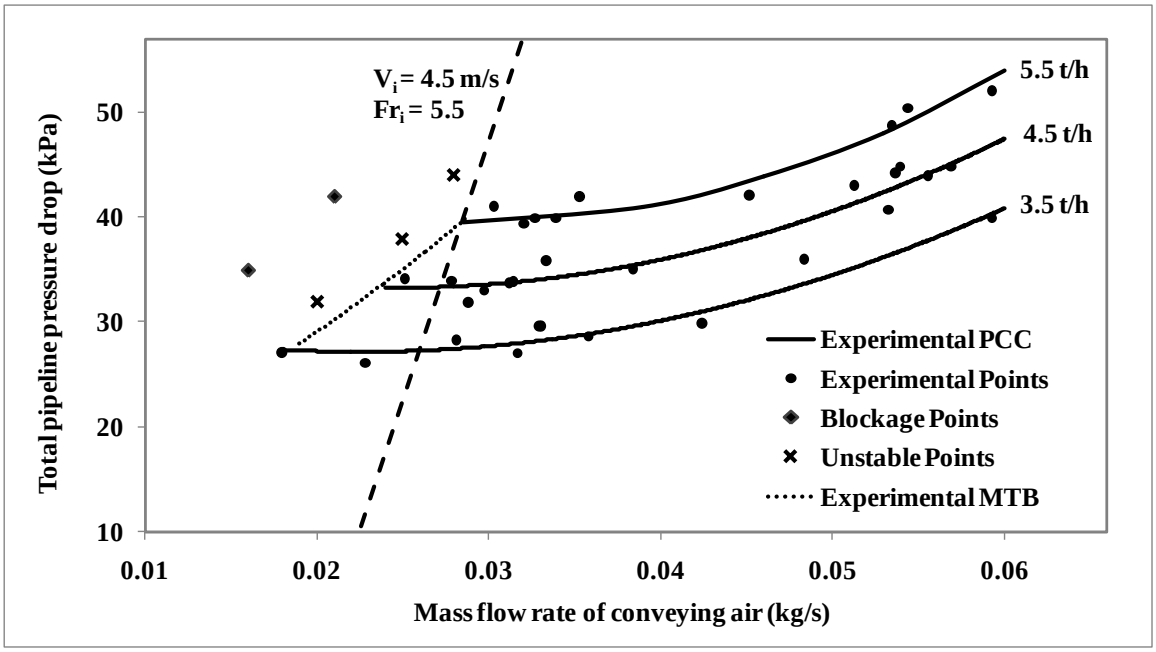

Figure 4.8: PCC for total pipeline pressure loss for fly ash at different solids mass flow rates through pipeline B3 (69 mm I.D. × 24 m long pipe)

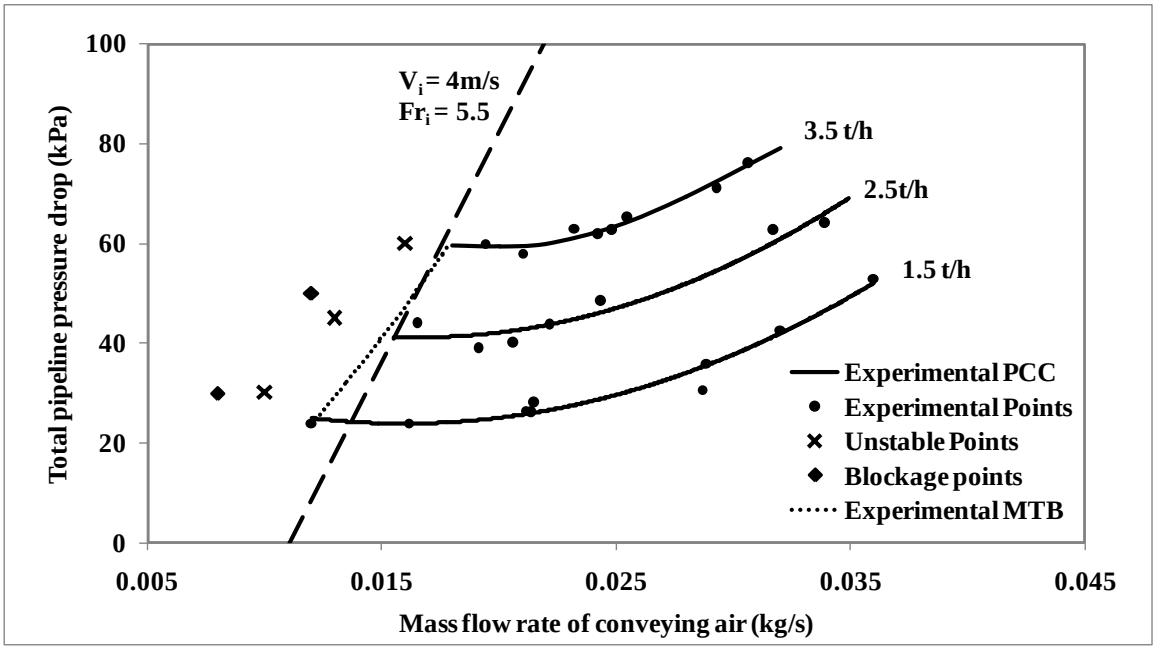

Figure 4.9: PCC for total pipeline pressure loss for fly ash at different solids mass flow rates through pipeline B4 (54 mm I.D. × 70 m long pipe)

Results show that the experimental minimum transport boundary values correspond to Fr_i = 5.5. For all the PCC, the pressure drop values for different solids flow rates increased with an increase in air flow rates (i.e. there was no apparent 'U' shaped trend in none of PCC), although non-suspension due type flow could be observed through sight glass. The reason for this increasing trend of pressure drop lines with an increase in air flow rates could be attributed to the pressure drop characteristics of the bends present in the pipeline. Figures 4.10 to 4.13 show total pipeline PCC based C1 and C2 pipelines for cement and fly ash.

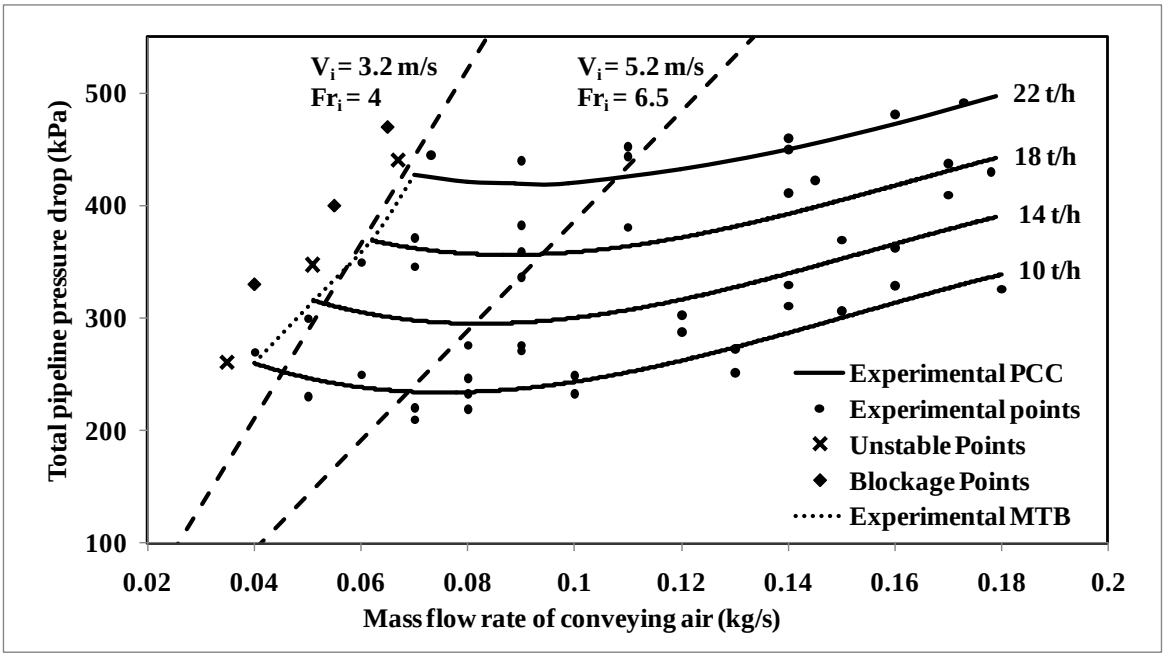

Figure 4.10: PCC for total pipeline pressure loss for cement at different solids mass flow rates through pipeline C1 (65 mm I.D. × 254 m long pipe)

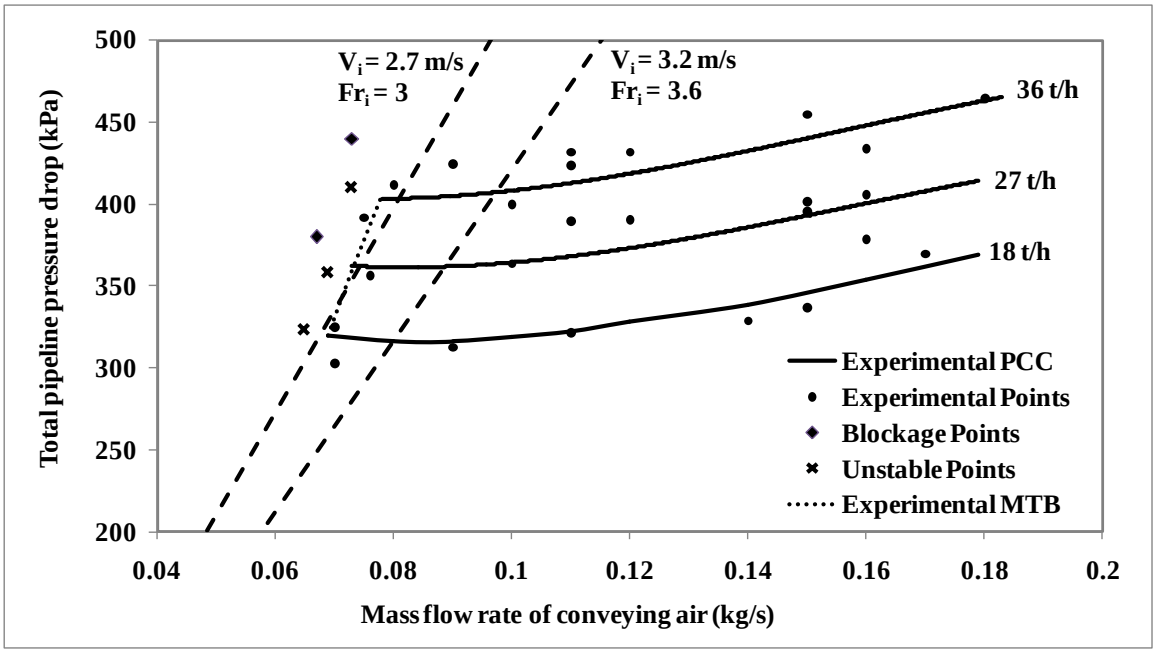

Figure 4.11: PCC for total pipeline pressure loss for cement at different solids mass flow rates through pipeline C2 (80/100 mm I.D. × 407 m long pipe)

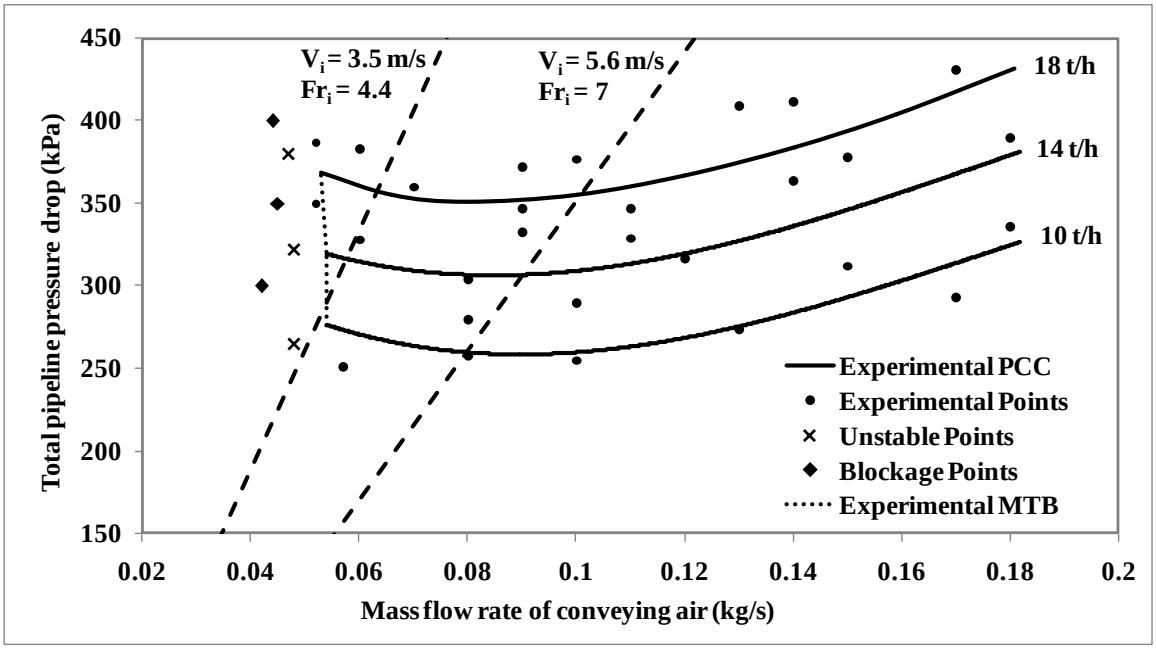

Figure 4.12: PCC for total pipeline pressure loss for fly ash at different solids mass flow rates through pipeline C1 (65 mm I.D. × 254 m long pipe)

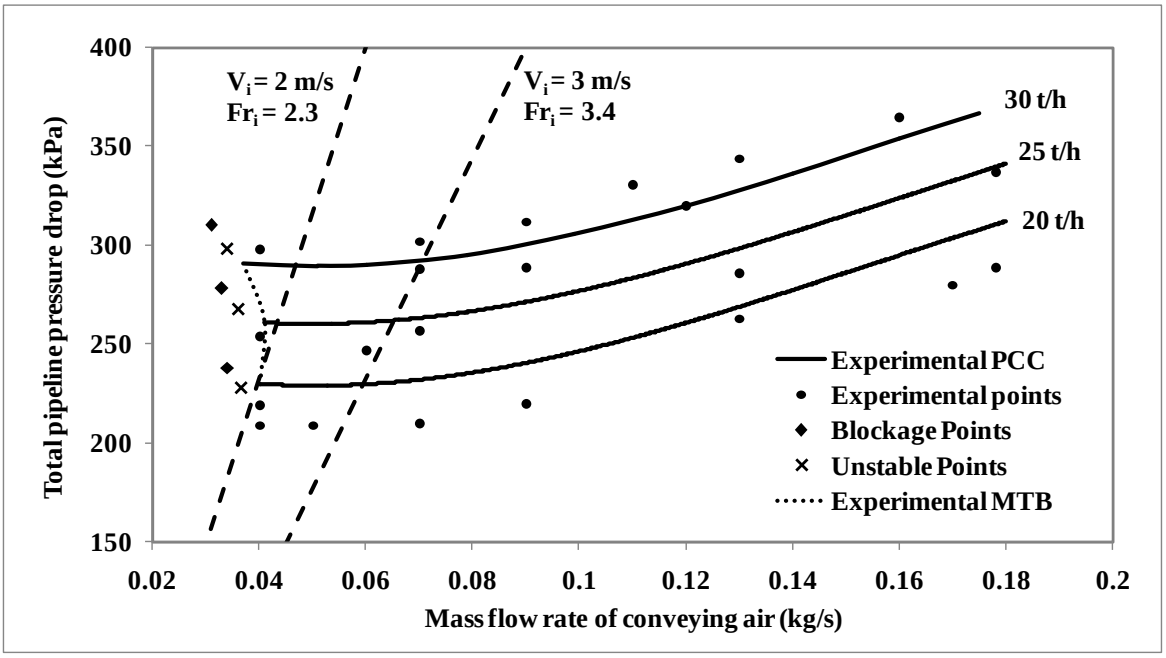

Figure 4.13: PCC for total pipeline pressure loss for fly ash at different solids mass flow rates through pipeline C2 (80/100 mm I.D. × 407 m long pipe)

It was found in Figures 4.10 to 4.13 that the PCC based on 65 mm I.D. × 254 m long pipe, provided more apparent 'U'-shaped trends than that obtained from the longer distance scale-up pipelines (80/100 mm I.D. × 407 m long pipe) for cement and fly ash. Comparing Figures 4.10 to 4.12 and Figures 4.11 to 4.13 (for both the products), it can be recognized that higher mass flow rate of products have resulted in reduced conveying velocity requirement (perhaps due to the self-pushing effect of the product). This aspect has been considered in detail in Chapter 6. Total pipeline PCC of fly ash and ESP dust based on experimental data of Wypych et al. (2005) (also shown by Mallick, 2009) also have been used in this thesis for the purpose of model validation. The values of V_{min} (minimum V_i value corresponding to the blockage condition) with the corresponding Froude numbers (i.e. Fr_{min}) for above PCC are provided in Table 4.1. Ranges of solids loading ratio values (m*) have been also included in Table 4.1.

Table 4.1: Minimum conveying condition and range of solids loading ratio for various products and pipelines (different PCC)

SL No.	Powder	Laboratory	d_{50} (μm)	ρ_s (kg/m^3)	ρ_{bl} (kg/m^3)	D (mm)	L (m)	Pipe tag	V_{min}	F_{min}	$(m^*)_{max}$	$(m^*)_{min}$
1	Fly ash	Thapar University	19	1950	950	43	24	B1	2.3	5.5	52.8	4.6
						54	24	B2	4	5.5	94.3	15.3
						69	24	B3	4.5	5.5	55.4	21.6
						54	70	B4	4	5.5	64.2	11.5
2	Cement	Fujian Longking Co.	19	2910	1080	65	254	C1	3.2	4	86.8	14.5
						80/100	407	C2	2.7	3	129.5	30.4
3	Fly ash	Fujian Longking Co.	22	2370	660	65	254	C1	3.5	4.4	118.8	13.9
						80/100	407	C2	2	2.3	208.7	24.5
4	ESP dust (Mallick, 2009)	University of Wollongong	7	3637	610	69	168	A1	3.3	4	62	12
						105	168	A2	4.1	4	84.2	10.9
						69	554	A3	2.6	3.8	34.2	2.5
5	Fly ash (Mallick, 2009)	University of Wollongong	30	2300	700	69	168	A1	2.6	3.2	133.3	19.8
						105	168	A2	3.6	3.5	121.5	17
						69	554	A3	2.8	3.4	77.1	8.4

CHAPTER 5

Modeling and Scale-up Validation of

Solids Friction Factor

5.1 Introduction

Total pipeline pressure drop mainly consists of losses in horizontal straight sections, verticals and in bends. For pipelines having relatively longer horizontal straight-pipe run (e.g. fly ash conveying pipelines in coal fired power plants that run from buffer hopper and/or electrostatic precipitator hoppers to remote silo), accurate prediction of pressure drop is of paramount importance. Over-estimation of total pipeline pressure drop would result in unnecessarily higher supply of air flow, energy cost and wearing of pipeline due to excessive conveying velocity. Under-prediction of total pipeline pressure drop would cause reduced material throughput rate. The pressure drop for the flow of solids and gas flow through a straight horizontal pipe section can be represented using equation (2.9). This equation was originally presented by Barth (1958) and believed to be for coarse particles in dilute-phase flow. However, various other researchers, such as Stegmaier (1978), Weber (1981), Rizk (1982), Wypych (1989), Pan and Wypych (1992), Pan and Wypych (1998) and Jones and Williams (2003) have subsequently used this equation to predict the pressure loss for the fluidized dense-phase pneumatic transport of powders, such as fly ash, for horizontal straight-pipes.

5.2 Development of new model for solids friction factor

The main task in equation (2.9) is to model the solids friction factor accurately. The solids friction factor term is a combined representation of energy loss due to solids to solids, solids to gas and solids to pipe wall interactions. While more fundamental modeling techniques based on powder mechanics have been developed for dense-phase low-velocity slug-flow of

granular products, the modeling of fluidized dense-phase conveying of fine powders has remained a relatively more difficult problem to solve at a similar depth of detail. Despite the widespread use and popularity of FDP, very little fundamental work has been done in trying to predict the total pipeline pressure drop (Δp_t) for the FDP conveying of powders. The main reasons are (Mallick, 2009): the nature of flow is quite complex (viz. moving turbulent fluidized bed of powder); it is extremely difficult to model the relevant particle and wall interactions and mechanisms; hence, it is very difficult to link the particle/bulk properties and the above interactions/mechanisms to actual conveying parameters or operating conditions. As a result of the above difficulties in modeling, only limited progress has been achieved so far towards fundamentally understanding the flow mechanisms and modeling of solids friction. Because of such difficulties, empirical power function type modeling has been generally preferred over the years by several investigators, such as Rizk (1982), Wypych (1989), Pan (1992), Pan and Wypych(1998), Jones and Williams (2003), Mallick (2009) (provided in Chapter 2), to avoid the need to establish fundamental equations between solids friction factor and the particle and bulk properties of powders. These models have used different dimensionless parameters and have shown only limited success under scale-up evaluation (Mallick, 2009). Hence, there is a requirement to conduct further studies on straight-pipe pressure drop models for solids friction with an aim to provide the industry a more accurate and reliable scale-up procedures for dense-phase pneumatic conveying of fine powders. Many popular methods of modeling solids friction factor (provided in Chapter 2) use dimensionless solids loading ratio and Froude number terms, as provided in equation 5.1.

$$\lambda_s = K\,(m^*)^a\,(Fr)^b \qquad (5.1)$$

These models have used different dimensionless parameters and have shown reliable results when applied to the researchers' own data. However, the physical significance of these dimensionless terms to represent the flow phenomenon of fluidized dense-phase conveying is not entirely clear and it is difficult to justify the use of the Froude number term to model particle-particle/wall interactions for a non-suspension layer (dense-phase flow). Moreover, recent scale-up evaluation by Mallick (2009) has shown that these existing choices of dimensionless terms can provide significant inaccuracy under meaningful scale-up conditions of pipeline length and diameter. Therefore, there is a requirement to develop improved modeling for solids friction factor using parameters that are better representatives of flow mechanism for fluidized dense-phase pneumatic conveying of fine powders.

Froude number, by definition, is the ratio of inertia to gravity force and finds application in estimating the resistance of ship movement due to wave action (Streeter and Benjamin, 1979). Therefore, the Froude number based approaches could be imagined to be valid for dilute-phase (suspension flow) conditions, where the gravity force of the particles are to be overcome by providing sufficient inertia force to keep particles in suspension. Bradley (1990) also raised similar skepticism over the use of Froude number term. Bradley (1990) did not provide any model for solids friction factor for straight-pipes as his work mainly concentrated on investigating the pressure drop caused by bends with a limited focus on modeling pressure loss through straight-pipes. However, Bradley (1990) used superficial air velocity for his bend model. It is considered here that superficial air velocity would be a more direct and appropriate representation of flow condition than Froude number. Solids loading ratio could be thought to be a relatively more suitable term for dilute-phase flow, where the volume fraction of pipe section occupied by the solids is relatively small compared to the gas volume.

However, for dense-phase flows, the solids loading ratio term (which is only a ratio of the mass of solids to mass of air) does not appear to consider important flow situations, such as the amount of pipe volume that is occupied by the solids. In the case of dense-phase flows, a significant amount of pipe cross section is occupied by the volume of solids which cannot be neglected in dense-phase flow. Therefore, the available space for the flow of most of the gas substantially decreases (i.e. the entire pipe section is not available for the main gas flow). This reduction in gas flow path would influence pressure drop of the gas phase. To account for this partial occupancy of pipe volume by the solids, a Volumetric Loading Ratio (VLR) term is proposed here, as defined by equation (5.2).

$$VLR = (m_s/\rho_s)/(m_f/\rho_f) \quad (5.2)$$

Rautiainen et al. (1999) and Behera et al. (2013a) employed solids volume fraction in modeling pneumatic transport. In fact, Rautiainen et al. (1999) mentions that solids volume fraction will influence the slip velocity of particles and clustering, which can be expected to be an important contributor to the pressure drop of solids-gas flows. Also, the occupied volume of solids is expected to influence the available free gas path (the gas has to pass through the tortuous path available between solid particles) and this movement of gas would contribute to the energy drop. Also, the solids and gas will influence to turbulence of each other. Elgobashi (1994) proposed that "one-way coupling" would exist when ε_p is in the range of 10^{-7}. However, the effect of "two-way coupling" will become prominent with increase in ε_p (to about 10^{-5}). Similar conclusions were also drawn in the work of Ahmed and Elgobashi (2000), where they proposed that the change in turbulence energy production rate of the carrier fluid occurs due to the modification of vorticity dynamics. It was stated that regions of

larger turbulence production rate become “sandwiched between counter rotating longitudinal vortex tubes”. Huber and Sommerfield (1998) carried out numerical analysis to study “two-way coupling” in dilute-phase pneumatic conveying. They proposed that at higher particle loading, turbulence of the gas-phase will be considerably altered by the presence of particles (i.e. either enhanced or reduced, depending on the particle size). They stated that higher particle mass flux near the bottom section of pipe would result in a stronger coupling with the gas-phase. Furthermore, it was suggested that small particles would get caught in the eddies and hence, they would have the similar velocities (i.e. not much relative velocities amongst the particles within an eddy). This would reduce the inter-particle collision effect. Due to the above reasons, it was considered prudent to assume that volume of pipe occupied by the particle (which could influence on the flow path and turbulence of gas-phase) should not be ignored. Hence, volumetric loading ratio has been used to model solids friction factor in the present study. Using volumetric loading ratio (VLR) and superficial air velocity as replacements of solids loading ratio and Froude number, respectively, the following new format (equation 5.3) is obtained for solids friction factor.

$$\lambda_s = K\ (VLR)^a\ (V)^b \qquad (5.3)$$

Subsequently it was thought that instead of superficial air velocity, use of a dimensionless term would be more appropriate which can better address the physical flow phenomenon. Therefore, a dimensionless term w_{f0}/V (ratio of free settling velocity to superficial air velocity) has been introduced in the model of solids friction factor, which attempts to represent whether the flow mode is non-suspension or suspension. Here, w_{f0} is free settling velocity of solid particles. Particles with larger size and/or higher particle density will have

higher free settling velocity and hence, are expected to require higher conveying velocity to keep them in motion. Thus, the following format for solids friction factor has been developed by incorporating the new dimensionless number (by replacing only 'V'):

$$\lambda_s = K\,(VLR)^a\,(w_{fo}/V)^b \qquad (5.4)$$

Using the straight-pipe data obtained from the P2-P3 tapping points of the 65 mm I.D x 254 m long pipe (conveying of cement and fly ash in the test pipes of Fujian Longking Co., Ltd.), models for solids friction factor were first developed in the existing modeling format (equation 5.3) and are included in Table 5.1 as Model 1 and Model 2. Similarly, models were generated using the existing modeling format for the fly ash and ESP dust of University of Wollongong, Australia. These are also provided in the Table 5.1 as Model 3 and Model 4 respectively. The purpose of first developing model in the existing format is to compare the possible improvements achieved with the new format (Table 5.1) under scale-up validation (i.e. model equation format 5.3 versus 5.4). Using the same set of straight-pipe data of cement and fly ash (tested at the laboratory of Fujian Longking Co., Ltd.), models for solids friction factor have been developed in the new format (equation 5.4), also given by Table 5.1 as Model 5 and model 6 respectively. Also, models were generated using the new format (equation 5.4), from the steady state straight-pipe static pressure drop data for the ESP dust and fly ash of University of Wollongong, Australia. These are provided in the Table 5.1 as Model 7 and Model 8, respectively.

Table 5.1: Models developed using existing and new model format

Product conveyed	**Pipeline**	**Straight-pipe section**	**Models developed**	R^2	**Model No.**
Models using existing model format (as per format given by equation 5.3)					
Cement	Pipeline C1	P2–P3, 47.5 m	$\lambda_s = 9.93(m^*)^{-0.63}(Fr)^{-1.81}$	0.98	Model 1
Fly ash	Pipeline C1	P2–P3, 47.5 m	$\lambda_s = 56.73(m^*)^{-0.91}(Fr)^{-2.12}$	0.99	Model 2
ESP dust	Pipeline A3	P9–P10, 26.91 m	$\lambda_s = 7.14(m^*)^{-0.498}(Fr)^{-2.01}$	0.98	Model 3
Fly ash	Pipeline A1	P11–P12, 40.41 m	$\lambda_s = 1.7(m^*)^{-0.34}(Fr)^{-1.63}$	0.99	Model 4
Models using new model format (as per format given by equation 5.4)					
Cement	Pipeline C1	P2–P3, 47.5 m	$\lambda_s = 11.02(VLR)^{-0.37}(w_{fo}/V)^{1.44}$	0.97	Model 5
Fly ash	Pipeline C1	P2–P3, 47.5 m	$\lambda_s = 14.50(VLR)^{-0.54}(w_{fo}/V)^{1.59}$	0.98	Model 6
ESP dust	Pipeline A3	P9–P10, 26.91 m	$\lambda_s = 2961(VLR)^{-0.21}(w_{fo}/V)^{1.73}$	0.97	Model 7
Fly ash	Pipeline A1	P11–P12, 40.41 m	$\lambda_s = 7.94(VLR)^{-0.26}(w_{fo}/V)^{1.51}$	0.98	Model 8

Figures 5.1 and 5.2 show the power function fit of models (Models 5 and 6) through the experimental data points. The high values of R^2 indicate good fit.

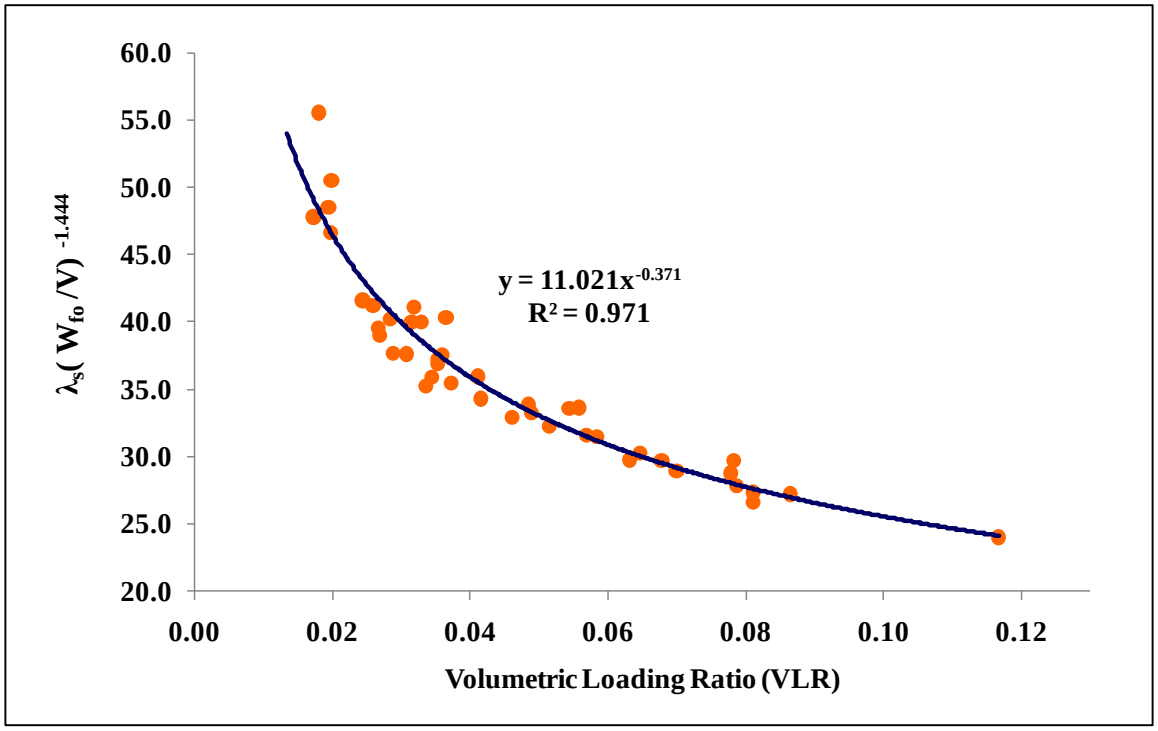

Figure 5.1: Model development using new model format for cement (Model 5)

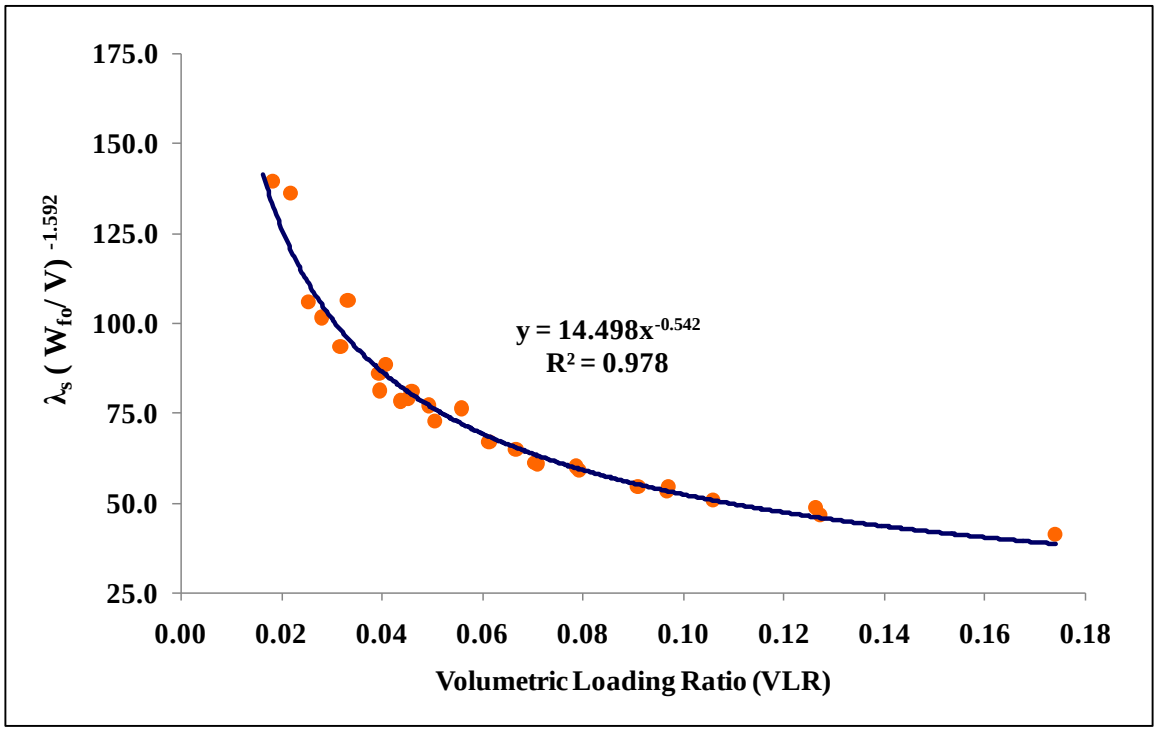

Figure 5.2: Model development using new model format for fly ash (Model 6)

5.3 Scale-up validation of models

In this section, solids friction factor models developed using the steady state conveying data for cement and fly ash, Models 3 and 4, respectively (obtained using tapping point data 47.5 m distance apart) have been evaluated for their accuracy and stability by using them to predict the total pipeline drop for the longer and larger pipelines (65 mm I.D. × 294 m and 80/100 mm I.D. × 407 m, thus for length and diameter scale-up conditions) for different solids and air mass flow rates and by comparing the predicted pneumatic conveying characteristics against the experimental plots. Model predictions using the existing format (Models 1 and 2) have been superimposed on the above predicted pneumatic conveying characteristics to demonstrate the possible improvement of pressure drop prediction capability of the new modeling format. The results are provided in Figures 5.3 to 5.6. Chambers and Marcus (1986) model was used to determine the losses in bends, as given by equation 5.

$$\Delta P_b = (N\ B\ (1+m^*)\ \rho\ V^2) / 2 \qquad (5.5)$$

Where, ΔP_b represents the pressure drop through a bend.

Pressure drops due to initial acceleration and verticals were calculated as per Klinzing et al. (2010). These losses are significantly less than the total straight-pipe losses in all pipes due to the rather short vertical length. An iterative solution based program using SOLVER and MACRO in Microsoft Excel 2007 has been developed to calculate total pipeline pressure drop. The flow diagram of the program is shown in Figure A 1.2 of Appendix indicating the input and output parameters, condition of convergence and equations used. The program starts

from a known condition, which generally prevails at the discharge or exist point of the pipeline (e,g. corresponding to the atmospheric condition). The entire pipeline is then divided into smaller sections of pipes by separately considering horizontal, vertical lengths and each bend. All such different sections or components were then linked using MACRO in MS EXEL. Knowing the exit condition of the pipeline, a pressure drop value through the first horizontal pipe section (starting from the exit) is initial assumed. This assumed pressure drop is then added to the exit pressure of the section to calculate the inlet condition (for the pipe section). From this, flow parameters (such as air density, superficial gas and dimensionless velocity, Froude number, VLR etc) corresponding to the mean condition across the section is calculated. Using these mean values, solids friction factor and pressure drop for horizontal section are calculated using equation (2.9) and the models given Table 5.1. This calculated pressure drop value is then compared with the initially assumed pressure drop value. Using the SOLVER function in MS EXCEL, an iterative criteria is set up in the program that the difference between the assumed and calculated values of pressure drops must converge to zero. When a solution for the first section is reached (i.e. pressure drop for first horizontal straight pipe section from the exit of the pipeline is calculated), the pressure at the inlet of the section is calculated by the program, which corresponds to the outlet pressure for the next pipe section. Subsequently, the MACRO programming shifts the program operation from the first section to the next (second) section and so on and terminates at the bottom of the blow tank. This method is based on a component approach and each of the horizontal straight sections, bends and verticals are separately considered by the program (i.e. losses due to the straight horizontal pipe, bends, verticals and initial acceleration are individually calculated for each section). It was found that convergence was achieved with the difference of assumed and

calculated values of pressure drop in all cases are in the range of 10^{-4} to 10^{-5} (which is almost zero). Such iterative solution methods have been also provided in [10, 20 and 21].

Figure 5.3 shows the results of scale-up evaluations for Model 1 and Model 5 using the conveying data of cement through the pipeline C1 (65 mm I.D. × 254 m long pipe).

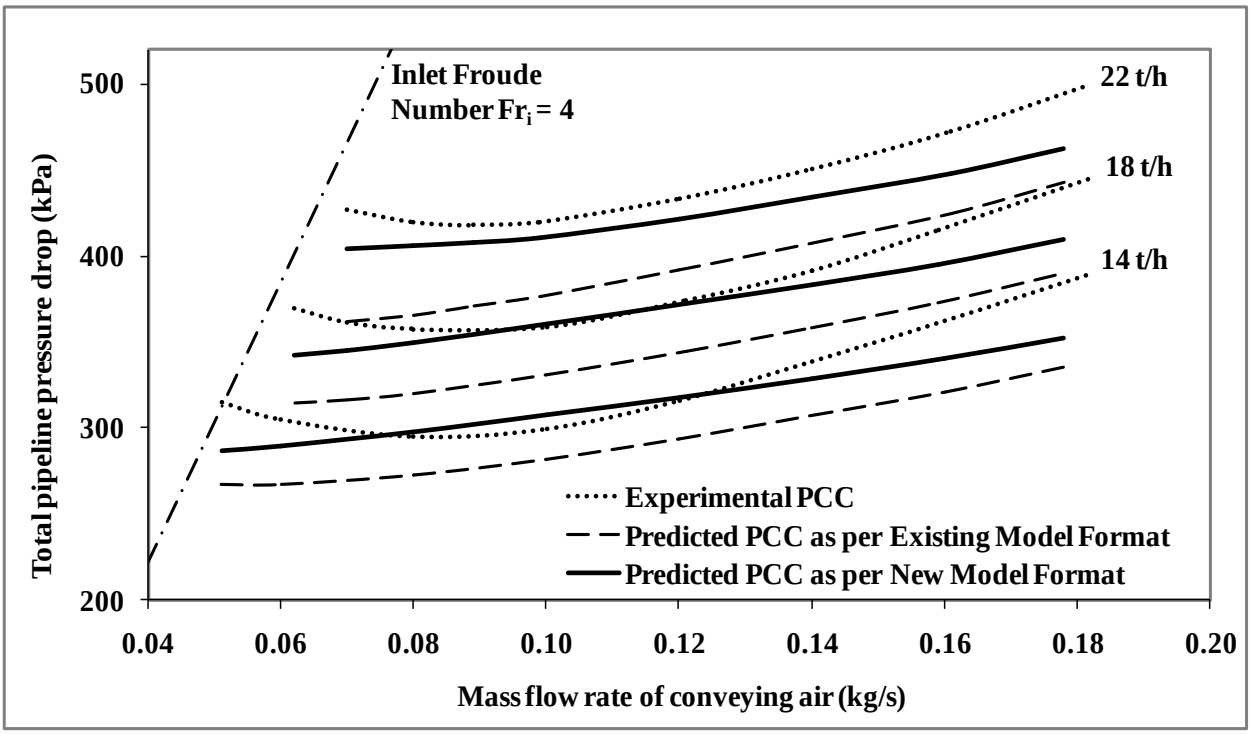

Figure 5.3: Experimental versus predicted PCC using Model 1 and Model 5 for cement through pipeline C1 (65 mm I.D. × 254 m long pipe)

In the above figure (Figure 5.3), for all the series of predicted PCC, the top lines represent m_s = 22 t/h, middle lines represent m_s = 18 t/h and bottom lines represent m_s = 14 t/h. Results show that the existing model provides under-predictions for all the solids flow rates in case of length scale-up. The new model provides better predictions in the range of air flows from about 0.09 to 0.14 kg/s. The model produces under-predictions beyond this air flow range on

either side, i.e. the new model has predicted well in the linear portion of the experimental plots. However, the new model has not been able to follow the rise in slope of the experimental PCC in the very dense-phase zone. Possible reason for this could be that the volumetric loading ratio term assuming a uniform distribution of solids across pipe cross section. However, in true non-suspension flow, more particle concentration is visible towards the bottom of the pipe. Figure 5.4 shows the results of scale-up evaluations for the same models (Model 1 and Model 5) using the conveying data of cement through the pipeline C2 (80/100 mm I.D. × 407 m long step-up pipe).

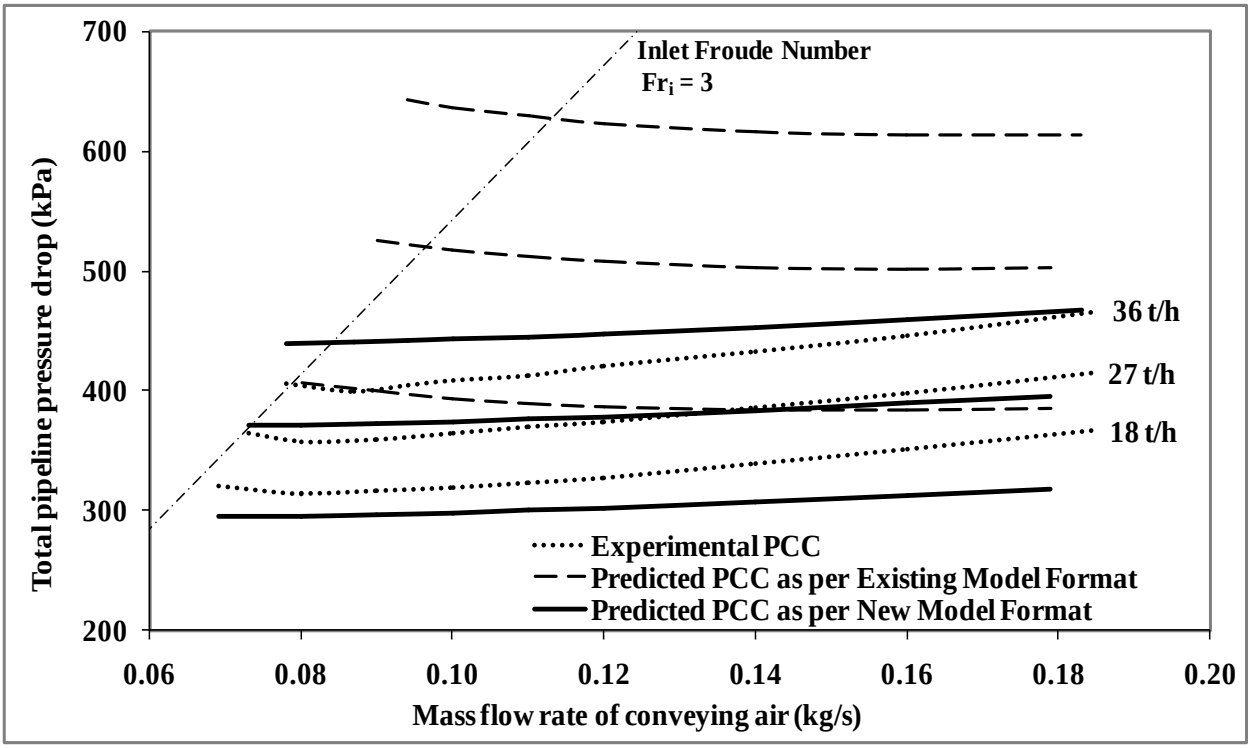

Figure 5.4: Experimental versus predicted PCC using Model 1 and Model 5 for cement through pipeline C2 (80/100 mm I.D. × 407 m long pipe)

In the above figure, for all the series of predicted PCC, the top lines represent m_s = 36 t/h, middle lines represent m_s = 27 t/h and bottom lines represent m_s = 18 t/h.

The results show that the existing models provide gross over-predictions for all the solids flow rates. Also, the existing model produces continuously decreasing trends of predicted pressure drops with an increase in air flow rate, whereas the trends of the experimental PCC are the opposite. It is evident that the existing model becomes significantly unreliable under proper diameter and length scale-up conditions. The new model produced relatively better predictions, with slight over-predictions for 36 t/h and slight under-prediction for 18 t/h line in the low velocity region. The trends of predicted PCC using the new format show mild increase in predicted pressure drop with increase in air flow rate (however, the slope is less prominent compared to the experimental PCC). Figure 5.5 shows the results of scale-up evaluations for Model 2 and Model 6 using the conveying data of fly ash through the 65 mm I.D. × 254 m long pipe.

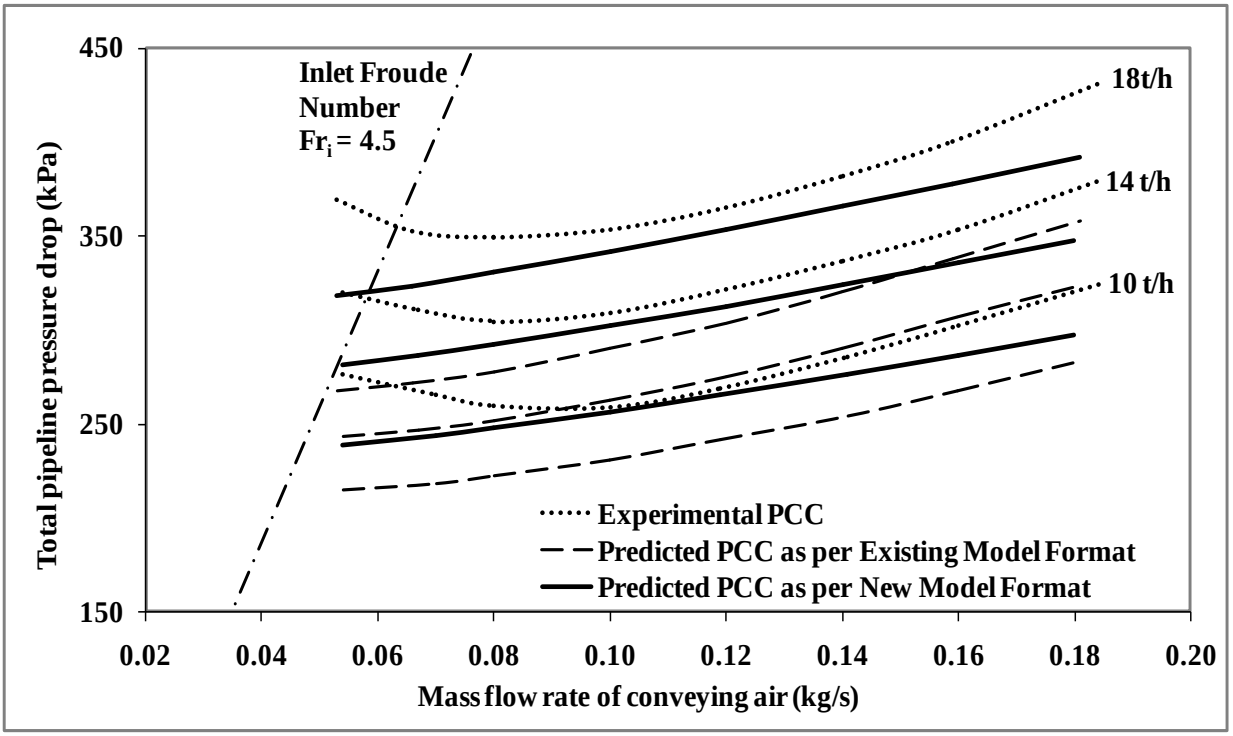

Figure 5.5: Experimental versus predicted PCC using Model 2 and Model 6 for fly ash through pipeline C1 (65 mm I.D. × 254 m long pipe)

In the above figure, for all the series of predicted PCC, the top lines represent m_s = 18 t/h, middle lines represent m_s = 14 t/h and bottom lines represent m_s = 10 t/h. The results show that the existing models provide gross under-predictions for all the solids flow rates. The existing model produces continuously decreasing trends of predicted pressure drops with increasing air flow rate, whereas the trends of the experimental PCC are the opposite. It is evident that the existing model becomes drastically unreliable under significant diameter and length scale-up conditions. The new model produced much better predictions, with slight under-predictions for 18 t/h and slight under-prediction for the 10 t/h line in the low velocity region. The trends of predicted PCC using the new format show a mild increase in predicted pressure drop with increase in air flow rate (however, the slope is less than the experimental PCC). Figure 5.6 shows the results of scale-up evaluations for Model 2 and Model 6 using the conveying data of fly ash through the pipeline C2 (80/100 mm I.D. ×407 m long pipe).

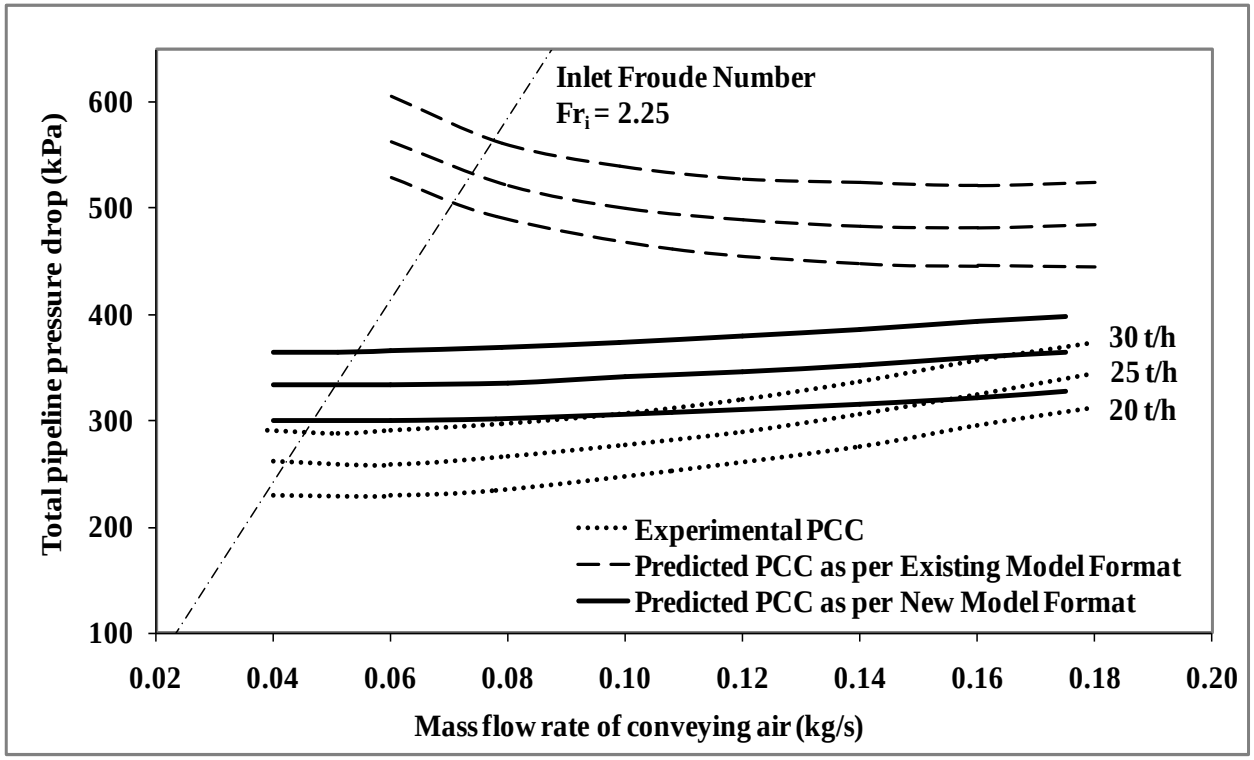

Figure 5.6: Experimental versus predicted PCC using Model 2 and Model 6 for fly ash through pipeline C2 (80/100 mm I.D. × 407 m long pipe)

In the above figure, for all the series of predicted PCC, the top lines represent m_s = 30 t/h, middle lines represent m_s = 25 t/h and bottom lines represent m_s = 20 t/h.The results show that the existing format provides drastic over-prediction. Compared to this, the new format provides much better predictions (with some over-predictions). Similar to the above, solids friction factor models developed using the steady state conveying data for ESP dust and fly ash, Models 7 and 8, respectively have been evaluated for their accuracy and stability by using them to predict the total pipeline pressure drop for the larger and longer pipelines i.e. pipelines A2 and A3 (105 mm I.D. × 168 m and 69 mm I.D. × 554 m, thus for length and diameter scale-up conditions) for different solids and air flow rates and by comparing the predicted pneumatic conveying characteristics against the experimental plots. Model

predictions using the existing format (Models 3 and 4) have been superimposed on the above predicted pneumatic conveying characteristics to demonstrate the improved prediction capabilities of the new format. These have been shown in Figures 5.7 to 5.10. Once again, Chambers and Marcus (1986) model was used to determine the losses in bends.

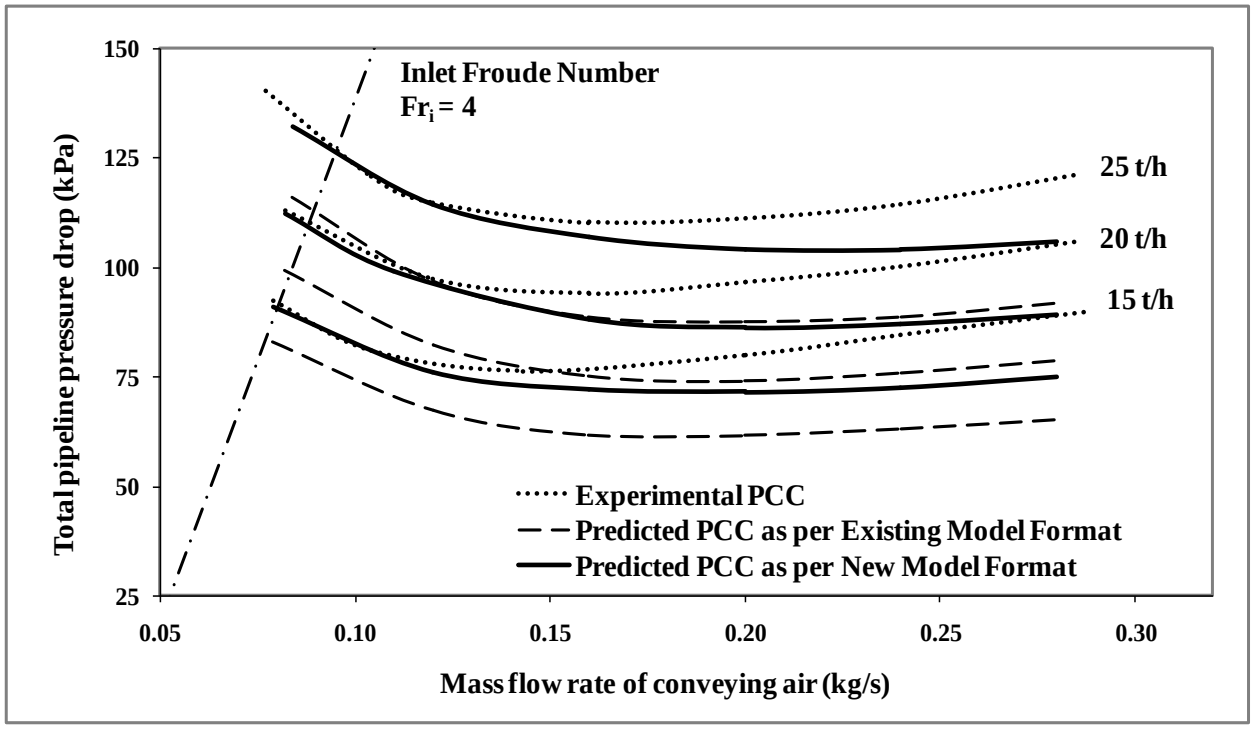

Figure 5.7: Experimental versus predicted PCC using Model 3 and Model 7 for ESP dust through pipeline A2 (105 mm I.D. × 168 m long pipe)

In the above figure, for all the series of predicted PCC, the top lines represent m_s = 25 t/h, middle lines represent m_s = 20 t/h and bottom lines represent m_s = 15 t/h.

Accurate modeling of fluidized dense-phase flow of fine powders is known to be a difficult task due to the highly turbulent nature of the flow. Models are developed using a straight pipe

section corresponding to some range of air velocities. In the actual pipeline certain velocities will be lower and certain velocities will be higher than this range due to the physical location of the test set-up and the location of the pressure tapping points. Near the blow tank the air velocity will be lower than the specified range (from where the models are generated); whereas near the exit to the pipeline the air velocity is more than the range. This causes the models to extrapolate to arrange of velocities that is outside the range from where the models were generated. Moreover, till date superficial air velocity has been used in the expression of solid friction factor. Superficial air velocity can be considered to be close to the actual air velocity in case of dilute-phase flow, where solid volume occupancy can be neglected compared to the pipe volume. However, in fluidized dense-phase the cross-sectional area occupied by the solids cannot be neglected. Furthermore, the predicted total pipelines PCC consist of individual prediction of straight pipe, losses due to bends and verticals. This thesis is aimed at addressing straight pipe losses through the horizontal section only. Any inadequacy in the prediction capability of the bend and vertical los models can result in some changes in nature of predicted total pipeline PCC, although this effect is expected to be low for dense-phase compared to dilute-phase. Due to these reasons and that the particle size distribution has been considered to be adequately represented a single median particle diameter term (which inherently assumes that the particles are spherical), the author consider that it is not unusual to find some predictions haven't exactly matched with the experimental data. Nonetheless, it is evident that a considerable amount of improvement has been achieved using the new developed models. For further improvement particle velocity and actual air velocity may need to be included in the models in future studies.

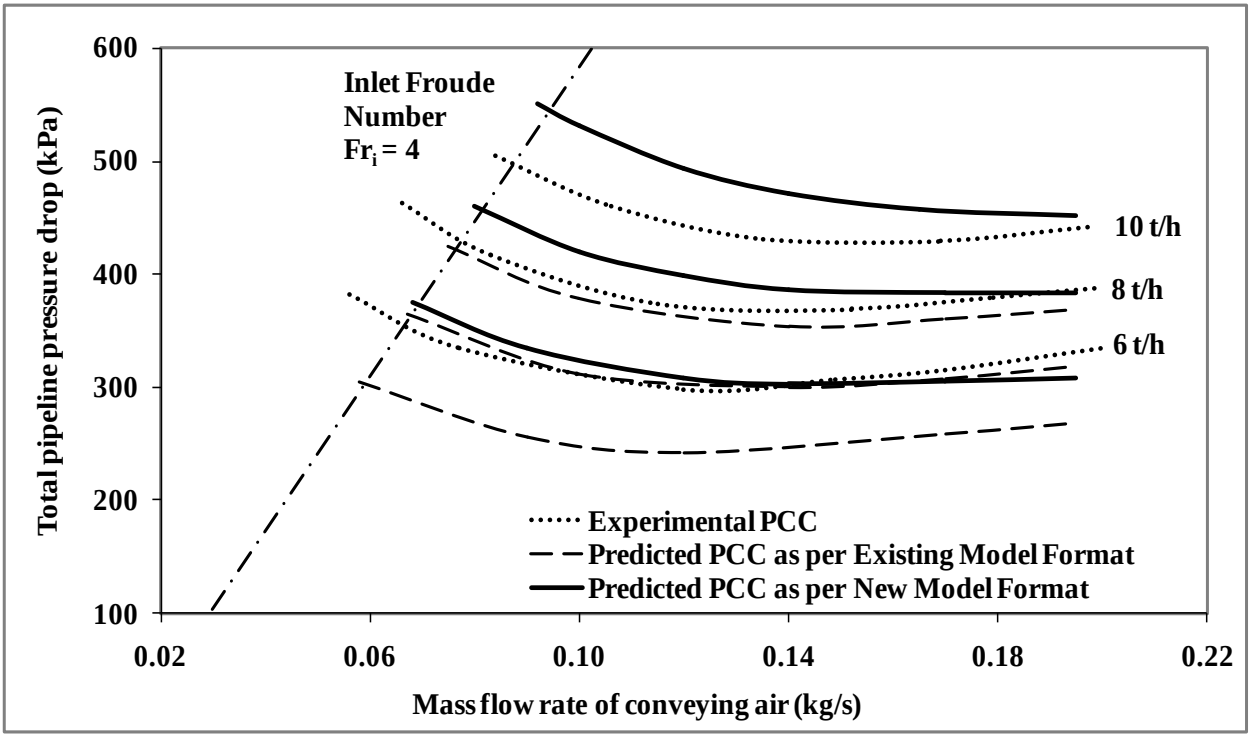

Figure 5.8: Experimental versus predicted PCC using Model 3 and Model 7 for ESP dust through pipeline A3 (69 mm I.D. × 554 m long pipe)

In the above figure, for all the series of predicted PCC, the top lines represent m_s = 10t/h, middle lines represent m_s = 8 t/h and bottom lines represent m_s = 6 t/h.

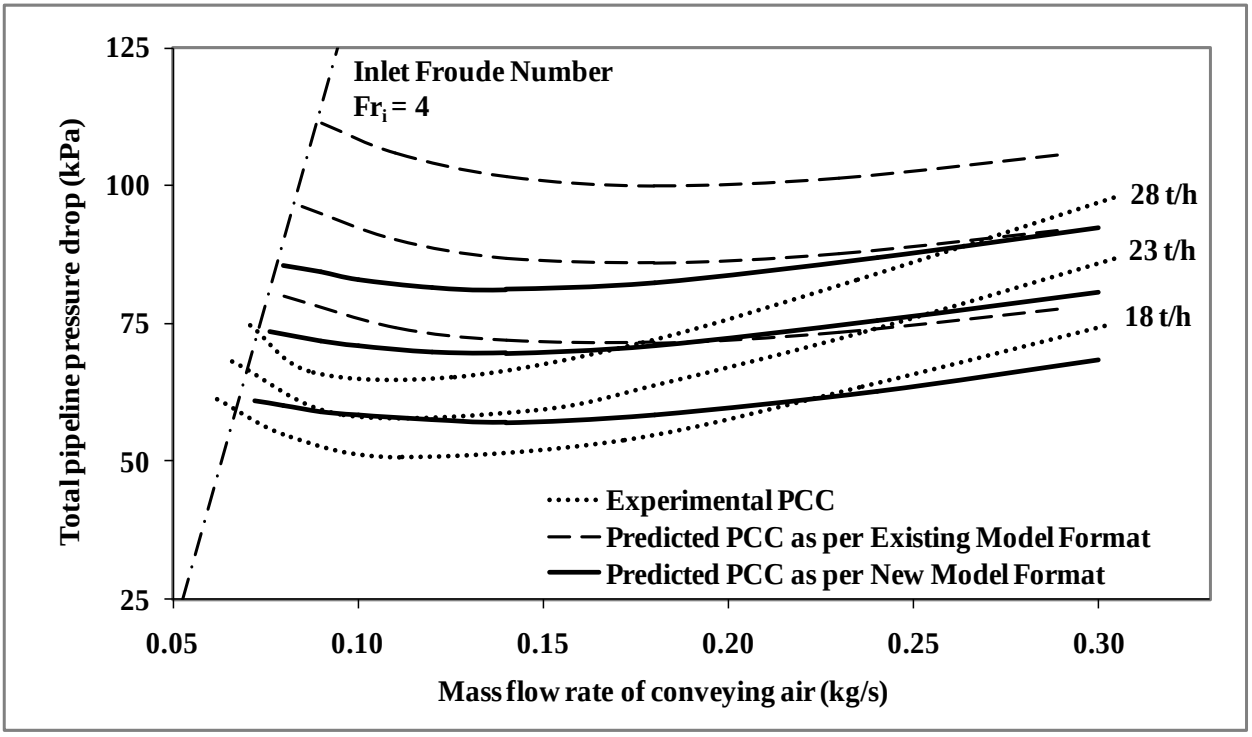

Figure 5.9: Experimental versus predicted PCC using Model 4 and Model 8 for fly ash through pipeline A2 (105 mm I.D. × 168 m long pipe)

In the above figure, for all the series of predicted PCC, the top lines represent m_s = 28 t/h, middle lines represent m_s = 23 t/h and bottom lines represent m_s = 18 t/h.

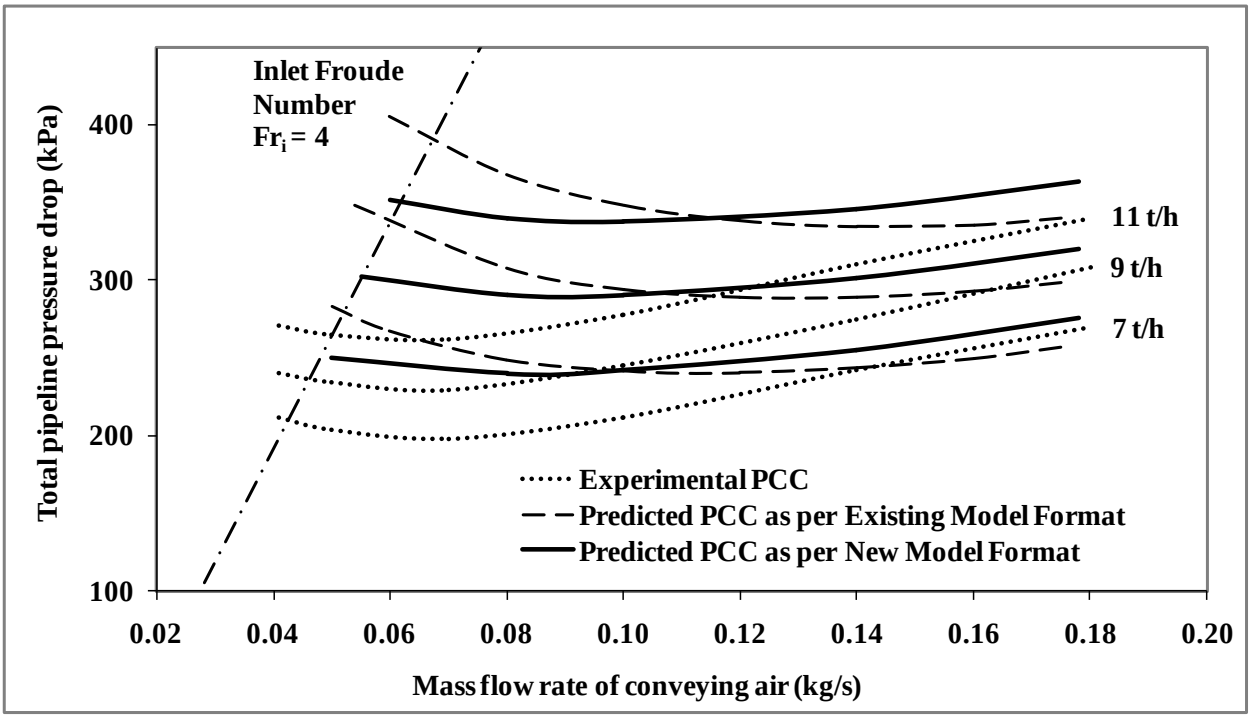

Figure 5.10: Experimental versus predicted PCC using Model 4 and Model 8 for fly ash through pipeline A3 (69 mm I.D. × 554 m long pipe)

In the above figure, for all the series of predicted PCC, the top lines represent m_s = 11 t/h, middle lines represent m_s = 9 t/h and bottom lines represent m_s = 7 t/h. Results show that for ESP dust, the existing formats have shown considerable under-predictions for both length and diameter scale-up conditions. The new format has provided excellent prediction in these cases, especially in the low velocity (dense-phase) zone. The new format tends to provide little under-prediction towards dilute-phase (high air flow region). For fly ash, the existing format has provided significant over-prediction for both length and diameter scale-up cases and for dense- to dilute-phase. The new format provided some over-estimation, but the predictions are considerably better compared to that provided by the existing format.

Table 5.2: Average absolute deviation of percentage error of various model predictions

Product	**Model No.**	**Pipeline and Figure No.**	**Existing Model**			**New Model**			**Improvement in predictions (**percentage)
			Max. error (kPa)	Mini. error (kPa)	Average absolute deviation of percentage error	Max. error (kPa)	Mini. error (kPa)	Average absolute deviation of percentage error	
Cement (Fujian Longking Co.)	Model 1 and Model 5	Pipeline C1, Figure 5.3	65.7	22.4	10.8	36.7	-7.9	4	6.8
Cement (Fujian Longking Co.)	Model 1 and Model 5	Pipeline C2, Figure 5.4	-258.8	-17.5	35.9	50.7	-41	5.8	30.1
Fly Ash (Fujian Longking Co.)	Model 2 and Model 6	Pipeline C1, Figure 5.5	101	26.5	24.2	46.5	2.2	13	11.2
Fly Ash (Fujian Longking Co.)	Model 2 and Model 6	Pipeline C2, Figure 5.6	-426	-133.4	85.5	-75.3	-16	19.3	66.2
ESP dust (Uni. of Wollongong)	Model 3 and Model 7	Pipeline A2, Figure 5.7	27.3	9.4	20.2	14.8	-1.6	7.6	12.6
ESP dust (Uni. of Wollongong)	Model 3 and Model 7	Pipeline A3, Figure 5.8	114.9	56.3	38.3	-65	21.4	10.5	27.8
Fly ash (Uni. of Wollongong)	Model 4 and Model 8	Pipeline A2, Figure 5.9	-46.6	-3.4	22.3	-16.6	5.8	6.5	15.8
Fly ash (Uni. of Wollongong)	Model 4 and Model 8	Pipeline A3, Figure 5.10	-209.5	12.1	23.2	-86.5	-6.1	15.5	7.7

Average absolute deviation of percentage error

$$= \frac{1}{n}\sum_{n}\left|\frac{\text{experimental value} - \text{predicted value}}{\text{experimental value}}\right| \times 100\ \% \qquad (5.6)$$

Table 5.2 shows that new model format provides significant improvement compared to the existing model format, e.g. upon comparing Model 1 versus Model 5, Model 2 versus Model 6, Model 3 versus Model 7 and Model 4 versus Model 8 in all the figures (Figure 5.3 to 5.10).

New model format has provided 6.8 to 66.2 % improved predictions. Also, whereas the existing formats can have wide range of inaccuracy; e.g. existing format can provide amount of error in estimation of total pipeline pressure drops ranging from 10.8 to 85.5%, the maximum variability range for new modeling format is 4 to 19.3%. This is a much narrower and desirable range of prediction capability compared to the existing models. The results indicate that the new modeling procedure provided in this chapter using solids volumetric loading ratio and dimensionless velocity will help designers to reliably estimate total pipeline pressure drop for larger and/or longer industrial systems. However, the predicted PCC (pneumatic conveying characteristics) did not provide adequate 'U' shaped characteristics, i.e. it could not follow the gradual change in flow mechanism from fluidized dense- to dilute-phase pneumatic conveying (i.e. non suspension to suspension flow mechanism). As a result, the pressure drop prediction lines were not adequately turning upward in very low and high velocity zones, i.e. instead of 'U'-shaped characteristics (with change in slope from low to high air flows), the predicted PCC had more pronounced regions of flat characteristics.

5.4 Modeling solids friction using two-layer flow theory

The newly developed modeling format for solids friction factor using volumetric loading ratio and dimensionless velocity developed by the author, as given by equation (5.4), considers that the air-solid mixture flows in the pipe as a uniform fluidized bed, i.e. there is no concentration gradient of powders across the pipe diameter. This flow mode typically has been seen during experimentation at the high dense-phase regions of pneumatic conveying characteristics (i.e. operating conditions near to the blockage boundary), where the dunes tend to cover a large amount of pipe cross-section. Previous scale-up validation have revealed that predictions from this recently developed uniform flow modeling format were relatively better compared to the other previously known existing popular modeling format (equations 5.1). The uniform model seemed to predict well near the pressure minimum point (at the mid portions of typical pneumatic conveying characteristics), but was unable to follow the 'U'-shaped trend of typical conveying characteristics (Klinzing et al., 2010; Mallick 2009). Sight glass observations during the conveying trials have revealed that although for highly dense-phase (near blockage boundary), the pipe was almost uniformly filled with non-suspension flow of dunes, but in the medium air flow range, more particle concentration was visible towards the bottom of the pipe (this layer transports most of the particles) and a dilute suspension layer of powder was seen to be flowing on top of the non-suspension layer (i.e. there exists a concentration gradient of powders across pipe diameter). It has been observed that for fine powders, such as fly ash and cement, the change in flow mechanism from non-suspension to suspension (with an increase in air flow rate) is gradual and spans over majority of the air flow rate range. This could be seen experimentally through sight glass and also evident from the gradual change in slopes in pneumatic conveying characteristics, i.e. absence of any sharp pressure minimum point in PCC.

Therefore, the actual dense-phase conveying condition in the pipe is not precisely just having a single non-suspension layer (wavy dunes of powders) travelling along the bottom of pipe, but actually there is a non-suspension dune flow occurring along the bottom of pipe, on top of which dilute-phase suspension flow of fine particles occurs. Figure 4a and b represents the complex flow phenomenon as observed through the sight glass. Due to the difficulties in obtaining good quality photograph through sight glass for fine powder flow (the glass gets coated with fine powder after few minutes of conveying), a sketch is provided (Figure 5.11a and b). Similar representations were also provided by Mason and Levy (2001) and Mallick (2009).

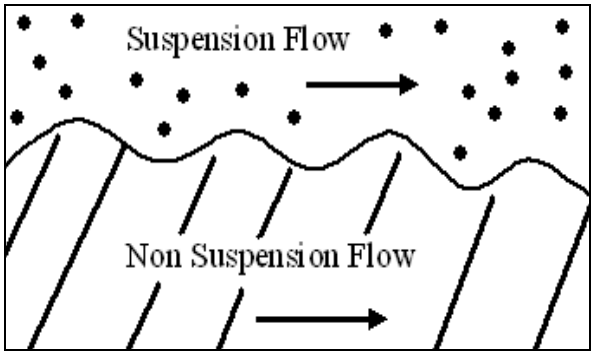

Figure 5.11a. Two-layer dune flow of fine powders in dense-phase under actual flow condition

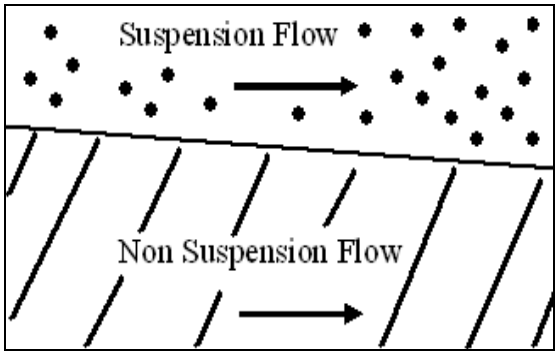

Figure 5.11b. Simplified representation of two-layer flow of fine powders in dense-phase

Figure 5.11a shows that the non-suspension layer is having a wavy/liquid type appearance with a turbulent top surface, where a rapid mass exchange of solids with the upper dilute-phase layer takes place. However, the interface between the non-suspension and suspension layers was not very distinct. With an increase in conveying air flow rate, the thickness of the non-suspension layer decreased (with more and more product getting into the suspension flow), ultimately resulting in the disappearance of the non-suspension layer and suspension

flow (dilute-phase) occurring through the whole cross section of the pipe. Recent work of other researchers (Jones et al., 2008; Williams et al., 2008) using Electrical Capacitance Tomography (ECT) to analyze the flow structure of dense-phase conveying of fine powders indicated similar considerations of flow mechanisms. Figure 5.11b is a simplified representation of the dune flow condition, where the top surface of dune has been considered as linear for the purpose of modeling solids friction factor. This line represents the interface between the non-suspension and suspension layers. It has been also considered that with an increase in gas velocity, more and more particles from the non-suspension layer gets picked up in the suspension layer. This results in gradual decrease in the thickness of non-suspension layer with an increase in superficial gas velocity. The non-suspension dense-phase layer behaves like a liquid/pseudo-fluid (being aerated fluidized powders) and suspension flow mechanics can be assumed to be prevailing in the dilute-phase layer. Since the flow mechanisms of both the layers are completely different from each other, it is inadequate to represent both the flow modes by a single model with the same set of flow parameters. Therefore, it is prudent to consider that a comprehensive model is to be developed that must have sub-models to separately represent the non-suspension and suspension flow phenomenon. These sub-models will then need to be suitably clubbed within the main model. For the non-suspension layer, volumetric loading ratio and dimensionless velocity are considered as apt parameters (from earlier validation in this chapter). For the suspension layer, a pure dilute-phase model, known as “Weber-A4” model (Wypych et al., 1990), has been considered. This model has been reported to provide good predictions for dilute-phase flow for different pipeline configurations. This model separates the solids friction factor loss into two components: losses due impact and friction between particle-particle/air/pipe wall and that due to keeping the particles in suspension. The model is given by equation (5.7).

$$\lambda_s = \lambda_s^* \, C/V + 2\beta_0/[(C/V)\, Fr^2] \quad (5.7)$$

Where, $\beta_0 = w_{fo}/V$ and λ_s* represents impact and friction components corresponding to dilute-phase condition (Wypych et al., 1990). The two layer modeling format is expressed as:

$$\lambda_s = \tau_1 \, (K \, (VLR)^a \, (w_{fo}/V)^b) \; + \; \tau_2 \, (\lambda_s^* \, C/V + 2\beta_0/[(C/V)\, Fr^2)] \quad (5.8)$$

Where, K, a, b are constant and exponents of power function format and τ_1 and τ_2 represent the relative contributions of non-suspension and suspension layers, respectively, based on the Froude number criteria. It is considered that with an increase in gas Froude number (i.e. air velocity for a particular pipe diameter), the flow mechanism shifts from non-suspension to suspension mode. τ_1 and τ_2 are represented as:

$$\tau_1 = \{1-(Fr - Fr_{min})/(Fr_{max} - Fr_{min})\} \quad (5.9)$$

$$\tau_2 = (Fr - Fr_{min})/(Fr_{max} - Fr_{min}) \quad (5.10)$$

Where, Fr_{min} corresponds to the minimum gas Froude number, below which unstable flow and pipeline blockage was found to occur. This was found to happen in the range of Fr = 3 to 4. Fr_{max} corresponds to high velocity (suspension flows). This was considered to be Fr = 50 as the extreme limit considering all the products and pipeline conditions. Froude number (Fr) refers to the value of Froude number at a section of straight-pipe (i.e. average value of Froude number across the pipe section). Models for solids friction factor developed for ESP dust, two different samples of fly ash and cement in two-layer format (format provided by equation 5.8) and are provided in Table 5.3. The tables contain the values of constants, exponents, w_{fo} and λ_s* for the modeling formats, as given by equation (5.8).

Table 5.3: Models developed using new two-layer modeling format (in the form of equation 5.8)

Product	**Pipeline**	**Horizontal length**	**Models (as per format given by equation 5.8)**					**R^2**	**Model No.**
			K	**a**	**b**	**w_{fo} (m/s)**	**λ_s***		
Cement	Pipeline C1	P2-P3, 47.5 m	17.31	-0.40	1.54	0.036	0.0081	0.98	Model 9
Fly ash	Pipeline C1	P2-P3, 47.5 m	23.54	-0.61	1.71	0.038	0.0074	0.99	Model 10
ESP dust	Pipeline A3	P9-P10, 26.91 m	3018	-0.20	1.72	0.005	0.0135	0.99	Model 11
Fly ash	Pipeline A1	P11-P12, 40.41 m	8.04	-0.22	1.48	0.06	0.0043	0.98	Model 12

High values of R^2 indicate good fit. The models as per recently developed uniform flow format (equation 5.4) which are already provided in Table 5.1 are again used for the purpose of comparing their scale-up predictions w.r.t those developed using two-layer format (Table 5.3).

5.5 Scale-up validation of models developed using two-layer flow theory

In this section, the newly develop two-layer models have been validated for longer and larger pipelines for different solids and air flow rates by comparing the predicted pneumatic conveying characteristics against the experimental plots. Solids friction factor models developed as per the newly developed two-layer modeling formats (shown in Table 5.3) have been evaluated and compared for their accuracy and stability to predict the total pipeline drop for four products and five pipeline combinations. Predictions as per the uniform modeling format (models shown in Table 5.1) have been superimposed on the above predicted pneumatic conveying characteristics to demonstrate the possible improvements of pressure drop prediction capability of the new two-layer modeling format (Table 5.3). The results are provided in Figures 5.12 to 5.21. Again, Chambers and Marcus (1986) model has been used to determine the losses in bends, as given by equation (5.5). Also, as in previous evaluation, pressure drops due to initial acceleration and verticals were calculated as per Klinzing et al., 2010. In all these figures, predictions using the uniform flow model (equation 5.4) have been superimposed to demonstrate the improvements achieved. Figure 5.12 shows the results of scale-up evaluations for Model 5 and Model 9 using the conveying data of cement through pipeline C1 (65 mm I.D. × 254 m long pipe).

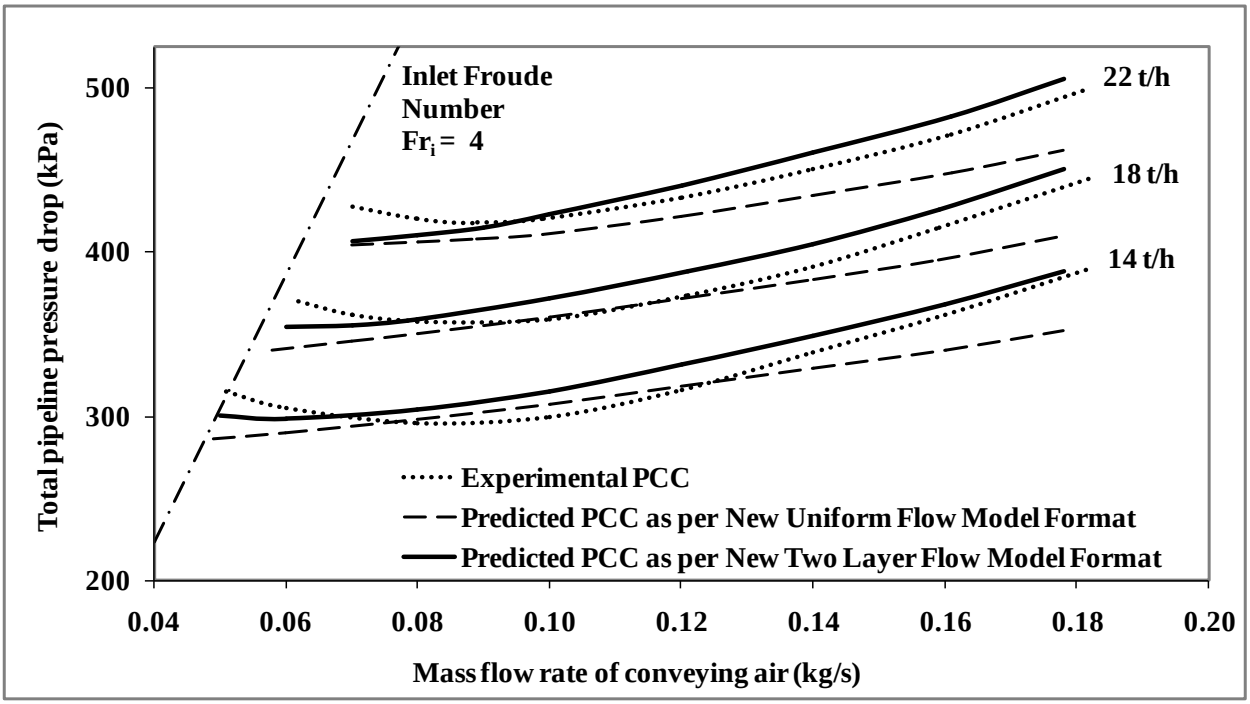

Figure 5.12: Experimental versus predicted PCC using Model 5 (Table 5.1) and Model 9 (Table 5.3) for cement through pipeline C1 (65 mm I.D. × 254 m long pipe).

In Figure 11, for all the series of predicted PCC, the top lines represent m_s = 22 t/h, middle lines represent m_s = 18 t/h and bottom lines represent m_s = 14 t/h. Results show that the uniform flow model (Model 5) provides under-predictions for all the solids flow rates. Also, Model 5 has not been able to follow the rise in slope of the experimental PCC in the very dense-phase zone. The new two-layer flow model provides better predictions in the higher range of air flows. However, both the model formats did not adequately follow the change in slope of predicted PCC (compared to the experimental PCC) in low air flow rates (close to the Fr = 4 line). Figure 5.13 shows the results of scale-up evaluations for the same models (Model 5 and Model 9) using the conveying data of cement through pipeline C2 (80/100 mm I.D. × 407 m long pipeline (step-up pipeline).

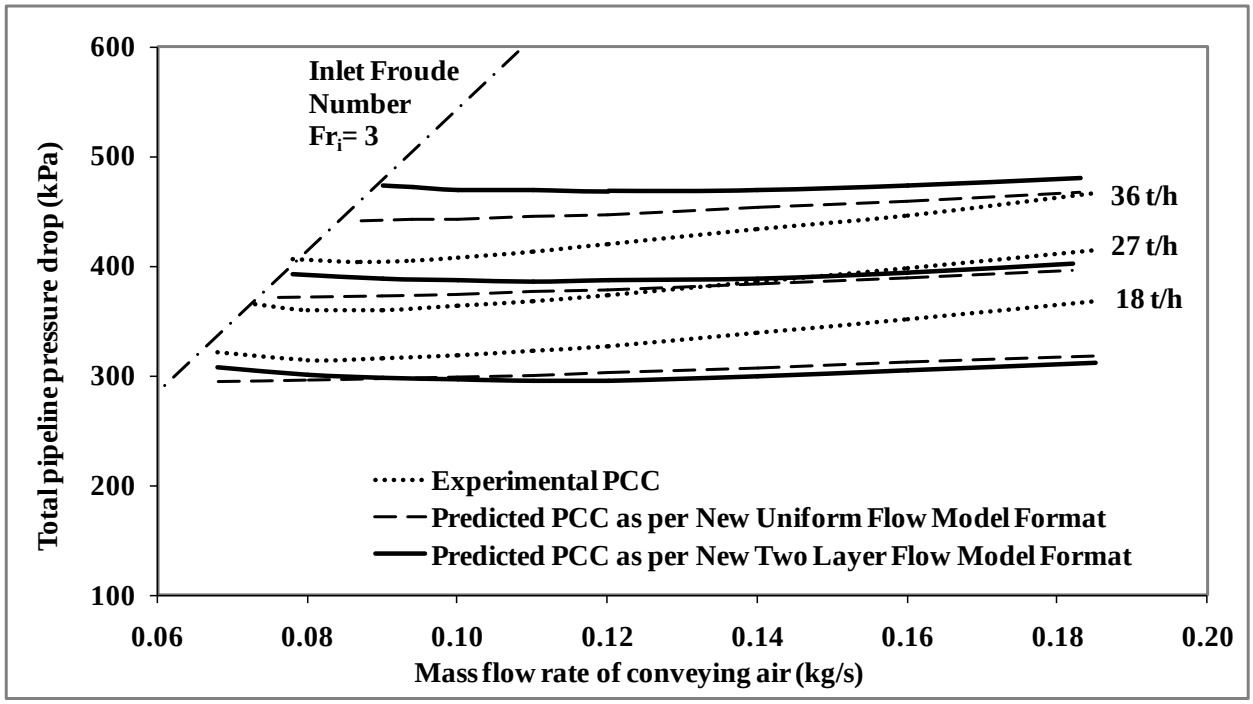

Figure 5.13: Experimental versus predicted PCC using Model 5 (Table 5.1) and Model 9 (Table 5.3) for cement through pipeline C2 (80/100 mm I.D. × 407 m long pipe)

In the above figure, for all the series of predicted PCC, the top lines represent m_s = 36 t/h, middle lines represent m_s = 27 t/h and bottom lines represent m_s = 18 t/h. Results show that both the models (Model 5 and Model 9) provided some under predictions for 18 t/h and over-predictions for the higher solids flow rates. The trends of predicted PCC using the two-layer format show moderate increase in predicted pressure drop values with an increase in air flow rates. Figure 5.14 shows the results of scale-up evaluations for Model 4 and Model 8 using the conveying data of fly ash through the pipeline C1 (65 mm I.D. × 254 m long pipe).

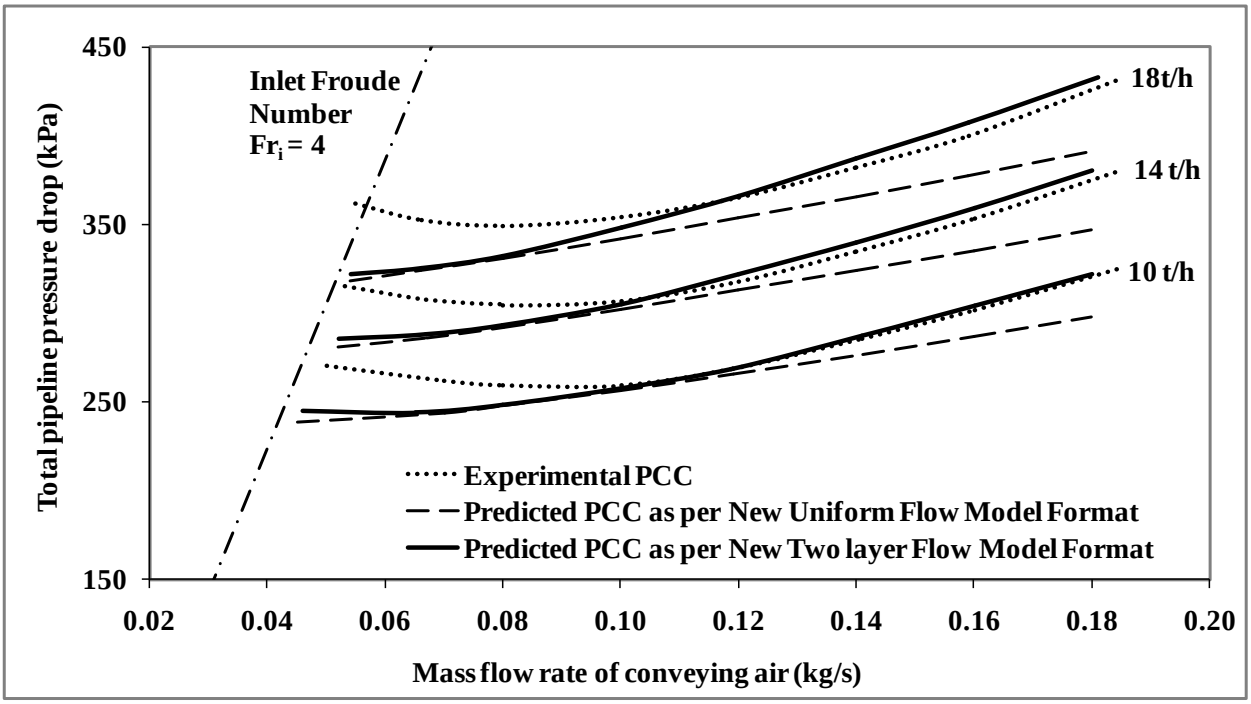

Figure 5.14: Experimental versus predicted PCC using Model 6 (Table 5.1) and Model 10 (Table 5.3) for fly ash through pipeline C1 (65 mm I.D. × 254 m long pipe)

In the above figure, for all the series of predicted PCC, the top lines represent m_s = 18 t/h, middle lines represent m_s = 14 t/h and bottom lines represent m_s = 10 t/h. Results show that the uniform flow model (Model 8) provides under-predictions for all the solids flow rates, whereas the two-layer flow model provides better predictions in the higher ranges of air flow. Compared to the uniform model, the predictions using two-layer model tends to follow the trends of pressure drop lines towards the dense-phase region, although the change in slope is not considerable. Figure 5.15 shows the results of scale-up evaluations for the same models (Model 6 and Model 10) using the conveying data of fly ash through pipeline C2 (80/100 mm I.D. × 407 m long pipe: step up pipeline).

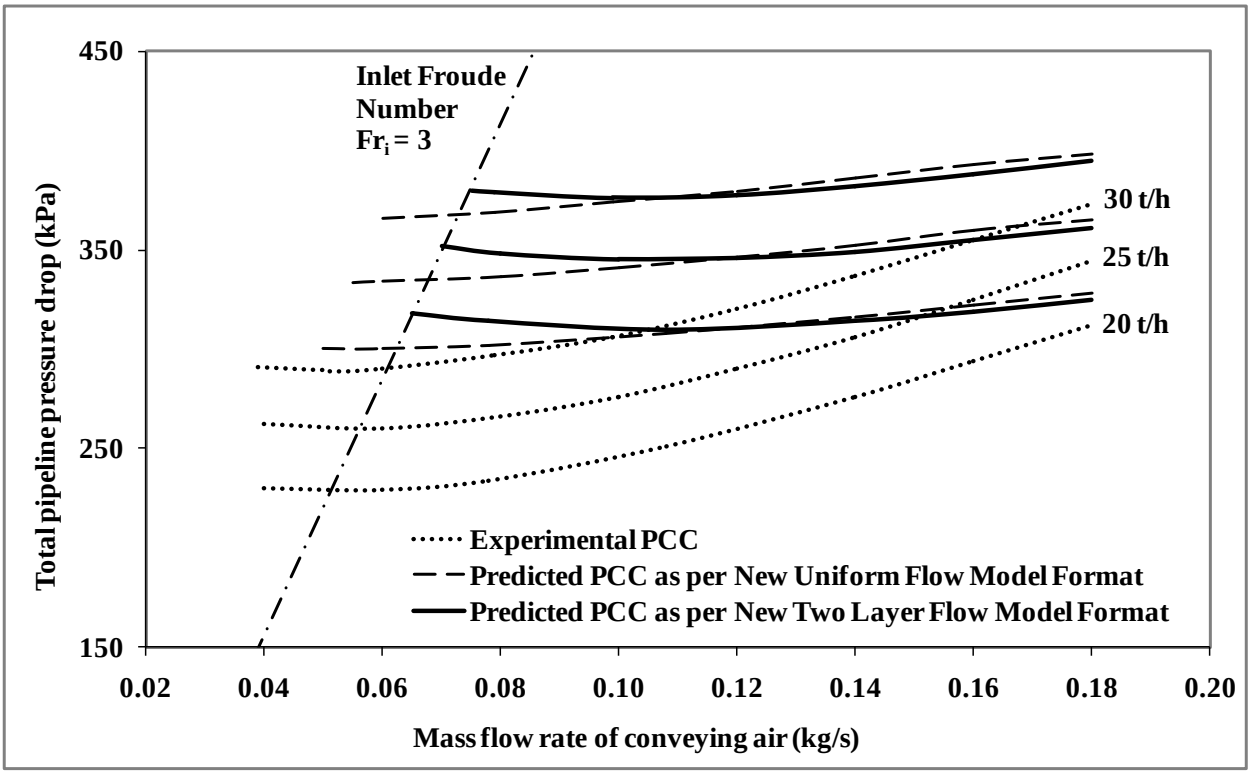

Figure 5.15: Experimental versus predicted PCC using Model 6 (Table 5.1) and Model 10 (Table 5.3) for fly ash through pipeline C2 (80/100 mm I.D. × 407 m long pipe)

In the above figure, for all the series of predicted PCC, the top lines represent m_s = 30 t/h, middle lines represent m_s = 25 t/h and bottom lines represent m_s = 20 t/h. Results show that predictions of both the models (Model 6 and Model 10) are comparable in case of scale-up for stepped pipeline. The two-layer model has not provided any apparent improvement over the uniform flow model, except that the two-layer model has shown a gradual change in slope in very dense-phase region (rise in pressure drop values with a decrease in air flow rates). Figure 5.16 shows the results of scale-up evaluations for Model 7 and Model 11 using the conveying data of ESP dust through 69 mm I.D. × 168 m long pipe.

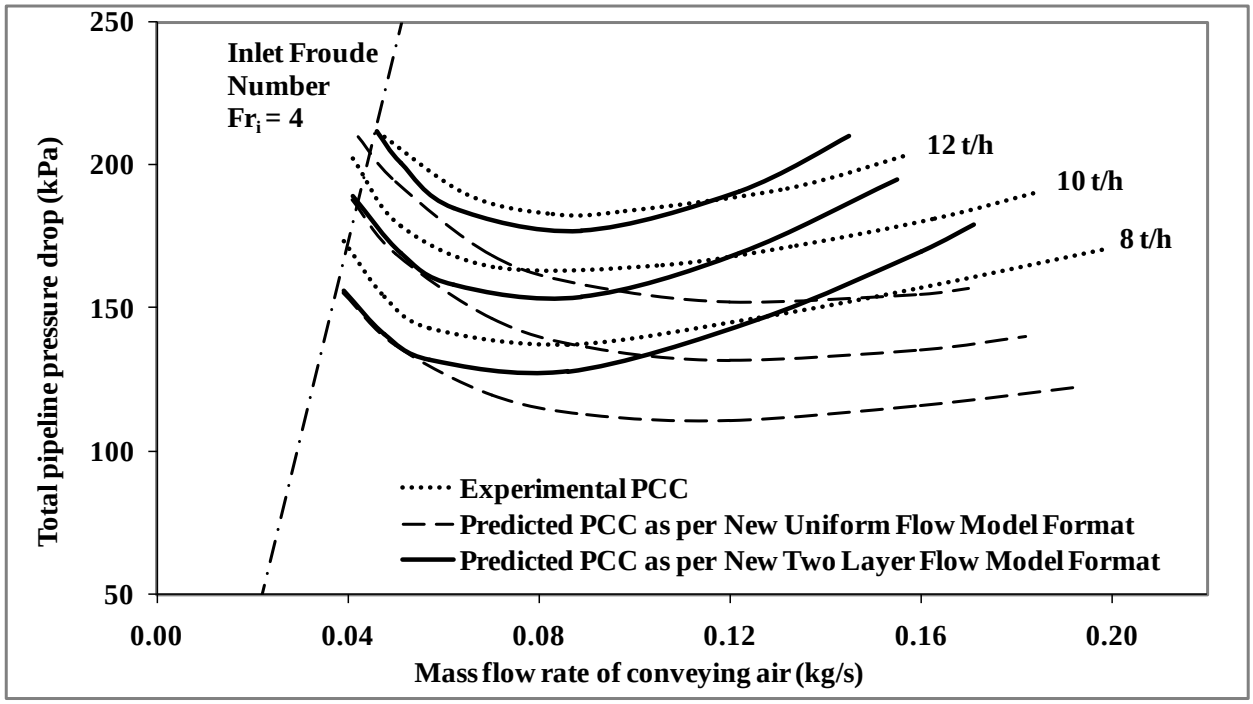

Figure 5.16: Experimental versus predicted PCC using Model 7 (Table 5.1) and Model 11 (Table 5.3) for ESP dust through pipeline A1 (69 mm I.D. × 168 m long pipe)

In the above figure, for all the series of predicted PCC, the top lines represent m_s = 12 t/h, middle lines represent m_s = 10 t/h and bottom lines represent m_s = 8 t/h. Results show that for ESP dust, the uniform model (Model 7) has shown acceptable predictions for dense-phase, but provided considerable under-predictions in the dilute-phase region. This behavior could be expected as the uniform model only addresses pure dense-phase flow phenomenon. The predictions were not able to follow the rise in slope (increase in predicted pressure drop with the rise in air flow rate) to the right of pressure minimum curve. The new two-layer model (Model 11) has provided excellent predictions in both flow modes covering the entire range of air flows, especially in the high velocity (dilute-phase) zone. The two-layer model also resulted in relatively better prediction towards the dense-phase (low air flow) region. Figure

5.17 shows model predictions versus experimental plots for larger diameter pipeline A2 (105 mm I.D. × 168 m long pipe) for ESP dust.

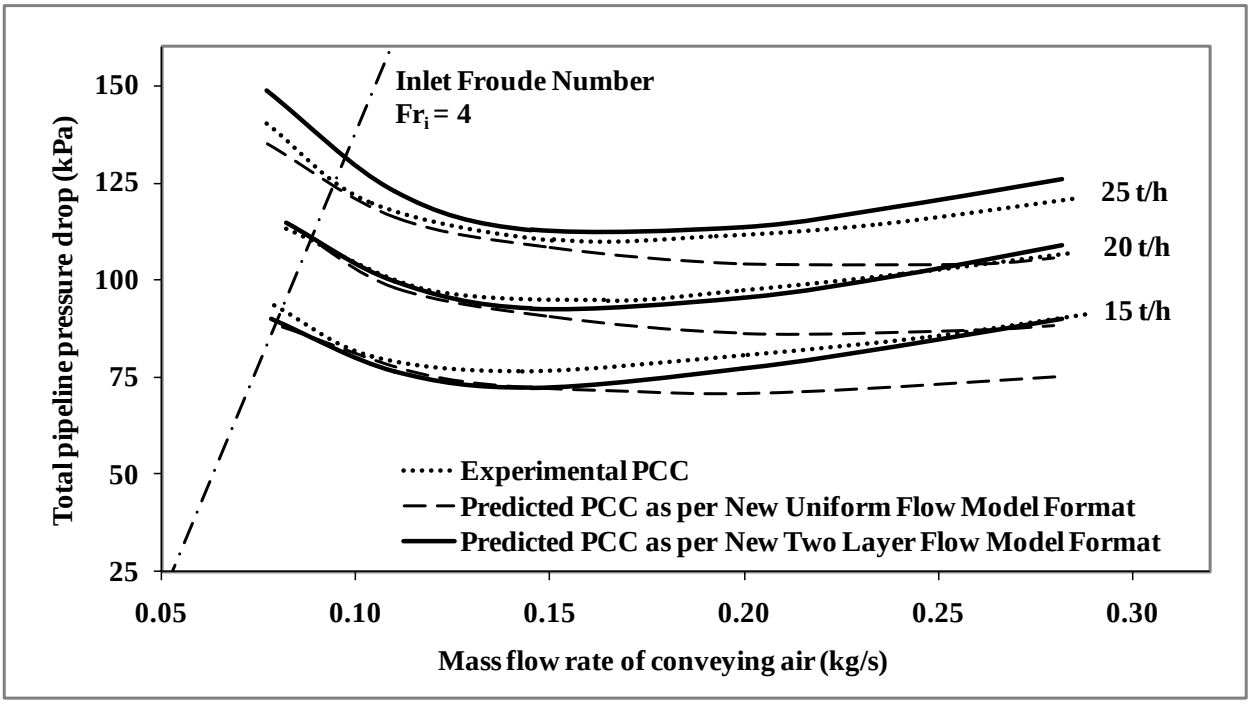

Figure 5.17: Experimental versus predicted PCC using Model 7 (Table 5.1) and Model 11 (Table 5.3) for ESP dust through pipeline A2 (105 mm I.D. × 168 m long pipe)

In the above figure, for all the series of predicted PCC, the top lines represent m_s = 25 t/h, middle lines represent m_s = 20 t/h and bottom lines represent m_s = 15 t/h. Results show that the new two-layer model (Model 11) not only provides overall better predictions throughout the PCC, but is also able to follow the 'U' shaped trend of the experimental PCC. Once again, the uniform flow model format (Model 7) could not follow the experimental trends of conveying characteristics and provided under-predictions in the medium to high air flow rates. Figure 5.18 shows predicted pressure drop values against experimental plots for longer pipeline A3 (69 mm I.D. × 554 m long Pipeline) for ESP dust.

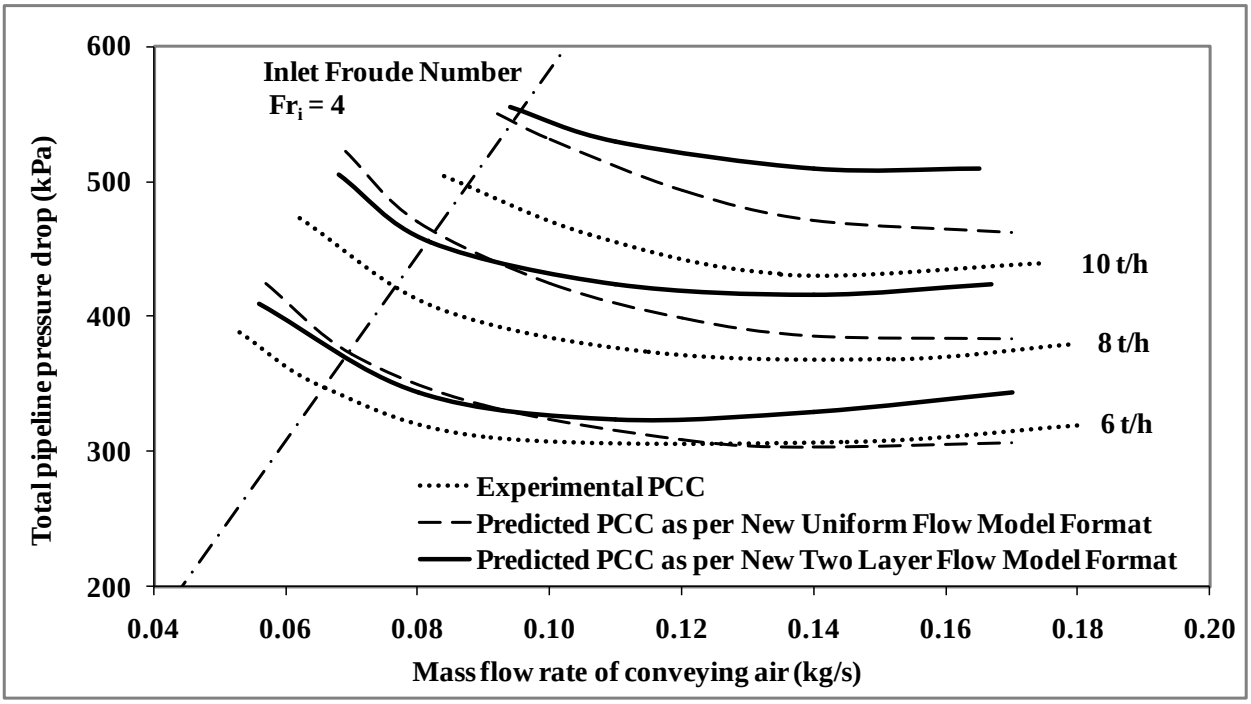

Figure 5.18: Experimental versus predicted PCC using Model 7 (Table 5.1) and Model 11 (Table 5.3) for ESP dust through pipeline A3 (69 mm I.D. × 554 m long pipe)

In the above figure, for all the series of predicted PCC, the top lines represent m_s = 10 t/h, middle lines represent m_s = 8 t/h and bottom lines represent m_s = 6 t/h. Results show that for ESP dust and length scale-up, the new two-layer model provides over-predictions especially for m_s =10 t/h in dilute-phase region. Both the models (Model 7 and Model 11) provide good predictions in extreme dense-phase or lower air flow region. With the increase in air flow rate, the new two-layer model (Model 11) followed the experimental 'U'-shaped trend of the PCC better than Model 7. Figures 5.20, 5.21 and 5.22 show the results of scale-up evaluations for Model 8 and Model 12 for the conveying data of fly ash through the pipeline A1 (69 mm I.D. × 168 m long pipe), pipeline A2 (105 mm I.D. × 168 m long pipe) and pipeline A3 (69 mm I.D. × 554 m long pipe).

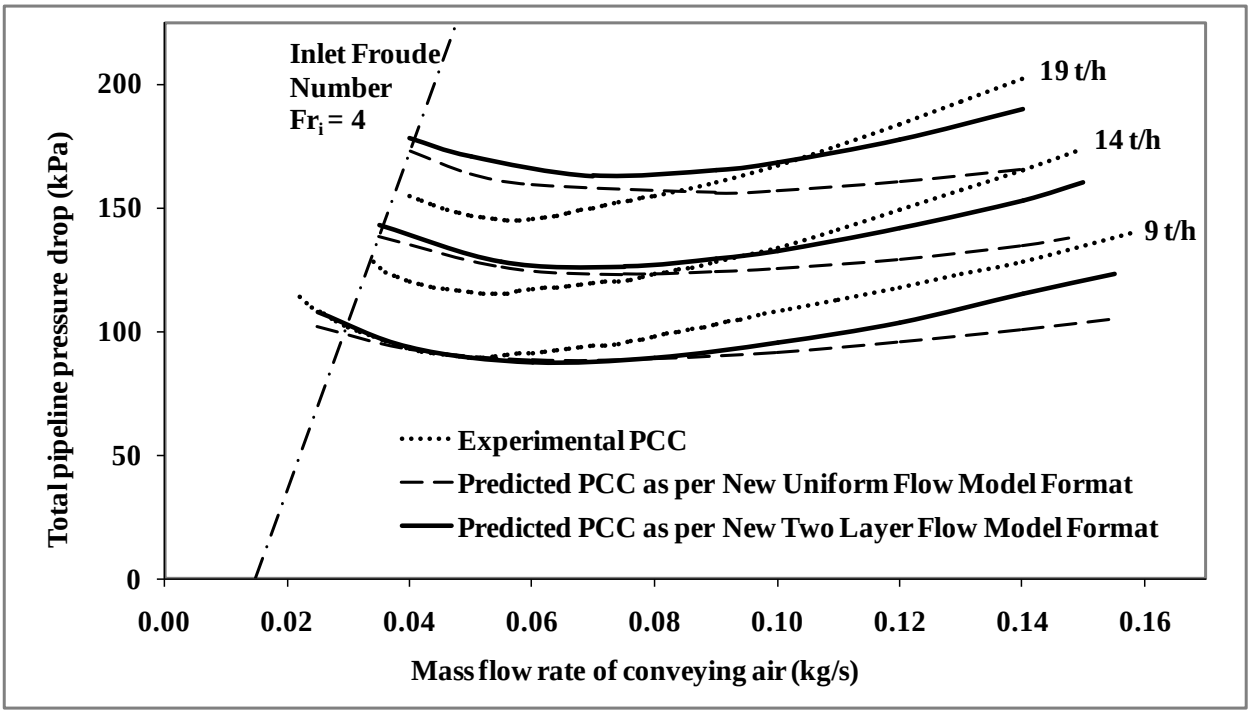

Figure 5.19 Experimental versus predicted PCC using Model 8 (Table 5.1) and Model 12 (Table 5.3) for fly ash through pipeline A1 (69 mm I.D. × 168 m long pipe)

In the above figure, for all the series of predicted PCC, the top lines represent m_s = 19t/h, middle lines represent m_s = 14 t/h and bottom lines represent m_s = 9 t/h. For fly ash, the new two-layer model (Model 18) provided better predictions compared to that provided by the uniform flow model format (Model 8) in the higher air flow range. The two-layer model showed change in slope ('U'-shaped trend) with an increase in air flow rate, whereas the same was less apparent for uniform flow model. This resulted in Model 8 providing under-predictions in higher air flow rates.

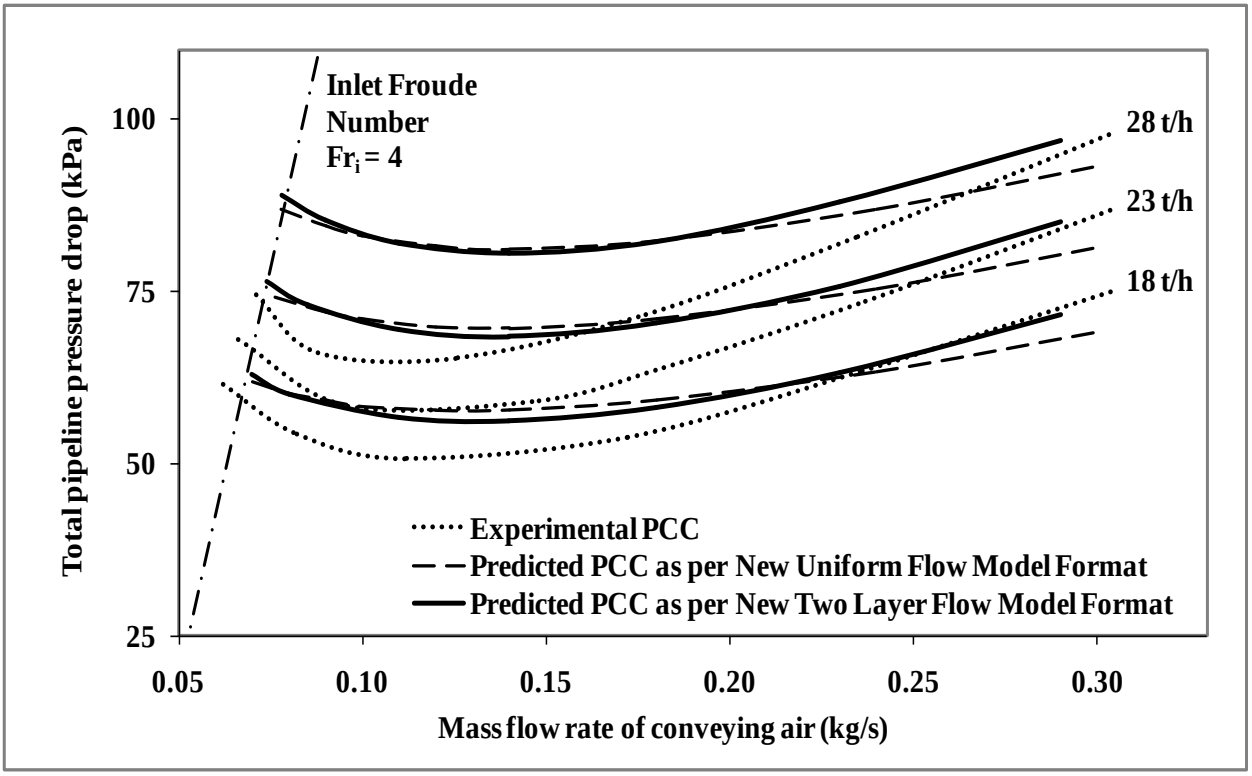

Figure 5.20 Experimental versus predicted PCC using Model 8 (Table 5.1) and Model 12 (Table 5.3) for fly ash through pipeline A2 (105 mm I.D. × 168 m long pipe)

In the above figure, for all the series of predicted PCC, the top lines represent m_s = 28 t/h, middle lines represent m_s = 23 t/h and bottom lines represent m_s = 18 t/h. For the case of diameter scale-up for fly ash, similar pattern of predictions were obtained as seen before in case of smaller diameter pipeline. Both the models (Model 8 and Model 12) have provided some over-estimation, but the predictions obtained using the two layer model (Model 12) are better compared to that provided by the uniform flow model (Model 8), with the predicted PCC showing relatively more pronounced change in slopes in higher air flow rate for the two-layer model.

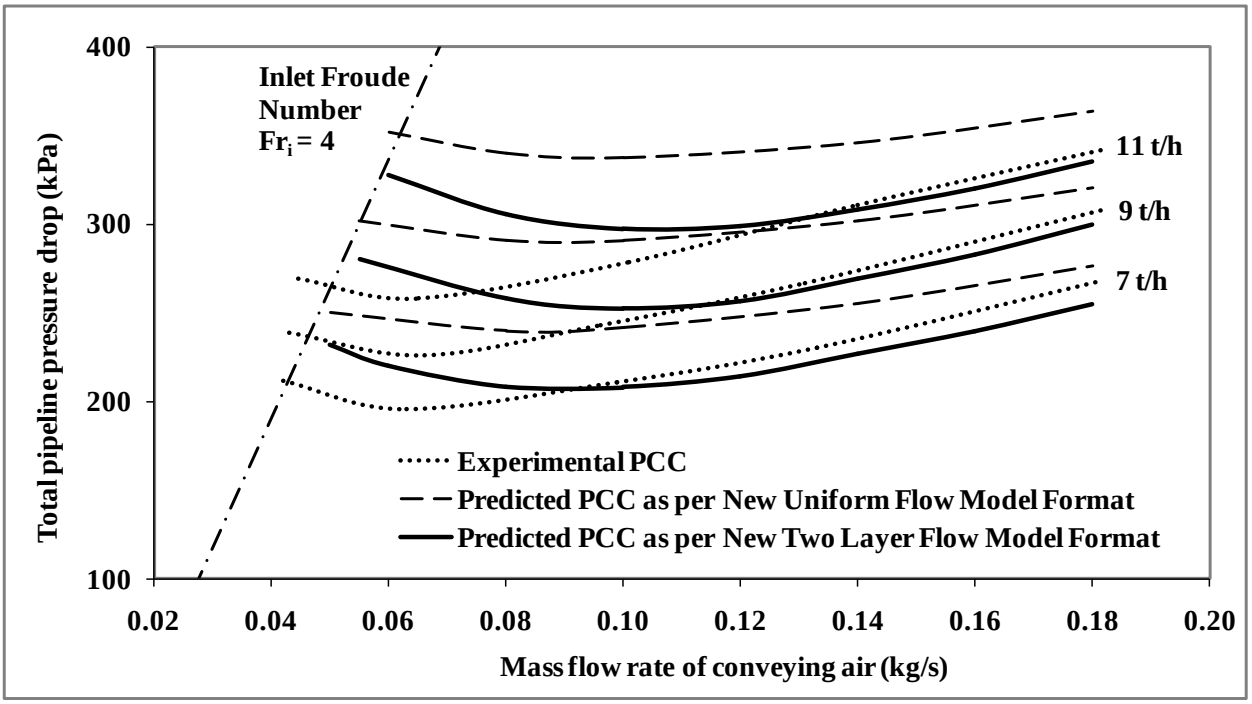

Figure 5.21 Experimental versus predicted PCC using Model 8 (Table 5.1) and Model 12 (Table 5.3) for fly ash through pipeline A3 (69 mm I.D. × 554 m long pipe)

In the above figure, for all the series of predicted PCC, the top lines represent m_s = 11 t/h, middle lines represent m_s = 9 t/h and bottom lines represent m_s = 7 t/h. For the length scale-up for fly ash, the two-layer model (Model 12) provided far better predictions compared to the uniform flow model (Model 8) both in terms of reduced range of over-predictions and in terms of trends of predictions following the experimental PCC.

Overall, it is evident that the two-layer model format has provided considerable improvements over the uniform flow model format in terms of better accuracy of predictions and more importantly, by being able to follow the 'U'-shaped trends (change in slopes of pressure drop lines from low to high air flows) of the experimental PCC more accurately. This demonstrates that the two-layer modeling approach is more representative of the actual flow phenomenon

of gradual change in flow mechanism from non-suspension to suspension mode. However, the two-layer model needs to be further amended in future to provide more accurate results in case of step-up pipelines. This would include a close observation of the change in flow mechanism just after step-up locations.

5.6 Modeling of pressure drop using rheological properties of powders

Two-layer flow phenomenon (explained earlier) considers majority of the powders are conveyed in the form of a highly concentrated non-suspension turbulent dunes flowing along the bottom of pipe and on top of this non-suspension layer, some particles are transported in suspension mode (dilute-phase flow). It has also been considered that with an increase in superficial gas velocity (along the flow direction), more and more particles would be gradually picked up from the non-suspension to the suspension layer. Thus, the thickness of the non-suspension layer gradually reduces in the direction of flow, as shown in Figures 11(a) and 11(b). This has been further shown with more detail in Figure 5.22.

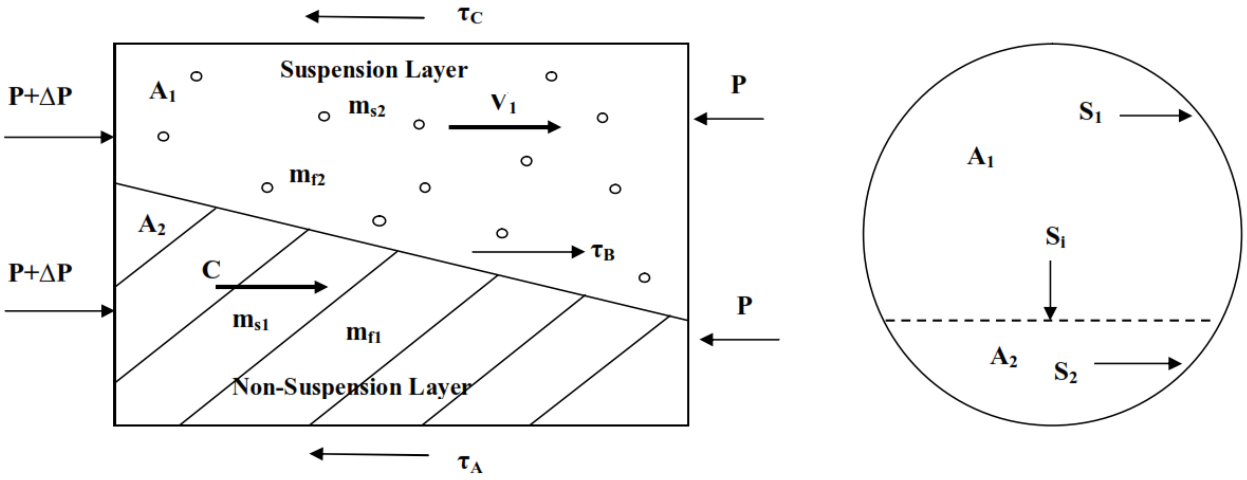

Figure 5.22: Free Body Diagram of two layer flow of fluidized powders

Where, τ_A, τ_B and τ_C are the shear stresses working at the interface of bottom of the dune layer and the pipe surface (wetted perimeter: S_1), non-suspension and suspension layer (S_i), suspension flow and top surface of pipe (wetted perimeter: S_2), respectively. The expressions for force balance can be given as (Mallick, 2009):

$$\Delta P = (L/A)\ (\tau_1 S_1 + \tau_2 S_2) \quad (5.11)$$

$$\tau_1 = 0.5\ (\lambda_{non\text{-}sus})\ (\rho_{app})\ V^2 \quad (5.12)$$

$$\tau_2 = 0.5\ (\lambda_f + m^*\lambda_{sus})\ \rho_f\ V^2 \quad (5.13)$$

With the supply of sufficient amount of air flows, sight glass observations revealed a significant amount of non-suspension flow, therefore confirming fluidized dense-phase conveying performance of the fine powders. Further reduction of air velocity provided pulse-type discontinuous dune structures. Even further reduction of air velocity resulted in unstable conveying, characterized by high pressure fluctuations and a gradual build-up of products in the pipeline. In the present study, this unstable-phase conveying is considered as the proximity of blockage condition. In the experience of the author, continuing air flow even after the onset of blocking would quickly form logs of products in the product, thus complete blockage of the line. This is characterized by the complete de-aeration of the powders. This is the limits to which the product could be conveyed without instability and is the left most point on the pneumatic conveying characteristics (as shown in Chapter 4). Here, Froude number values corresponding to these points have been calculated for fly ash and cement were conveyed in C1 and C2 pipelines (65 mm I.D × 254 m long, 80/100 mm I.D stepped diameter × 407 m long) (as shown in Chapter 4). These Froude number values (for minimum transport

condition) can be considered as the limiting condition where the powders (dunes) are just on the verge of flow or undergoing yield phenomenon. Again, yield stress corresponds to a point where the material starts to deform plastically and begins to flow. In a similar way, it can be imagined that this is the same point corresponding to the point of minimum transport on the PCC, as it also depicts the onset of material flow in a pipeline. Complete blockage of the pipeline corresponds to a situation where the product has got significantly de-aerated forming immovable logs of powders in the pipe. At this point, the pressure of the system starts to sharply increase, causing high pressure air further pressing the immovable bed of powder, causing the products to be compressed and de-aerate further. At this condition, the powders significantly lose their fluidized nature. Because of this reason, the yield stress values corresponding to unfluidized states are more applicable here.

Powder rheology is an important parameter to understand the flow mechanism and to model fluidized dense-phase pneumatic conveying of fine powders (Geldart Group A) (Mallick, 2009; Anjaneyulu and Khakhar, 1995; Wei and Chen, 2001; Bruni et al., 2005 and Chen, 2013). These powders are naturally able to retain air and exhibit liquid-like flow characteristics (in the form of moving dunes) (Mallick, 2009). Einstein (1956) conducted rheological studies on two-phase systems considering suspension of mono dispersed particles in Newtonian fluid and provided the following model (equation 5.14) to estimate the viscosity of the mixture. This model was further revised and provided by equation 5.15.

$$\mu_r = 1 + [\mu]\emptyset + O(\emptyset^2) \quad (5.14)$$

$$\mu_r = 1 + [\mu]\emptyset + B\,\emptyset^2 + \cdots \quad (5.15)$$

Where, the value of 'B' has been considered as 6.2 and 7.6 for Brownian and non- Brownian suspensions, respectively (Batchelor, 1970 and Natchelor and Green, 1972. A model proposed for the non-Newtonian fluids by incorporating the effect of yield stress using Mercury as the fluid (Bingham and Thompson, 1928) is given by equation (5.16) to (5.18) (Dogadkin and Pewsner, 1931). For different non-Newtonian fluids (pseudoplastic and dilatants), different values of 'n' are to be selected.

$\dot{\gamma} = 0, \qquad if\ \tau < \tau_o$ (5.16) $\tau =$

$\tau_0 + \mu_o\, \dot{\gamma}, \qquad if\ \tau > \tau_o$ (5.17)

$\tau = \mathrm{m}\, \dot{\gamma}^{\mathrm{n}-1}\dot{\gamma}$ (5.18)

An indirect technique to measure the viscosity of powdered bed was developed by (Grace 1970) in which the value of viscosity was determined using the wake angle of the rising bubble in the fluidized bed. Reynolds number of the bubble was used to represent the viscosity, as provided below:

$Re_b = 23 \exp(-0.049)$ (5.19)

Where, $Re_b = \frac{d_b\, u_b \rho_p (1 - \varepsilon_{mf})}{\mu_{app}}$ (5.20)

Falling sphere technique has been employed to determine the apparent viscosity of fluidized beds (Kai et al., 1991), where different powders with mean particle sizes ranging from 35 to 83 μm were used and the terminal velocity of the sphere was estimated in the fluidizing bed.

A model (equation 5.21) was established relating apparent viscosity, bed voidage and mean particle size (Kai et al., 1991).

$$\mu_A = \frac{5.58\ X\ 10^{-5}\ d_p^{0.634} \rho_p^{1.39}\ (1-\varepsilon)}{(\varepsilon - 0.98\varepsilon_{mf})^{\ 0.494}} \tag{5.21}$$

Wei and Chen (2001) assumed that fluidized powders follow Bingham plastic model and estimated the drag coefficient of spherical objects in fluidized granular bed using the method of falling sphere and provided the following model:

$$C_D = \frac{24}{Re_m}\ (1 + 0.15\ Re_m^{0.687}\ ) \tag{5.22}$$

$$Re_m = \frac{d_0\ u_t\ \rho_{bf}}{\mu + \frac{\tau_0 d_0}{3u_t}} \tag{5.23}$$

Bruni et al. (2005) used a mechanically stirred fluidized bed rheometer (MsFBR) to investigate into the rheology of ballotini (d_{50}: 350 μm) and alumina (d_{50}: 75 μm) by measuring the torque near minimum fluidization velocities for different impeller depths of immersions and rotational speeds. Considering uniform stress distribution at any horizontal section of the powder, the following model was provided:

$$\frac{d\ \sigma_z}{dz} + \frac{4\tau_w}{D} + \frac{dP}{dz} = \rho_{bl}\ g \tag{5.24}$$

Reiling (1992) employed a four-bladed paddle viscometer to measure the apparent viscosity of fine powders. The viscosity values obtained were high in the un-fluidized state and it was

observed that the apparent viscosity decreased with an increase in bed voidage. Other comprehensive work on powder rheology was carried out by Gibilaro et al. (2007). In recent years, Mallick (2009) proposed that rheological properties of bulk solids need to be considered for better fundamental and accurate modeling of the transport of dunes during fluidized dense-phase pneumatic conveying. He advocated two-layer dune flow structure to represent the dense-phase flow having a non-suspended highly turbulent dune of powders (liquid-like appearance) flowing along the bottom of the pipeline and a dilute suspension of fine powders was assumed to be transported on top of these dunes. He attempted to incorporate a pseudo-viscosity term to represent solids friction. However, this work was limited due to the lack of rheological data for fine powders. Chen (2013) measured the yield stress of three different powders, alumina, cement and fly ash, at different aeration levels using of double ended cone penetration method. It was concluded that the yield stress decreases with an increase in air flow rates and the decreasing trend ceases at minimum fluidization velocity. An empirical model was developed to establish a relation between yield stress and bulk density. Chen (2013) advocated that the values of yield stress are largely dependent on the type of measurement technique adopted, i.e. the dimension of the spindle used and the quantity of aeration. These studies tend to emphasize the importance of rheological study for accurate modeling of fluidized dense-phase. Overall it can be stated that only limited attempts have been made so far to include rheological parameters of aerated dunes (which tend to behave like pseudo-fluids) in the modeling of important parameters of fluidized dense-phase conveying, such as solids friction factor. Considering the non-Newtonian nature of non suspension layer of the turbulent dune, yield stress of powders is considered to be an important parameter that would govern the limits of powder flow.

Rheological testing of powders was carried out at the Laboratory for Particle and Bulk Solids Technologies, Thapar University. Brookfield YR 1 rheometer with different vane spindles (V-72 to V-75) were used to measure the yield stress values at varying depths of spindle immersion and different rotational speeds of the spindle. The rotational speeds are limited to low values (close to the yield point) for the YR 1 rheometer. The set up has been developed as part of an ongoing research (Chaudhry, 2015) and Figure 5.23 provides the schematic of the set-up. The set up consisted of a 400 mm long acrylic fluidizing chamber attached to the distributor plate. A 5 μm pore-sized mesh was used above the distributor plate to separate the upper and lower fluidizing columns. The mesh prevented the powder from dropping into the lower fluidizing column from where the air was supplied. The powder was poured into this chamber and the spindle was lowered slowly to measure the yield stress. The experiments were performed at an ambient room temperature of 25°C. Low rotational speeds were used from 0.1 to 5 rpm (close to zero strain rate). Three different depths of immersions (for the spindle) were selected as 1.6, 2.3 and 3.4 cm. Before measurement of the yield stress, the powders were heated in an oven for 2 hours and at 90°C to drive off any moisture. Yield stress was measured corresponding to unfluidized state of powders, as the intended solids friction factor model using yield stress value would be used for prediction of pressure drop near the minimum transport boundary (as explained before). The experimental procedure to determine yield stress values have been explained in detail in Chaudhry (2015).

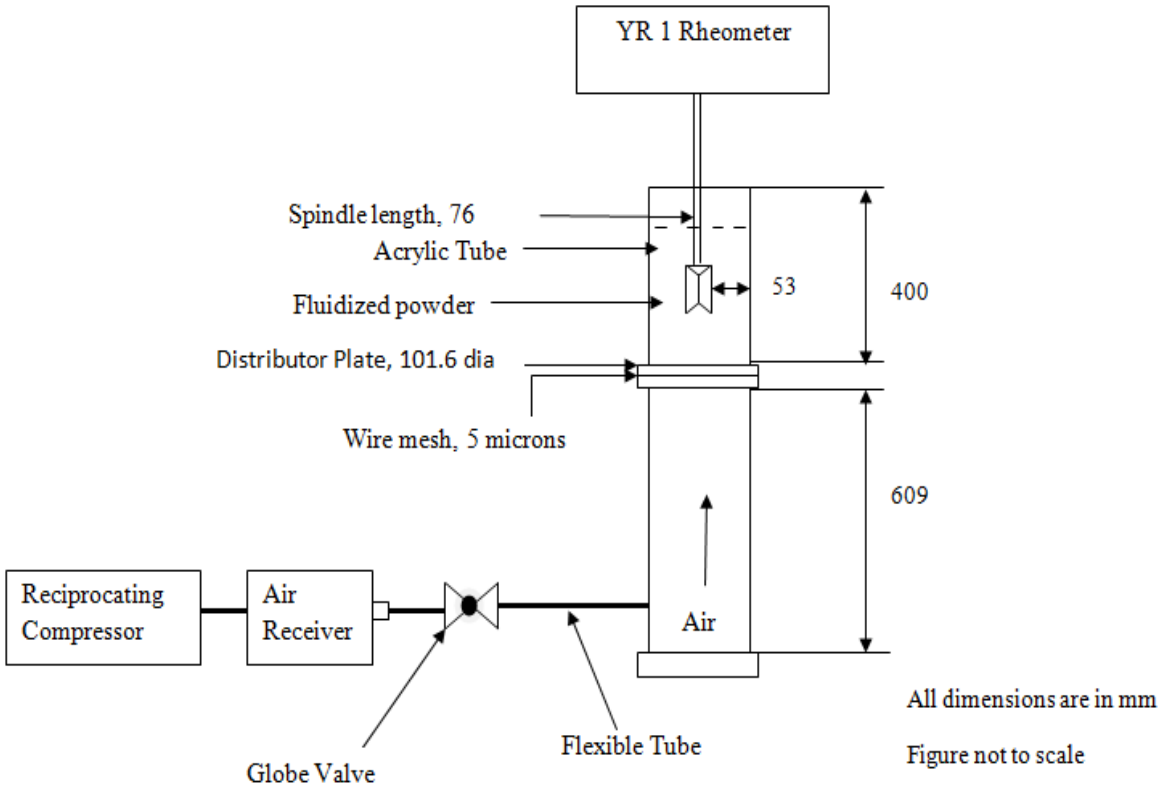

Figure 5.23: Schematic of the set up for powder rheology testing

Table 5.4 provides the measured yield stress values used in thesis for the subsequent modeling work.

Table 5.4: Yield stress and Froude number (at minimum transport limit) for different powders

Material	**Pipeline**	**Yield Stress (Pa)**	$\mathbf{Fr_{min} = \frac{V_{min}}{\sqrt{gD}}}$
Cement	C1	224	4
Fly ash	C1	198	4.4
Cement	C2	224	3
Fly ash	C2	198	2.3

Table 5.4 shows that for the same pipe, an increase in the value of yield stress has resulted in higher Froude number requirement. It can be considered that higher yield stress (caused by inadequate aeration of powders) would require larger amount of air flow to keep the dunes under flow condition. Higher yield stress could be related to the increased tendency of pipeline blockage and to compensate for this, appropriate amount of air flow must be provided. The measured yield stress values can be further used to model the pressure drop in very dense-phase region of pneumatic conveying characteristics. Considering all or most of the solids are transported in the non-suspension flow (Figure 5.22), equation (5.11) (Mallick, 2009) is reduced to:

$$\Delta P = (L/A)\, \tau_w S_1 \qquad (5.25)$$

Where, τ_w ($\tau_w = \tau_1$) is the wall shear stress

It can be considered that with an increase in gas velocity and depletion of the thickness of non-suspension layer (in the director of flow), the non-suspension layers would start to get more aerated (due to an increase in air ingress to the layer). This would result in decrease in wall stress as the dunes would start to flow. To represent the loss of wall stress with an increase in gas velocity, the work of Anjaneyulu and Khakhar (1995) can be referred. An experimental study was carried out on the rheology of glass beads (d_{50}: 400-1000 μm) using a rotary viscometer (Anjaneyulu and Khakhar, 1995) and it was concluded that the yield stress decreases with an increase in the amount of aeration into the fluidization camber. The following relation was proposed relating the yield stress and viscosity of powders (Anjaneyulu and Khakhar, 1995):

$$\tau = \tau_o - \mu r \frac{d}{dr}\left(\frac{v_\theta}{r}\right) \quad (5.26)$$

In this model, v_θ is angular velocity as provided by Chen (2013). The above model for pneumatic conveying through horizontal pipes (translational flow) can be represented as:

$$\tau_w = \tau_o - \mu_{app}\frac{dV}{dy} \quad (5.27)$$

Where, 'y' is counted from the bottom of the pipe to the top surface of the dune. It has been assumed that: (a) the average velocities of the gas and the non-suspension dune layer are the same and is equal to the superficial gas velocity (V) (i.e. there is a consideration of no-slip between the two-phases); (b) the apparent or the pseudo-viscosity of the dune is constant in very dense-phase; (c) the top layer of the dune is flat; (d) all the mass flow rate of solids is happening through the non-suspension layer (i.e. it is a condition of highly dense-phase flow). With the consideration of no-slip condition between the two-layers, S_1 (Figure 5.22) can be represented as:

$$S_1 = 4\, m_s/(\rho_{bl}\, D) \quad (5.28)$$

The hydraulic radius of the non-suspension layer (R_h) is given as:

$$R_h = \sqrt{\frac{m_s}{\rho_{bl} V \pi}} \quad (5.29)$$

Incorporating the above terms in the expression of ΔP and since equation (5.25) is modified to:

$$\Delta P = (L/A)\ \{4\ m_s/(\rho_{bl}\ VD)\}\ (\tau_o\ - \mu_{app}\frac{\Delta V}{\Delta y}) \quad (5.30)$$

Considering the velocity difference ΔV is the velocity difference between the average dune velocity (V) (at y = R_h, hydraulic radius) and the velocity of dune at the bottom of pipe (V= 0, at y = 0) (due to boundary layer formation), equation (5.30) can be further modified to:

$$\Delta P = (L/A)\ \{4\ m_s/(\rho_{bl}\ VD)\}\ (\tau_o\ - \mu_{app}\frac{V}{\sqrt{\frac{m_s}{\rho_{bl}V\pi}}}) \quad (5.31)$$

Fly ash and cement were conveyed from 10 to 18 t/h and 10 to 22 t/h, respectively through pipeline C1 (65 mm I.D × 254 m long pipe). For the given values of pressure drops close to the minimum transport limits (275 and 260 kPa for fly ash and cement, respectively), the apparent viscosity values were calculated corresponding to the minimum Froude number values provided in Table 5.5.

Table 5.5: Experimental versus predicted pressure drops for fly ash and cement

Material	**Pipeline**	**Fr_{min}**	**Mass flow rate of solids (t/h)**	**Experimental pressure drop (kPa) (A)**	**Predicted pressure drop (equation 5.31) (kPa) (B)**	**Percentage Relative error: (B-A)/A × 100**
Cement	C1	4	22	430	405	6%
Fly ash		4.4	18	370	388	5%

The results show that the model (equation 5.31) has predicted the pressure drop values for higher material flow rates quite accurately. This indicates that the new model is able to adequately address the dense-phase flow mechanism. The model in its present form appears suitable for the scaling up of solids flow rate near the minimum transport limit. Future scope will include amending the model further to incorporate the effect of change of pipe diameter (diameter step-up).

5.7 Conclusion

Existing models for solids friction factor use solids loading ratio and Froude number as dimensionless parameter groupings in the power function format. This model format, when tested under proper scale-up conditions of pipe diameter and length, generally result in significant under- or over-predictions. The new model format developed using a new combination of dimensionless terms, volumetric loading ratio and dimensionless velocity (ratio of free setting velocity of particle to superficial gas velocity) by the replacing solids loading ratio and Froude number terms, has provided improved predictions (from 6.8 to 66.2 %) when the model predictions are tested under significant scale-up conditions for 4 different products conveyed through 4 different test rigs in two different laboratories. The new model format is intended to address the occupancy of solids volume fraction in the pipe, which contributes to solids to solids, solids to air and solids to pipe wall interactions and the associated pressure drop. Moreover, the dimensionless velocity ratio term is aimed at addressing the transition from non-suspension to suspension flow. A two-layer based model for solids friction has been developed by separately considering the solids friction

contributions of the non-suspension and suspension layer of particles and suitably combining them using a Froude number based criteria. Models developed for two different samples of fly ash, cement and ESP dust, when tested under scale-up conditions by using them to predict the pressure drops for larger and longer pipelines and by comparing the experimental and predicted pneumatic conveying characteristics, have resulted in better reliable predictions compared to the newly developed uniform flow models. The predicted pneumatic conveying characteristics have shown 'U'-shaped trends that are following the shapes of experimental PCC more closely compared to the existing models indicating that the new two-layer model has the capability to address the gradual transition of dense- to dilute-phase flow mechanisms of fine powders with an increase in conveying gas velocity. Future work should be focused to improve the accuracy of the model for step-up pipelines. Also, a new model has been developed to predict pressure drop using powder yield stress. The model has been validated by using it to predict the pipeline drop for higher tonnages by comparing the experimental values of pressure drops versus the predicted values. Results have shown the new model could predict pressure drop quite accurately. Future scope of research would include validation of the model for pressure drop for other powders and pipelines.

CHAPTER 6

Modeling Minimum Transport Boundary

6.1 Introduction

For the reliable design of fluidized dense-phase pneumatic conveying systems, it is of paramount importance to accurately estimate blockage conditions or the minimum transport boundary. Over-estimation of the minimum transport boundary would cause unnecessarily high velocities, thus nullifying many of the advantages of low-velocity dense-phase conveying. Under-estimation of the minimum transport boundary would result in unstable conveying, product build-up in the line and/or pipe blockage. Therefore, it is essential that the blockage condition or the minimum air velocity requirement to sustain stable conveying be modeled and scaled-up reliably. The existing models (such as Weber, 1981; Rizk, 1982; Martinussen, 1996; Mills, 2004; Mallick, and Wypych, 2009; Mallick et al., 2011) are mostly empirical and have not been adequately examined for their accuracy for different products and pipeline scale-up conditions. These models are provided in detail in Chapter 2. The aim of this chapter is to test the reliability of the existing models and to validate a new unified model to predict the minimum transport boundary for the fluidized dense-phase pneumatic conveying of powders.

6.2 New model development for minimum transport criteria

In this section, an attempt has been made to develop a unified model (and not particle specific model) for a wider range of applications and usability. In this approach, models in two different formats have been developed by using a large number and variety of data points of 22 different powders conveyed through 38 pipelines (covering high to low solids flow rates).

The various products and pipelines are summarized in Table 6.1. The first format (New model 1) is provided by equation (6.1); however, the 'K' and 'a' values are to be determined not for individual products, but by combining the large number of data sets (viz. 22 products and 38 pipelines). Setia et al. (2013) provided a format (given by equation 6.1), where Froude number (Fr) term signifies that higher minimum conveying velocity is required for larger pipe diameters and solids loading ratio (m*) signifies that with an increase in solids loading ratio, the product exhibits a self-pushing or self-cleaning effect. It has been experimentally observed that for larger diameter pipes, higher air velocity is required. The same has been reported in Mallick and Wypych (2009). Hence, it was considered prudent to continue to use Froude number in the minimum transport criteria model. Also, it has been found experimentally that products are able to be conveyed at somewhat lower velocities for higher mass flow rates of solids, e.g. 22 t/h of cement was conveyed with a minimum Froude number of $Fr_i = 4$ (see Figure 4.5), but the same product could be conveyed at $Fr_i = 3$ for 36 t/h (see Figure 4.6). Similarly, 18 t/h of fly ash was conveyed with a minimum Froude number of $Fr_i = 4.4$ (see Figure 4.7), but the same product could be conveyed at $Fr_i = 2.3$ for 30 t/h (see Figure 4.8). Similar observations were also found in Mallick (2009). These show that higher product throughput may actually be assisting self-cleaning or self-pushing of dunes through the pipes, but of course too high product flow rate could lead to pipeline blockage. Considering these aspects, the new model format (format 1, equation 6.1) has been provided below.

New model format 1: $Fr_i = K\,(m^*)^{a}$ (6.1)

In the second format, further improvement in modeling has been attempted by directly incorporating some particle parameters in the form of a particle Froude number. The format is

given by equation (6.2). In this format, the gas velocity requirement to prevent pipeline blockage is a function of pipe diameter, particle Froude number (based on free settling velocity of particles and averaged diameter of particle) and solid loading ratio (representing the self-cleaning effect). Therefore, this model incorporates the effect of particle properties (particle size and density). Hence, this format can be used for different powders. The 'K', 'a' and 'b' values are to be determined from the large number of data sets (viz. 22 products and 38 pipelines). The new model includes important parameters such as the solids loading ratio and particle properties in addition to the pipe diameter effect. Thus, the new model is significantly more capable than the existing model ($Fr_{min} = 6$). It has been experimentally seen that at higher solids loading ratios, the products seem to be self-pushing and needing relatively low velocities for reliable transport. Therefore the effect of m* should not be ignored. Additionally, the aim of the new model was to incorporate the particle parameters in the model, so that the model can be applied reliably for different products. With this view, a particle Froude number term has been incorporated that aims to include the effects of particle diameter and density.

New model format 2: $Fr_i = K\,(m^*)^{a}\,(Fr_p)^{b}$ (6.2)

Where, Fr_p is particle Froude number defined as $Fr_p = w_{fo} / (g\,d)^{0.5}$

Table 6.1: Summary of 22 products conveyed and 38 pipeline configurations

No.	Powders	d_{50} (μm)	ρ_s (kg/m^3)	ρ_{bl} (kg/m^3)	Blow tank type	D (mm)	L (m)	L_h (m)	L_v (m)	$L_v/L \times 100\%$	No. of bends	Percentage loss of pressure in verticals	Percentage loss of pressure in bends
1	ESP dust (Mallick, 2009)	7	3637	610	BD	69 69 105	168 554 168	161 547 161	7 7 7	4 1 4	5 17 5	7.2 2.2 7.2	10 11 10
2	Fly ash (Mallick, 2009)	30	2300	700	BD	69 69 105	168 554 168	161 547 161	7 7 7	4 1 4	5 17 5	7.2 2.2 7.2	10 11 10
3	White powder (Mallick, 2009)	55	1600	620	BD	69	148	142	6	4	6	6.7	14
4	Barytes (Ratnayake, 2005)	12	4200	*	TD	75 75 100 125	72 66 66 68	64 66 66 68	8 0 0 0	11 0 0 0	5 4 4 4	16 0 0 0	20 20 20 19
5	Cement (Ratnayake, 2005)	15.5	3100	*	TD	75 75 100 125	72 66 66 68	64 66 66 68	8 0 0 0	11 0 0 0	5 4 4 4	16 0 0 0	20 20 20 19

No.	Powders	d_{50} (μm)	ρ_s (kg/m^3)	ρ_{bl} (kg/m^3)	Blow tank type	D (mm)	L (m)	L_h (m)	L_v (m)	$L_v/L \times 100\%$	No. of bends	Percentage loss of pressure in verticals	Percentage loss of pressure in bends
6	Ilmenite (Ratnayake, 2005)	9.5	4600	*	TD	75 100 125	66 66 68	66 66 68	0 0 0	0 0 0	4 4 4	0 0 0	20 20 19
7	Bentonite (Ratnayake, 2005)	25	2800	*	TD	75	72	64	8	11	5	16	20
8	Alumina 1 (Ratnayake, 2005)	59.2	2800	*	TD	75	138	130	8	6	9	8.8	20
9	Alumina 2 (Ratnayake, 2005)	72	2800	*	TD	75	138	130	8	6	9	8.8	20
10	Alumina 3 (Ratnayake, 2005)	79.3	2800	*	TD	75	138	130	8	6	9	8.8	20
11	Alumina 4 (Ratnayake, 2005)	86.7	2800	*	TD	75	138	130	8	6	9	8.8	20
12	Alumina 5 (Ratnayake, 2005)	90.5	2800	*	TD	75	138	130	8	6	9	8.8	20

No.	Powders	d_{50} (μm)	ρ_s (kg/m^3)	ρ_{bl} (kg/m^3)	Blow tank type	D (mm)	L (m)	L_h (m)	L_v (m)	$L_v/L \times 100\%$	No. of bends	Percentage loss of pressure in verticals	Percentage loss of pressure in bends
13	Cement (Mills, 2004)	14	3060	1070	TD	81 53	95 101	95 101	0 0	0 0	9 17	0 0	28 40
14	Fly ash (Pan, 1992)	15.5	2197	634	BD	52.5 52.5 69 69	102 135 172 553	96 129 165 547	6 6 7 6	6 4 4 1	4 4 5 17	9.6 7.6 7 2	13 10 10 11
15	Tallawarra fly ash (Wypych, 1989)	20	2350	500	BD	52	71	67.4	3.6	5	11	6	37
16	Eraring fly ash (Wypych, 1989)	27	2160	880	BD	52	71	67.4	3.6	5	11	6	37
17	Munmorah fly ash (Wypych, 1989)	25	2100	650	BD	52	71	67.4	3.6	5	11	6	37
18	Vales Point fly ash (Wypych, 1989)	19	2130	700	BD	52	71	67.4	3.6	5	11	6	37
19	Gladstone fly ash (Wypych, 1989)	18	2250	1030	BD	52	71	67.4	3.6	5	11	6	37

No.	Powders	d_{50} (μm)	ρ_s (kg/m^3)	ρ_{bl} (kg/m^3)	Blow tank type	D (mm)	L (m)	L_h (m)	L_v (m)	$L_v/L \times 100\%$	No. of bends	Percentage loss of pressure in verticals	Percentage loss of pressure in bends
20	Wallerawang fly ash (Wypych, 1989)	12	2195	455	BD	52	71	67.4	3.6	5	11	6	37
21	Liddell fly ash (Wypych, 1989)	13	2415	640	BD	52	71	67.4	3.6	5	11	6	37
22	Cement (Wypych et al.,1984)	20	3100	950	BD	69	168	161	7	4	5	7.2	10
* Not provided in source reference													

Using the minimum transport boundary data provided in Table 6.1, the values of 'K', 'a' and 'b' have been calculated. The new models and the correlation coefficient values are provided by equations (6.3) and (6.4), as follows:

New model 1: $Fr_{min} = 40(m^*)^{-0.48}$ $[R^2 = 0.87]$ (6.3)

New model 2: $Fr_{min} = 23.5\,(m^*)^{-0.396}\,(Fr_p)^{0.131}$ $[R^2 = 0.89]$ (6.4)

6.3 Validation of models of minimum transport boundary criteria

The above models (existing and new models) have been validated for their reliability by using them to predict the blockage boundary for two fly ash and cement samples conveyed through different pipelines in dense-phase. Conveying trails were performed using fly ash at the Laboratory for Bulk Solids and Particulate Technologies of Thapar University (India) and with fly ash and cement at the pneumatic conveying test set-up of Fujian Longking Co., Ltd. (China) with different pipeline configurations. The product properties and pipeline details are provided in Table 6.1. The new models 1 and 2 were not developed from the data of these products and pipelines for proper validation. Figure 6.1 shows the predictions of different models for cement conveyed through the 65 mm I.D. and 254 m long pipe**.**

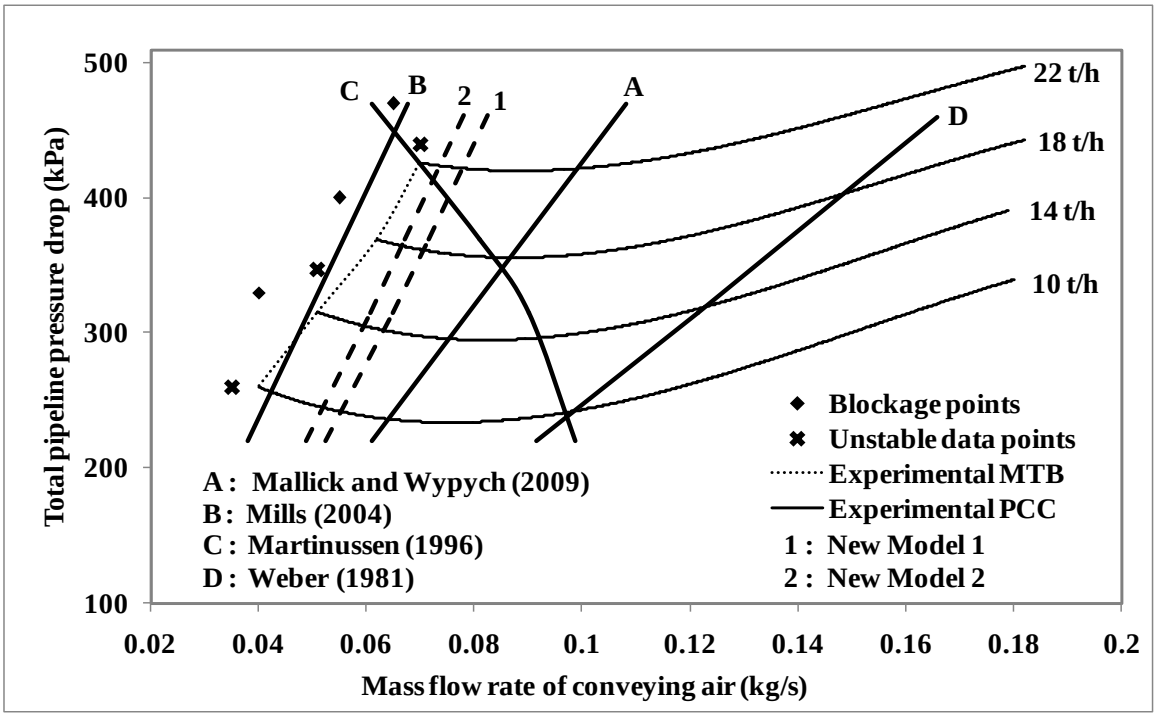

Figure 6.1: Validation of models of minimum transport boundary for cement through pipeline C1 (65 mm I.D. × 254 m long pipe)

It can be seen that the Mallick and Wypych (2009) and Weber (1981) models provide over-predictions; in fact, the Weber (1981) model predicts significantly higher air flow rate requirements. This could be due to the positive exponents of solids loading ratio in the expression of the Weber (1981) model. As a result, it has predicted higher velocities for larger tonnages. The Mills (2004) model has provided some under-predictions; hence use of this model for this product and pipeline could result in unstable flow and pipe blockage. The new models 1 and 2 provided reasonably good predictions (with trivial amounts of over-predictions), with model 2 providing the best results. The Martinussen (1996) model predicted trends of minimum transport boundary that contradicted the slopes of the experimental blockage boundary. The Martinussen (1996) model provided significantly lower air flow rate requirements at higher solids flow rates; i.e. the model would predict unnecessarily high amount of air flows in lower tonnages, but would result in unstable

conveying or pipe blockage at higher air flows. This could be because the minimum conveying velocity requirement decreases with an effective exponent of 1.5 to m* as per this model, i.e. the minimum predicted velocity according to this model would rapidly decrease with an increase in m*. As a result, the model predicts significantly lower transport limits at higher solids flow rates (due to rise in m*). As a result, it has been decided not to further evaluate the model in subsequent figures. Figure 6.2 shows the predictions of different models for cement conveyed through 80/100 mm I.D. and 407 m long stepped-diameter pipeline**.**

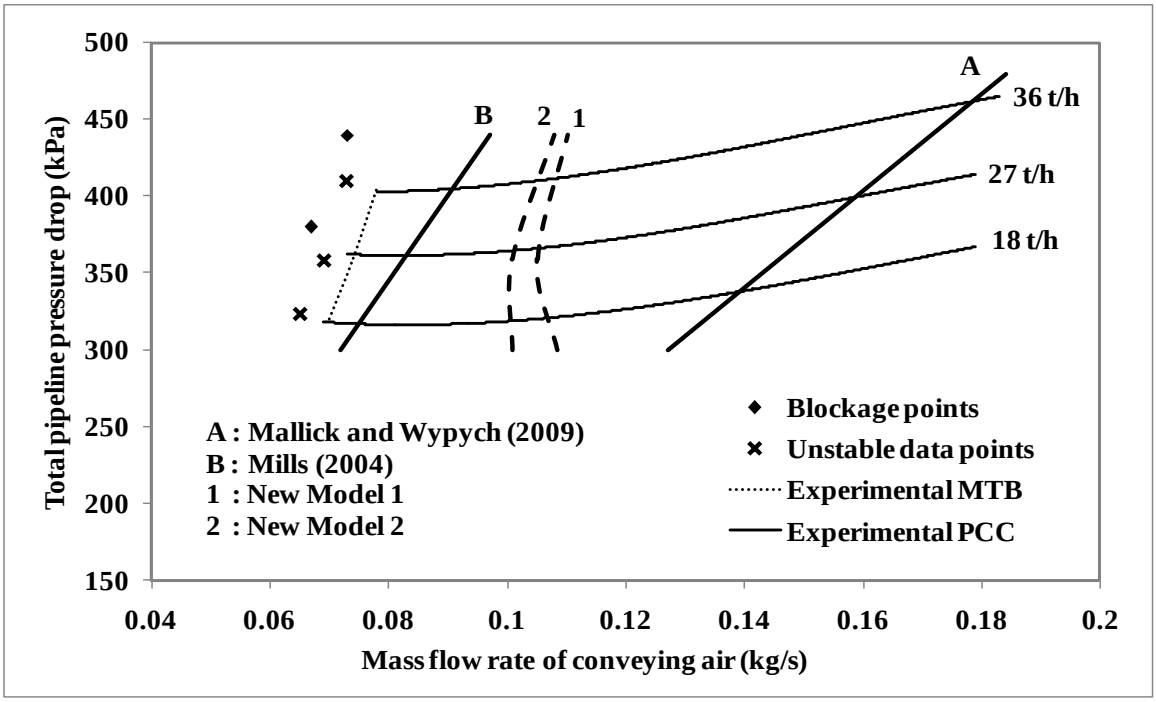

Figure 6.2: Validation of models of minimum transport boundary for cement through pipeline C2 (80/100 mm I.D. × 407 m long stepped-diameter pipeline)

It can be seen from Figure 6.2 that for longer pipe (407 m length) and higher mass flow rate of solids, conveying was possible with relatively lower velocities (compared to Figure 6.1). As a result, the Mills (2004) model provided good predictions in this case. The Mallick and Wypych (2009) model provided large over-predictions. The new models 1

and 2 provided similar results, with the new model 2 providing predictions that are closer to the experimental blockage boundary. The Martinussen (1996) model provided similar trends as shown in Figure 4. Also, the Weber (1981) model predicted excessively high air flows (beyond the range of Figure 4.5). Hence prediction with the Weber (1981) model has not been included in Figure 6.2. Figure 6.3 and 6.4 show the predictions of different models for fly ash conveyed through pipeline C1 and C2 (i.e. 65 mm I.D. and 254 m long and 80/100 mm I.D. and 407 m long pipes)

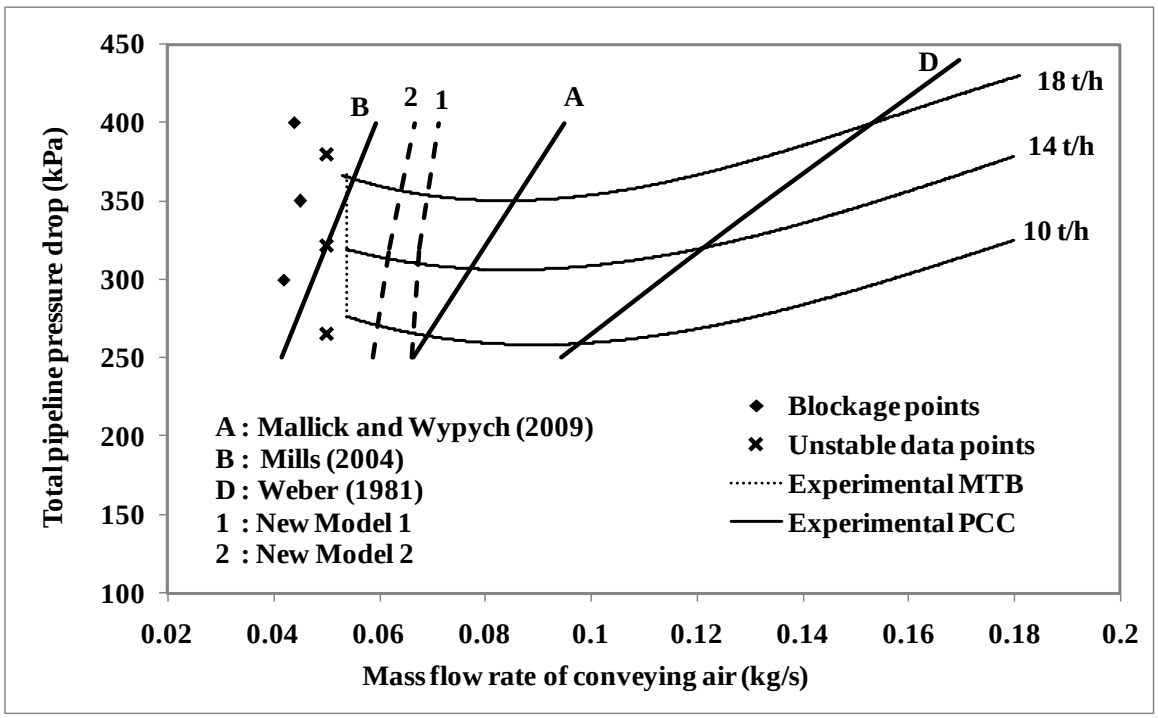

Figure 6.3: Validation of models of minimum transport boundary for fly ash through pipeline C1 (65 mm I.D. × 254 m long pipe)

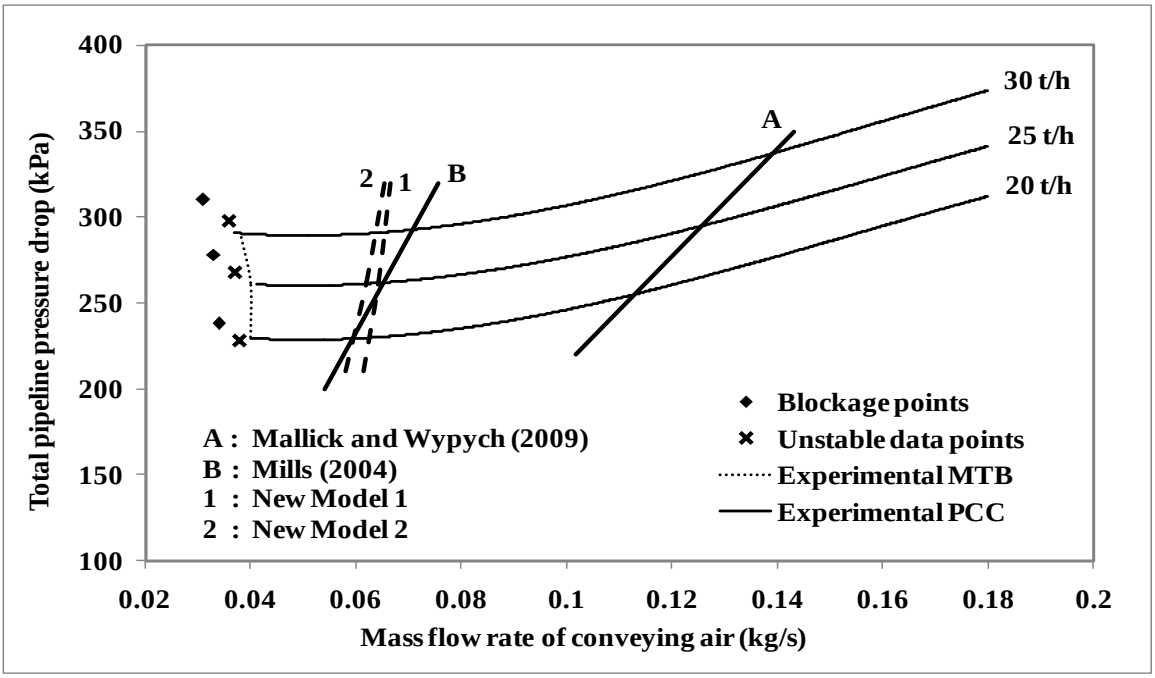

Figure 6.4: Validation of models of minimum transport boundary for fly ash through pipeline C2 (80/100 mm I.D. × 407 m long stepped-diameter pipeline)

Figures 6.3 and 6.4 show that the trends of predictions with the models for fly ash are similar to that of cement. Figure 6.3 shows that the model of Mills (2004) shows under-predictions. The Weber (1981) and Mallick and Wypych (2009) models provided significant over-predictions. Hence, these models would result in unnecessarily higher air flows than what would be sufficient to achieve stable conveying, thus affecting system optimization and increasing the operating and maintenance costs of the system. The new models have provided stable-predictions, of which the new model 2 has resulted in most optimized predictions (i.e. the minimum transport boundary predicted by new model 2 is closest to the experimental blockage boundary and does not predict operating conditions to the "left "of the experimental blockage boundary). It is again found (similar to cement) that for higher tonnages, transport is possible with lower air velocity. This is perhaps due to the "self-pushing" effect of the products. Figures 6.5 to 6.8 show the predictions of different models for fly ash conveyed at Thapar University through pipelines B1, B2, B3

and B4. In Figures 6.5, 6.6 and 6.7, the pipe length was kept at 24 m for both cases and only the internal diameters were different – ranging from 43, 54 and 69 mm (B1, B2 and B3 pipeline). Therefore, Figures 6.5, 6.6 and 6.7 are intended to represent the effect of increase in pipe diameter on the experimental minimum transport boundary and prediction of the same using different models. Figure 6.8 shows results from the model evaluations for the 54 mm I.D and 70 m long pipe (Pipeline B4). Comparison of Figures 6.6 and 6.8 is intended to address the effect of length scale-up (for the same pipe diameter, pipeline B2 and B3) on the prediction capability of models.

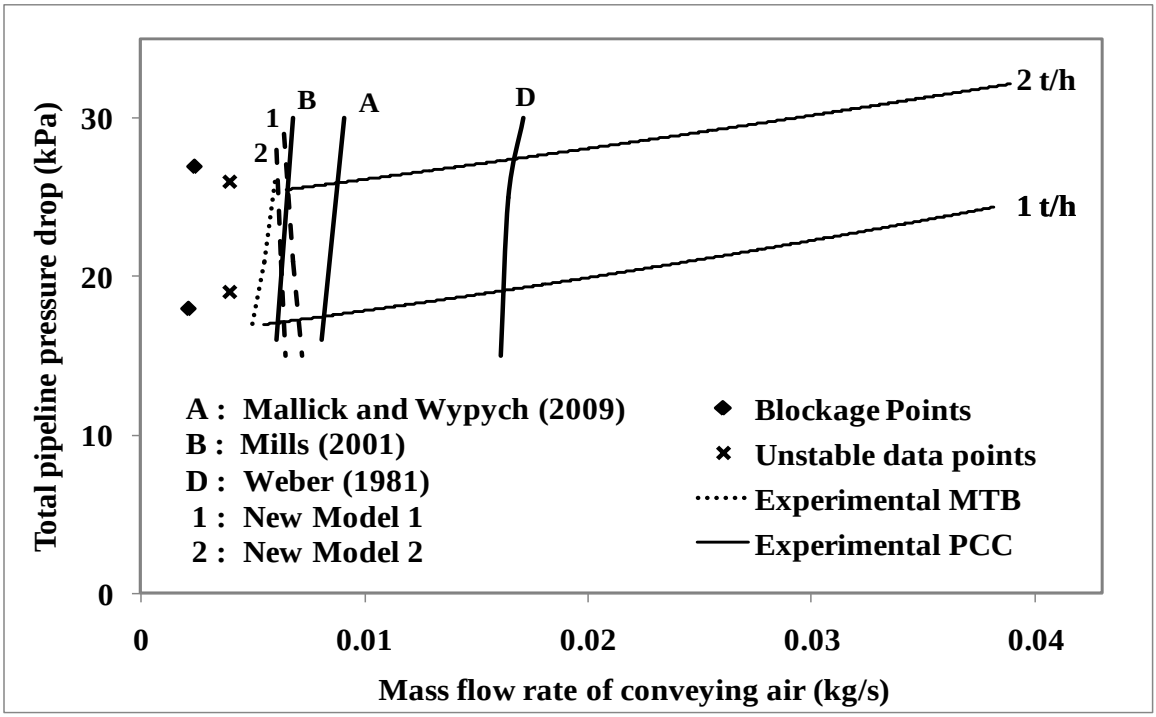

Figure 6.5: Validation of models of minimum transport boundary for fly ash (Thapar University) through pipeline B1 (43 mm I.D. × 24 m long pipe)

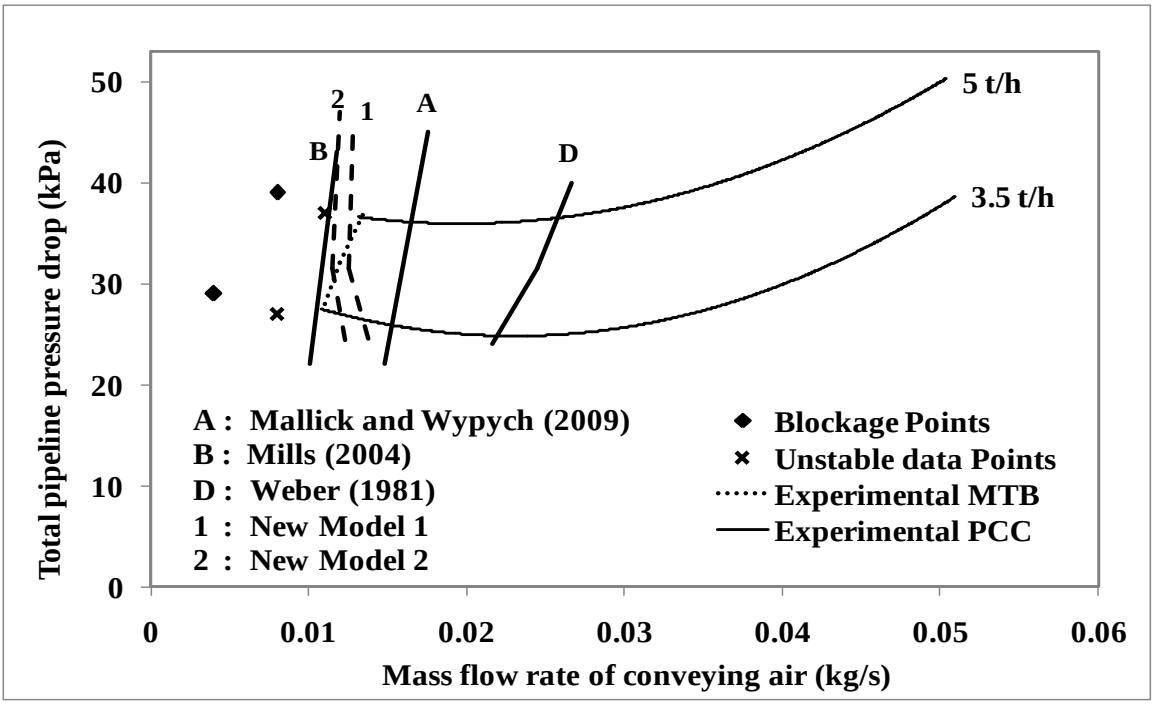

Figure 6.6: Validation of models of minimum transport boundary for fly ash (Thapar University) through pipeline B2 (54 mm I.D. × 24 m long pipe)

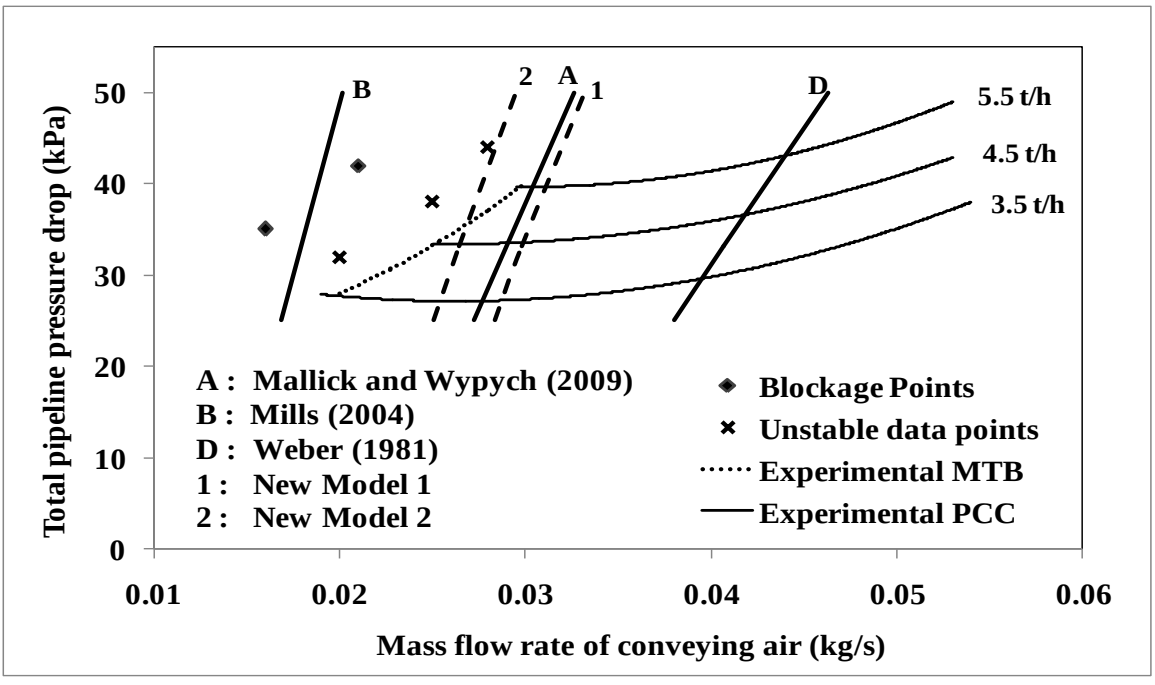

Figure 6.7: Validation of models of minimum transport boundary for fly ash (Thapar University) through pipeline B3 (69 mm I.D. × 24 m long pipe)

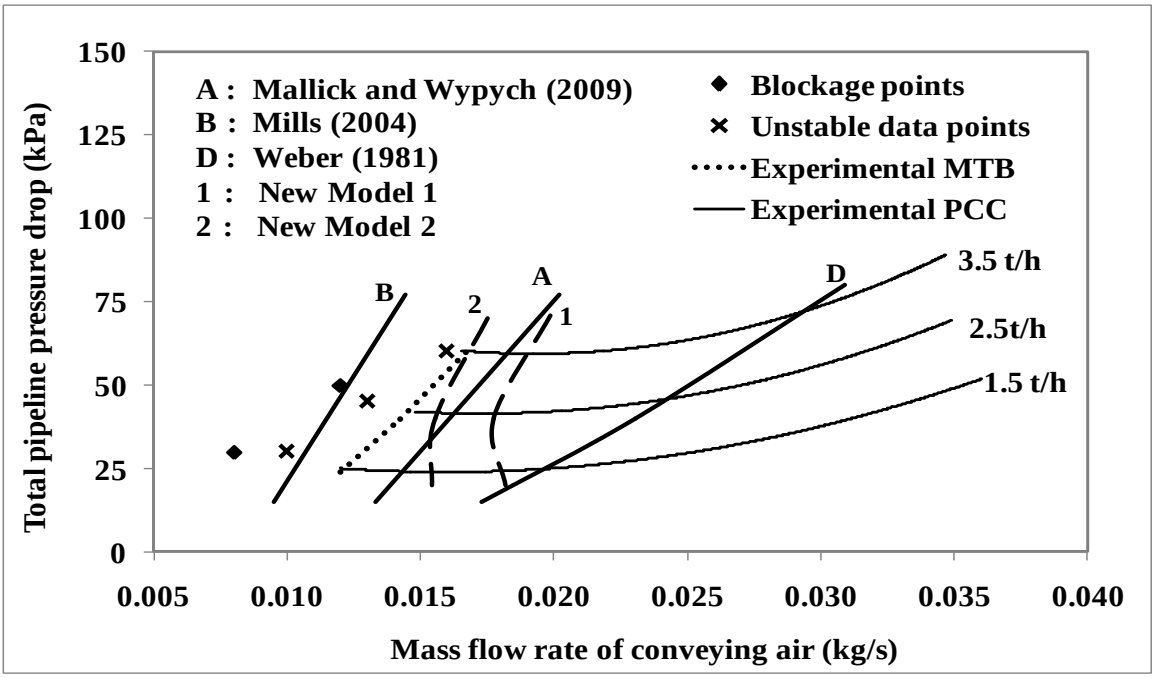

Figure 6.8: Validation of models of minimum transport boundary for fly ash (Thapar University) through pipeline B4 (54 mm I.D. × 70 m long pipe)

Figures 6.5, 6.6 and 6.7 show that the Weber (1981) model consistently provided large amounts of over-prediction. The Mills (2004) model provided good predictions for smaller pipelines. However, this model resulted in under-predictions (i.e. predicting possible transport within the blockage zone) when the diameter was scaled-up from 54 to 69 mm. This demonstrates that a constant velocity based model is not adequate and the effect of pipe diameter must be incorporated in selecting minimum transport boundary criteria. The Mallick and Wypych (2009) model provided some over-predictions in each case. New models 1 and 2 resulted in predictions that are very close to the actual blockage boundary. However, they tend to show some under-predictions for Figure 6.6 and partially for Figure 6.7. It seems that the new models are better for larger tonnages. A comparison between Figures 6.6 and 6.8 shows that the relative prediction capabilities of new models remain unaffected due to the change in pipe length (for the same diameter of pipe). However, they

tend to show some under-predictions partially for Figure 6.7. It seems that the new models are better for larger tonnages.

6.4 Conclusions

In this chapter, based on the test results of 22 powders conveyed through 38 pipelines, unified models for minimum transport boundaries have been developed using 2 formats, which are: gas Froude number represented as a power function of only solids loading ratio; and as a power function of solids loading ratio and particle Froude number. The models were evaluated by predicting the blockage boundary for three different products, conveyed through six different pipelines by comparing the predicted versus experimental blockage boundaries. Seven other models were also evaluated against the same set of test results. Results showed that the existing models provided considerable over- or under-predictions and could become unexpectedly unreliable causing either unnecessarily high air flow rates or pipe blockage. The new model developed and presented in this chapter that is based on gas Froude number as a power function of solids loading ratio and particle Froude number appears to provide the relatively better accurate and stable predictions. The model incorporates both pipe diameter effect and some important physical properties of the particles. The model has the potential to serve the purpose for minimum transport boundary criteria for wide range of products, as the model incorporates a particle settling velocity term, which in turn depends on particle density and size. In this chapter, the variation in pipe diameter is from 52 to 125 mm (about a factor of 2.5). Future work will include validation of the model in large industrial set-ups.

CHAPTER 7

Conclusions and Future Scope of Work

7.1 Conclusions

Test facilities were developed at the laboratory for Particle and Bulk Solids Technologies, Thapar University, India for the fluidized dense-phase flow of fine powders having different pipeline configurations. Fly ash was conveyed through this test rig and another sample of fly ash and cement were conveyed through the large diameter and long diameter test rigs of Fujian Longking Co., China. These and the additional test data obtained from the University of Wollongong, Australia were used for the purpose of modeling of solids friction factor and minimum transport boundary and validation of the same under scale-up conditions. The major outcomes of this thesis are:

A new model format has been developed using a new combination of dimensionless terms: volumetric loading ratio and ratio of free setting velocity of particle to superficial gas velocity. It is found that the new model generally provided improved predictions in the dense-phase region. Whereas the existing models (using solids friction factor and gas Froude number) predicted pressure drop with average absolute relative errors varying between 10.8 to 85.5% (depending on product and pipeline conditions), the new developed model resulted in predictions within 19.3% accuracy for a wide range of scale-up conditions, which provides better reliability and narrower range of predictions and more suitable for industrial scale-up requirements.

A two layer flow modeling format has been developed considering a dense non-suspension dune type flow is occurring along the bottom of pipe and on top of which a dilute-phase suspension layer of powders is believed to be occurring. Two different models were used to represent the two different flow mechanisms (non-suspension and suspension flow) and were coupled by suitable factors. Validation of this approach

resulted in predictions within 14 % accuracy for a wide range of scale-up conditions. More importantly, the trends of predicted Pneumatic Conveying Characteristics could follow the experimental data much better (more pronounced 'U'-shaped characteristics), representing that the two-layer model could better address the dense- to dilute-phase flow transition.

A new unified model for minimum transport boundary criteria has been developed using dimensionless solids loading ratio and particle Froude number. The particle Froude number terms contains different particle properties, thus making the model useful for a variety of fine powders. The model was validated and the results showed considerable improvement in prediction capability.

7.2 Future scope of work

Further scope of work will include:

- Incorporation of specific material characteristics to model minimum transport boundary criteria and solids friction factor, e.g. in the models, the median particle diameter or d_{50} has been used instead of particle size distribution. Attempt should be made to incorporate the effects of particle size distribution in the proposed models. The effects of particle shape on the flow characteristics (such as pressure drop, minimum transport and dense to dilute-phase transition criteria) need to be investigated. Effort is to be made to incorporate the fluidization and deaeration characteristic of the bulk powders in the models of solids friction factor and minimum transport.

- Development of reliable methods for the measurement of powder rheology representing the actual flow condition (measured at different bed depths and aeration conditions for various powders) and incorporation of these data in the model for solids friction factor.
- Investigation into the effects of blow tank operation and design towards optimizing the solids flow rate, e.g. the optimum combination of pre-pressurization, amount of conveying and fluidization air, bottom versus side discharge for different powders.
- Development of accurate technique for the measurement of the flow velocity of the non-suspension and suspension layers.
- Overall, more fundamental approach is required to represent fluidized dense-phase flow of fine powders.

REFERENCES

Ahmed, A.M. and Elghobashi, S. 2000. On the mechanisms of modifying the structure of turbulent homogeneous shear flows by dispersed particles. Physics of Fluids. 12: 2906-2920.

Anjaneyulu, P. and Khakhar, D. V. 1995. Rheology of a gas-fluidized bed. Powder Technology, 83, 29-34.

Arnold, P.C., Wypych, P.W. and Reed, A.R. 1994. Advances in the design of pneumatic transport systems. Powder Handling and Processing. 6 (1): 9-19.

Bansal, A. 2012. ME Dissertation: Investigation into straight pipe pressure drop and flow-mode transition criteria for fludised dense-phase pneumatic conveying systems, Thapar university.

Barth, W. 1958. Strömungsvorgänge beim transport von festteilchen und flüssigkeitsteilchen in gasen. Chemie – Ing. – Techn. 30 (3): 171-180.

Batchelor, G. K. 1970. The stress system in a suspension of force-free particles. Journal of Fluid Mechanics, 41, 545-570.

Batchelor, G. K. and Green, J. T. 1972. The determination of the bulk stress in a suspension of spherical particles to order c2. Journal of Fluid Mechanics, 56, 401-427.

Behera, N., Agarwal, V. K., Jones, M. G. and Williams, K. C. 2013a. CFD modeling and analysis of dense phase pneumatic conveying of fine particles including particle size distribution. Powder Technology, 244, 30-37.

Behera, N., Agarwal, V. K., Jones, M. G. and Williams, K. C. 2013b. Modeling and analysis for fluidized dense phase conveying including particle size distribution. Powder Technology, 235, 386-394.

Bingham, E. C. and Thompson, T. R. 1928. The fluidity of mercury1, 2. Journal of the American Chemical Society, 50, 2878-2883.

Bradley, M.S.A. 1990. PhD Dissertation: Prediction of pressure losses in pneumatic conveying pipelines, Thames Polytechnic.

Bruni, G., Colafigli, A., Lettieri, P. and Elson, T. 2005. Torque Measurements in Aerated Powders Using a Mechanically Stirred Fluidized Bed Rheometer (msFBR). Chemical Engineering Research and Design, 83, 1311-1318.

Chambers, A. J., and Marcus, R. D. 1986. Pneumatic conveying calculations. In the proceedings of 2nd International Conference on Bulk Materials Storage and Transportation, Wollongong, Australia, 7–9 July: 49-52.

Chaudhry, B. 2015. ME Dissertation An experimental investigation into the Rheology of fine powders for modelling fluidized dense-phase pneumatic conveying, Thapar university.

Chen, W. 2013. PhD Dissertation: The rheology of aerated fine powders: theory and application in pneumatic conveying systems. University of Newcastle, Australia.

Chen, W., Williams, K. C., Jabs, I. and Jones, M. G. 2014. A qualitative study on the pulsatile flow phenomenon in a dense fly ash pneumatic conveyor. Particuology, 17, 81-91.

Datta, B.K. and Ratnayaka, C. 2003. A simple technique for scaling up pneumatic conveying systems. Particulate Science and Technology. 21: 227-236.

Datta, B.K. and Ratnayaka, C. 2005. A possible scaling-up technique for dense phase pneumatic conveying. Particulate Science and Technology. 23: 201-204.

Dogadkin, B. and Pewsner, D. 1931. The Structure Viscosity of Rubber Solutions. Rubber Chemistry and Technology, 4, 345-353.

Eckhoff, R. K. 1997. Understanding Dust Explosions. The Role of Powder Science and Technology. KONA Powder and Particle Journal, 15, 54-67.

Einstein, A. 1956. Investigations on the Theory of the Brownian Movement, Courier Corporation.

Elgobashi, S. 1994. On predicting particle laden turbulent flows. Applied Scientific Research. 52: 309-329.

Gibilaro, L. G., Gallucci, K., Di Felice, R. and Pagliai, P. 2007. On the apparent viscosity of a fluidized bed. Chemical Engineering Science, 62, 294-300.

Gidaspow, D., 1994. Multiphase flow and fluidization: continuum and kinetic theory descriptions. Academic press.

Grace, J. R. 1970. The viscosity of fluidized beds. The Canadian Journal of Chemical Engineering, 48, 30-33.

Guo, X., Lu, W., Lu, H., Cong, X., Xie, K., Liu, H. and Gong, X. 2013. Pressure drop prediction for horizontal dense-phase pneumatic conveying of pulverized coal associated with feeding to gasifier. Chemical Engineering Research and Design, 91, 2509-2514.

Hilgraf, P. 1988 Influencing Variables in the Energy Optimization of Dense-phasePneumatic Conveying Systems.ZKG (Zement-Kalk-Gips) International.8(41): p. 374-380.

Huber, N. and Sommerfeld, M. 1998. Modelling and numerical calculation of dilute-phase pneumatic conveying in pipe systems. Powder Technology. 99: 90-101.

Jones, M.G. and Williams, K.C. 2003. Solids friction factors for fluidized dense phase conveying. Particulate Science and Technology. 21: 45-56.

Jones, M.G. Williams, K.C. and Busteed, S.S. 2008. Analysis of transient behaviour in the dense phase conveying of powders. In the Proceedings of 4th International Symposium Reliable Flow of Particulate Solids, Norway.

Kai, T., Murakami, M., Yamasaki, K.-I. and Takahashi, T. 1991. Relationship between Apparent Bed Viscosity and Fluidization Quality in a Fluidized Bed with Fine Particles. Journal of Chemical Engineering of Japan, 24, 494-500.

Kalman H., Satern, A. Meir, D. and Rabinovich E. 2005. Pickup (critical) velocities of particles, Powder Technology, Vol. 160: 103-113.

Keys, S. and Chambers, A.J. 1995. Scaling pneumatic conveying characteristics for Pipeline Pressure. Powder Handling and Processing. 7 (1): 59-62.

Knowlton, T.M., Mountziaris, T.J. and Jackson, R., 1986. The effect of pipe length on the gravity flow of granular materials in vertical standpipes. Powder technology, 47(2), pp.115-128.

Klinzing, G.E. and Rizk F., Marcus R.D., Leung L.S. 2010. Pneumatic conveying of solids - A theoretical and practical approach. Third edition. Springer.

Li, K., Kuang, S. B., Pan, R. H. and Yu, A. B. 2014. Numerical study of horizontal pneumatic conveying: Effect of material properties. Powder Technology, 251, 15-24.

Ma, A. C., Williams, K. C., Zhou, J. M. and Jones, M. G. 2010. Numerical study on pressure prediction and its main influence factors in pneumatic conveyors. Chemical Engineering Science, 65, 6247-6258.

Mallick, S.S. 2009. PhD Dissertation: Modelling dense-phase pneumatic conveying of powders, University of Wollongong.

Mallick, S.S. and Wypych, P.W. 2009. Minimum transport boundaries for pneumatic conveying of powders. Powder Technology. 194: 181-186.

Mallick, S.S., Wypych, P.W. and Pan, R. 2011. Minimum Transport Boundaries for Dense-Phase Pneumatic Conveying of Powders. In the proceedings of Bulk Solids India, Mumbai.

Martinussen, S.E., 1996. PhD Dissertation: The Influence of the Physical Characteristics of Particulate Materials on their Conveyability in Pneumatic Transport Systems, Technological Department, Telemark University College, Porsgruun, Norway.

Mason, D.J. and Levy, A. 2001. A model for non-suspension gas-solids flow of fine powders in pipes. International Journal of Multiphase Flow. 27: 415-435.

Mills, D. 2004. Pneumatic conveying design guide. Elsevier/Butterworth-Heinemann, 2nd edition.

Mills, D. 2004a. An investigation of the unstable region for dense phase conveying in sliding bed flow. Grannular Matter. 6: 173-177.

Mills, D., Mason, J.S. and Stacey, R.B. 1982. A design study for pneumatic conveying of fine particular material. In the proceedings of Solidex 82: The solids handling conference, Harrogate, England, pp. C1-C75.

Mountziaris, T.J. and Jackson, R., 1991. The effects of aeration on the gravity flow of particles and gas in vertical standpipes. Chemical engineering science, 46(2), pp.381-407.

Pan, R. 1992. PhD Dissertation: Improving scale-up procedures for the design of pneumatic conveying systems, University of Wollongong.

Pan, R. and Wypych, P.W. 1992. Scale up procedures for pneumatic conveying design. Powder Handling and Processing. 4 (2): 167-172.

Pan, R. and Wypych, P.W. 1998. Dilute and dense phase pneumatic conveying of fly ash. In the proceedings of 6th International Conference on Bulk Materials Storage and Transportation, Wollongong, NSW, Australia: 183-189.

Ratnayake C. 2005. PhD Dissertation: A Comprehensive Scaling Up Technique for Pneumatic Transport Systems, Norwegian University of Sceince and Technology (NTNU).

Rautiainen A., Stewart G., Poikolainen V., Sarkoma P. 1999. An experimental study of vertical pneumatic conveying. Powder Technology. 104: 139–150.

Rabinovich, E. and Kalman, H. 2009. Incipient motion of individual particles in horizontal particle–fluid systems: B. Theoretical analysis. Powder Technology, 192, 326-338.

Rao, K. K., Nott, P. R. and Sundaresan, S. 2008. An introduction to granular flow, Cambridge University Press New York.Reiling, V. G. 1992. The effects of ultrafine particles on powder cohesion and fluidization. Case Western Reserve University.

Rizk, F. 1982. Pneumatic transport in dilute and dense phase. Bulk Solids Handling. 2 (2): 235-241.

Schügerl, K., Merz, M. and Fetting, F. 1961. Rheologische eigenschaften von gasdurchströmten fliessbettsystemen. Chemical Engineering Science, 15, 1-38.

Setia, G., Mallick, S. S., Wypych, P. W. and Pan, R. 2013. Validated scale-up procedure to predict blockage condition for fluidized dense-phase pneumatic conveying systems. Particuology, 11, 657-663.

Stegmaier, W. 1978. Zur berechnung der horinentalen pneumatischen forderung feinkorniger feststoffe - for the calculation of horizontal pneumatic conveying of fine grained solids. Fordern and Heben. 28: 363-366.

Streeter, V. L. and Benjamin, W.E. 1979. Fluid mechanics. Publ. McGraw-Hill.

Weber, M. 1981. Principles of hydraulic and pneumatic conveying on pipes. Bulk Solids Handling. 1 (1): 57-63.

Weber, M. 1991. Friction of the air and the air/solid mixture in pneumatic conveying. Bulk Solids Handling. 11 (1): 99-102.

Wei, L. and Chen, Q. 2001. Calculation of Drag Force on an Object Settling in Gas-Solid Fluidized Beds. Particulate Science and Technology, 19, 229-238.

Williams, K., Olszewski, T., Jones, M. and Singh, B. 2008. Electrical capacitance tomography of dense-phase pneumatic conveying of fly ash powder. In the proceedings of Bulk Europe 2008, Czech Republic.

Williams, K.C. and Jones, M.G. 2004. Numerical model velocity profile of fluidised dense phase pneumatic conveying. In the proceedings of 8th International Conference on

Bulk Materials Storage and Transportation, Wollongong, NSW, Australia, 5-8 July: 354-358.

Wirth, K.E. and Molerus, O. 1983. Prediction of pressure drop with pneumatic conveying of solids in horizontal pipes. Journal of Powder and Bulk Solids Technology. 7 (2): 17-20

Wypych, P. W. 1989. PhD Dissertation: Pneumatic conveying of bulk solids, University of Wollongong.

Wypych, P.W and Yi, J. 2003. Minimum transport boundary for horizontal dense-phase pneumatic conveying of granular materials. Powder Technology. 129: 111-121.

Wypych, P.W. and Arnold, P.C. 1984. The use of powder and pipe properties in the prediction of dense phase pneumatic transport behaviour. In the proceedings of Proceedings of the Technical Program, Pneumatech 2, International Conference on Pneumatic Conveying Technology, University of Kent, Canterbury, England, 4-6 September, Organised by the Powder Advisory Centre, London, England. Wypych, P.W. and Reed A.R. 1990. The Advantages of Stepping Pipelines for the Pneumatic Transport of Bulk Solids. Powder handling and processing, 2(3): p. 217.

Wypych, P.W. and Arnold, P.C. 1987. On improving scale-up procedures for pneumatic conveying design. Powder Technology. 50: 281-294.

Wypych, P.W., Hastie, D. B. and Yi, J. 2005. Prediction of optimal operating conditions for dense-phase pneumatic conveying systems. Final research report for the International Fine Particle Research Institute, Inc, USA.

Wypych, P.W., Kennedy, O.C. and Arnold, P.C. 1990. The future potential of pneumatically conveying coal through pipelines. Bulk Solids Handling. 10 (4): 421-427.

Yi, J., Wypych, P.W. and Pan, R. 1998. Minimum conveying velocity in dilute-phase pneumatic conveying. Powder Handling and Processing. 10 (3): 255-261.

Zhang, X., Zhang, D., Wang, A. and Geng, Y. 2015. Transportation characteristics of gas–solid two-phase flow in a long-distance pipeline. Particuology, 21, 196-202.

APPENDIX A

A1.1 Results of scale-up evaluation

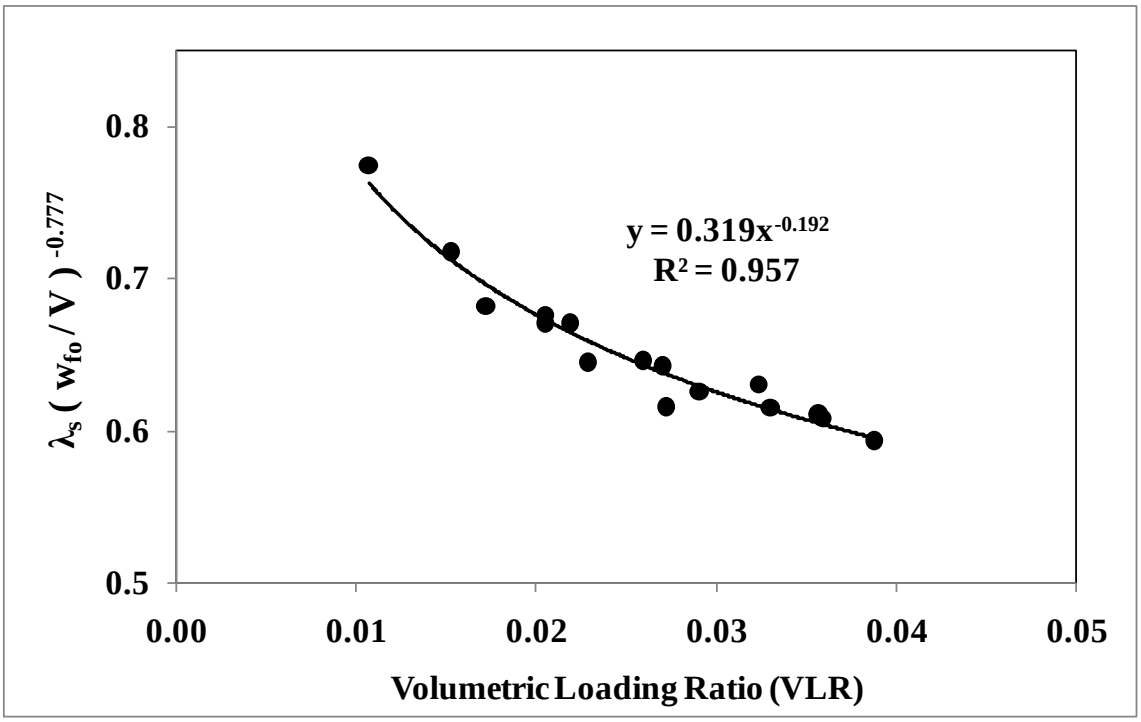

Figure A1.1: Model development for fly ash using new model format (as per Equation 5.1) for fly ash conveyed at Thapar University

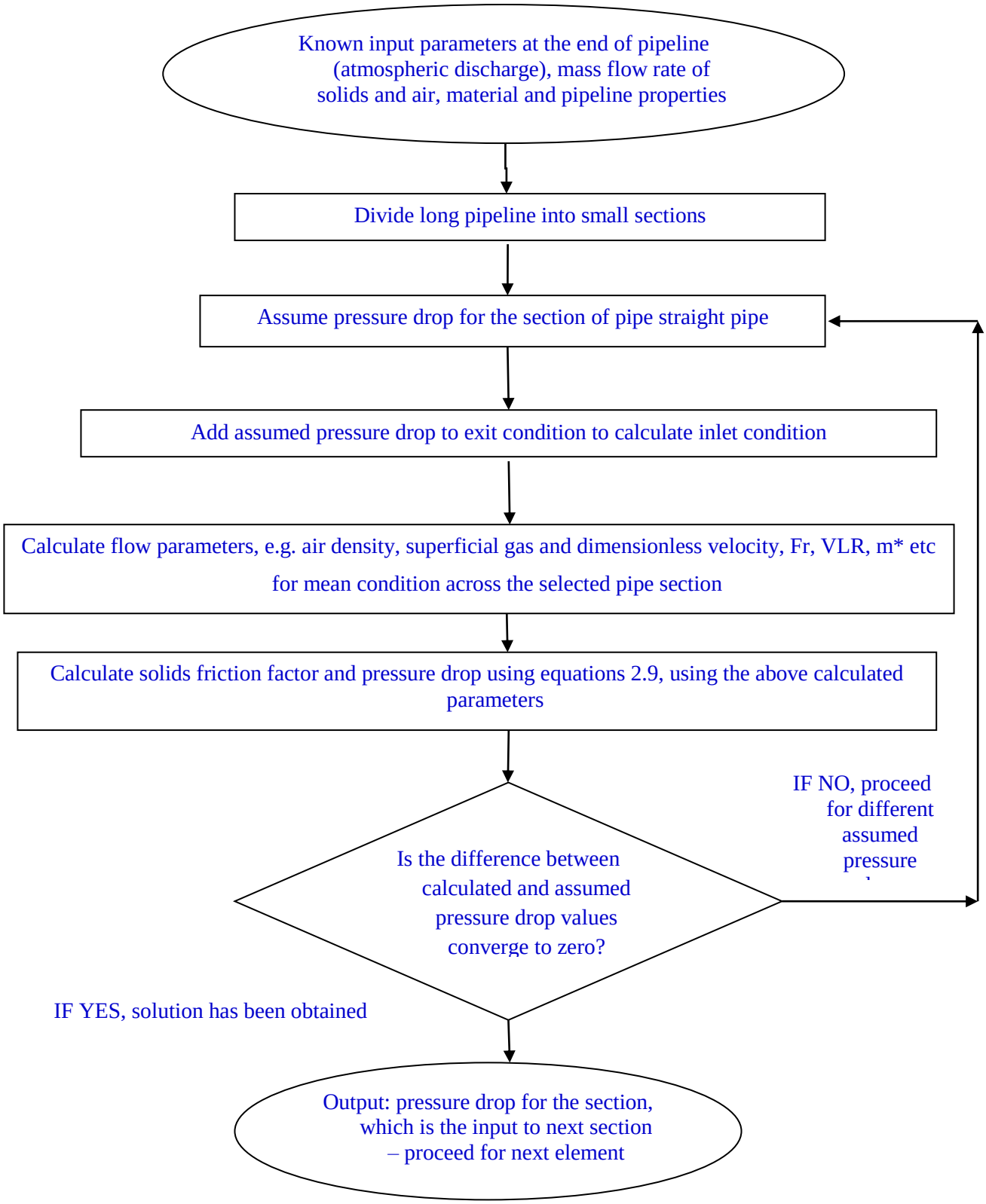

Figure A1.2 Flow chart for the Computer Program to calculate total pipeline pressure drop

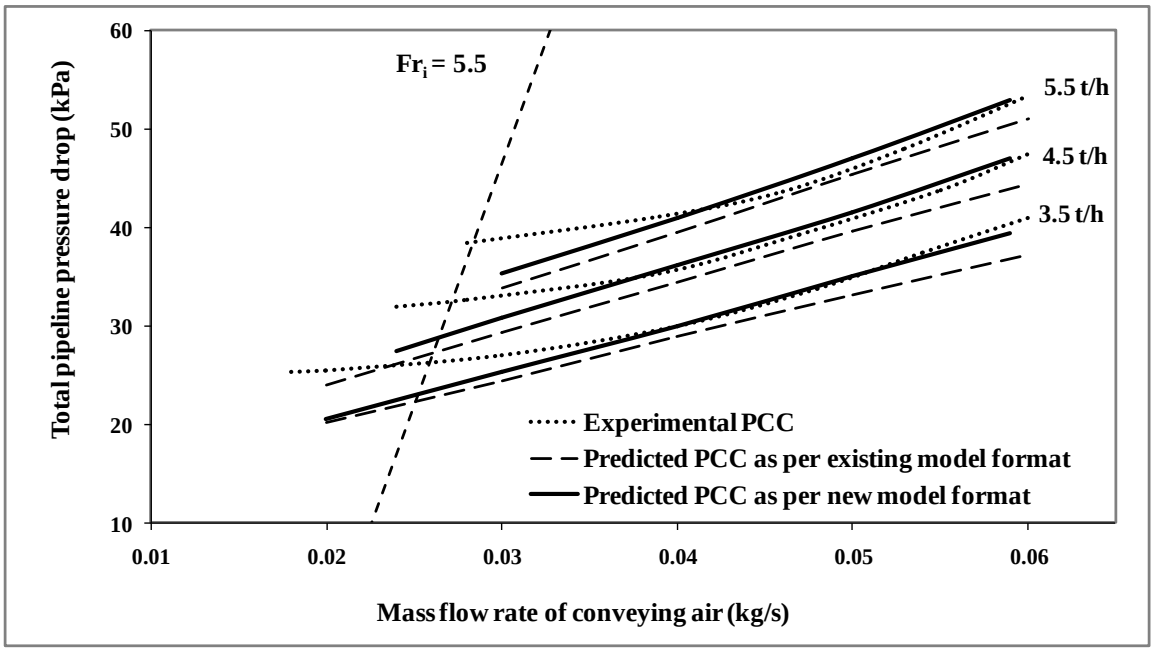

Figure A1.3: Experimental versus predicted PCC using Model 3 and Model 7 for fly ash through pipeline B3 (69 mm I.D. × 24 m long pipe)

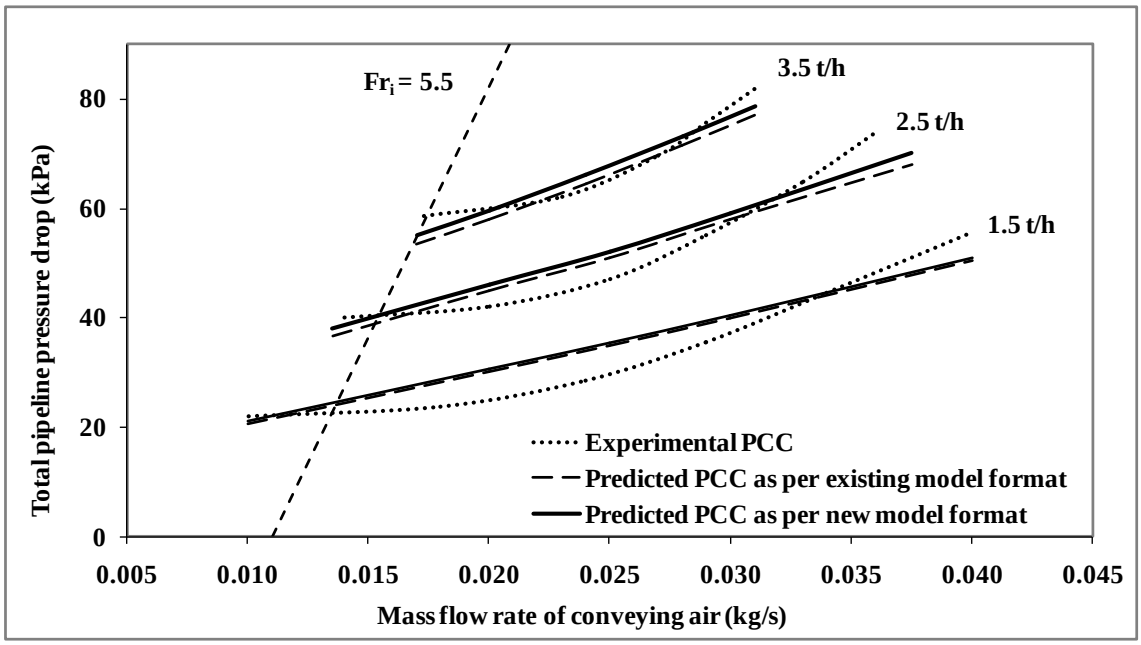

Figure A1.4: Experimental versus predicted PCC using Model 3 and Model 7 for fly ash through pipeline B4 (54 mm I.D. × 70 m long pipe)

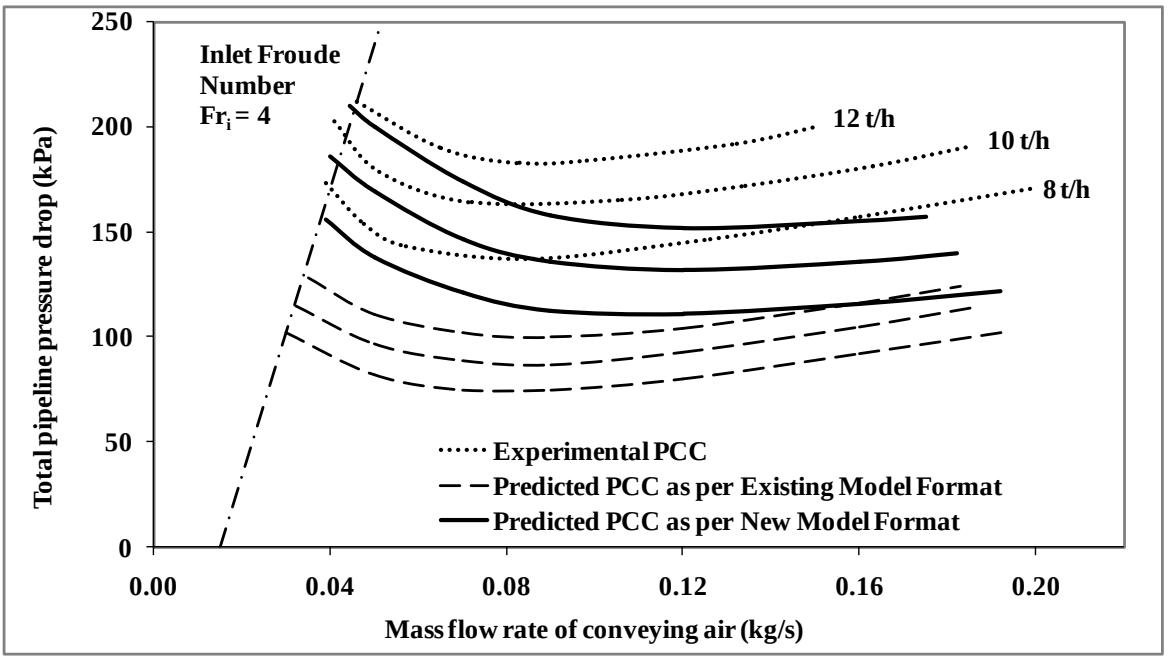

Figure A1.5: Experimental versus predicted PCC using Model 3 and Model 7 for ESP dust through pipeline A1 (69 mm I.D. × 168 m long pipe)

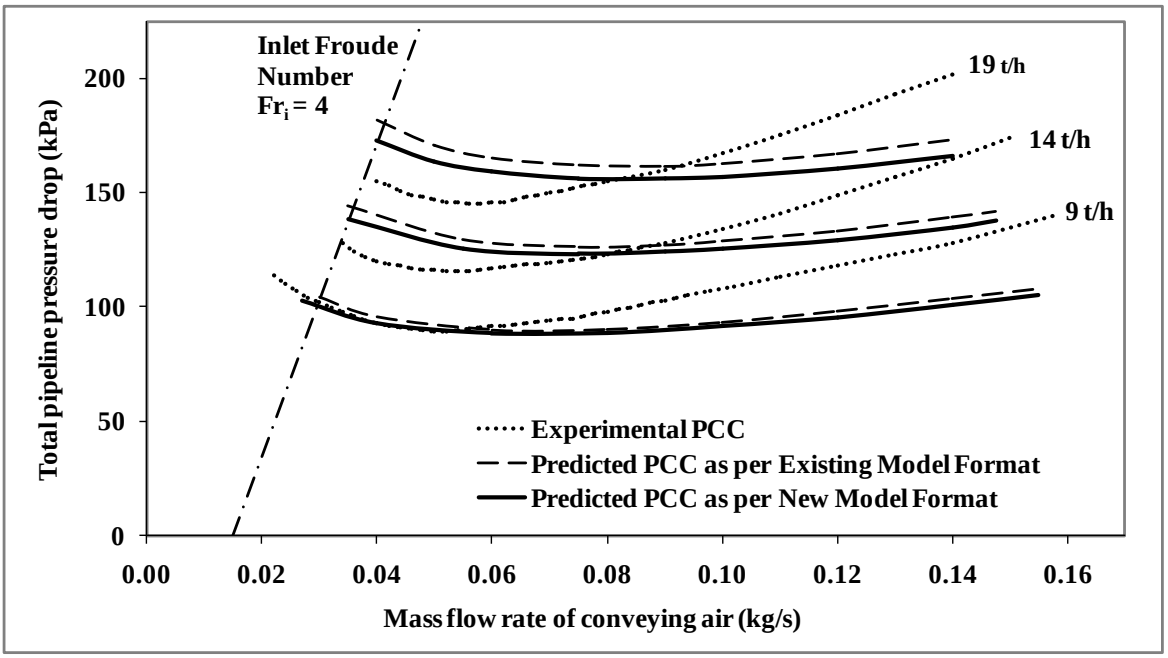

Figure A1.6: Experimental versus predicted PCC using Model 4 and Model 8 for fly ash through pipeline A1 (69 mm I.D. × 168 m long pipe)

LIST OF PUBLICATIONS DURING COURSE OF PhD

Referred SCI journal papers (published/accepted) – 6 Nos.

Sr. No.	Title of paper	Authors' Names	Journal	Volume, Year, Page no.	Impact factor
1.	An experimental investigation into modeling solids friction for fluidized dense-phase pneumatic transport of powders	**G. Setia** S.S. Mallick, R. Pan, P. Wypych	**Particuology** (Elsevier)	Accepted	2.110
2.	Modeling solids friction factor for fluidized dense-phase pneumatic transport of powders using two layer flow theory	**G. Setia** S.S. Mallick, R. Pan, P. Wypych	**Powder Technology** (Elsevier)	294, 2016, 80-92	2.349
3.	Modeling minimum transport boundary for fluidized dense-phase pneumatic conveying systems	**G. Setia,** S.S. Mallick, R. Pan, P.W. Wypych	**Powder Technology** (Elsevier)	277, 2015, 244-251	2.349
4.	Modelling fluidized dense-phase pneumatic conveying of fly ash	**G. Setia,** S.S. Mallick	**Powder Technology** (Elsevier)	270, 2015, 39-45	2.349
5.	An investigation into pressure fluctuations and improved modeling of solids friction for dense-phase pneumatic conveying of powders	A. Mittal, **G. Setia,** S.S. Mallick, P.W. Wypych	**Particulate Science and Technology** (Taylor and Francis)	33, 2015, 67-75	0.523
6.	On improving solid friction factor modeling for fluidized dense-phase pneumatic conveying systems	**G. Setia,** S.S. Mallick, P.W. Wypych	**Powder Technology** (Elsevier)	257, 2014, 88-103	2.349

Referred SCI journal papers (under review) – 1 nos.

Sr. No.	Title of paper	Authors' Names	Journal	Volume, Year, Page no.	Impact factor
1.	An experimental investigation into the rheology of fine powders for modeling fluidized dense-phase pneumatic conveying	B. Chaudhry, **G. Setia,** S.S. Mallick	**Powder Technology** (Elsevier)	Under Review	2.349

Referred conferences (published/accepted) – 3 nos.

Sr. No.	Title of paper	Authors' Names	Conference-year	Country
1.	Improved scale-up procedures for fluidized dense-phase pneumatic conveying systems	**G. Setia,** S.S. Mallick	**CHoPS-2015** (*8th International Conference for* Conveying and Handling of Particulate Solids, 2015)	Tel-Aviv, **Israel**
2.	Investigating pneumatic conveying characteristics and minimum transport velocity for fluidised dense-phase transport of fine powders	**G. Setia,** S.S. Mallick, P.W. Wypych	**IPS -2014 (***International Operation and Maintenance Conference on* Indian Power Stations, 2014**)**	New Delhi, **India**
3.	Study of pressure fluctuations during and improved modeling methods for dense phase pneumatic conveying of powders	A. Mittal, **G. Setia,** S.S. Mallick, P.W. Wypych	**PGBSIA-2013** (*First International Conference on* Powder, Granule and Bulk Solids: Innovations and Applications, 2013)	Thapar University, Patiala, **India**